Investigation of the strength loss of heat treated glass fibre

by

Peter Jenkins, MEng

A thesis presented for the degree of Doctor of Philosophy

2016

Department of Mechanical and Aerospace Engineering

Faculty of Engineering

University of Strathclyde

Signed:

Date:

Acknowledgements

I would firstly like to thank my supervisor Professor Jim Thomason for all of the guidance and support provided throughout the course of my studies. In addition, I am very grateful to Dr Liu Yang, and indeed all of the present and past members of the Advanced Composites Group and Strathclyde, for their advice and assistance over the past few years. It was a pleasure to work with them all.

I gratefully acknowledge the financial support of my studies received from University of Strathclyde and from the Engineering and Physical Sciences Research Council (EPSRC) through the project EP/I038616/1.

I owe thanks to all of the technical support staff at Strathclyde, who have been generous with their time and support towards my research. In particular I would like to thank James Kelly for help with microscopy and Dr Fiona Sillars for her significant support of all my activities in the Advanced Materials Research Laboratory.

I am thankful for the assistance of Dr John Liggat in the Department of Pure & Applied Chemistry for allowing me extensive access to equipment in his laboratories and for the many helpful discussions he was involved in.

I wish to thank Prof John Watts and Dr Steve Hinder at the University of Surrey for allowing me access to their Surface Analysis Laboratory and for assisting me with my XPS analysis and interpretation of data.

I owe thanks to Prof Xinjong Chen at the University of Nottingham's Laboratory of Biophysics and Surface Analysis (School of Pharmacy) for his great assistance with my AFM analysis and equally so for his guidance with data interpretation.

Finally I would like to thank all of my family and friends who have been very supportive throughout the length of my studies.

Abstract

Mechanical reinforcement glass fibre has been shown to demonstrate significant loss of tensile strength following exposure to elevated temperatures; for example when heat treatment is performed, or due to thermal recycling. Numerous previous studies have confirmed this phenomenon and, while some have attempted to explain possible mechanisms of strength loss, a complete understanding has not yet been presented in the literature.

In the work presented in this thesis the phenomenon of strength loss due to heat treatment was investigated using boron-free E-glass fibres, which were coated with either γ-aminopropyltriethoxysilane (γ-APS) or had no surface coating applied during manufacture (unsized/bare). Novel methods of heat treatment were developed and techniques including tensile testing and various thermal analyses were employed. The fibre surface was investigated by X-ray Photoelectron Spectroscopy (XPS), Atomic Force Microscopy (AFM) and Scanning Electron Microscopy (SEM) with Energy Dispersive X-ray spectroscopy (SEM-EDX).

By application of a single fibre heat treatment approach it was found that the retained fibre tensile strength after conditioning can be underestimated when using the standard method of heat treating fibre bundles. Strength loss may be comprised of two components: the first component, mechanical handling damage, was carefully controlled using the single fibre heat treatment approach, but is also minimised by presence of sufficient surface γ-APS coating.

The second component is the fundamental strength loss due to thermal effects, which was found to be most critical in the temperature range 450 – 600 °C.

The effect of water during heat treatment of unsized fibre was studied using a Thermal Volatilisation Analyser (TVA) in which simultaneous application of vacuum and elevated temperature is possible. It was found that single fibres conditioned using TVA at 450 °C had a strength that was not significantly different from that of fibres that were conditioned similarly but in a standard air furnace.

Surface chemical changes of heat treated fibres were investigated. Results of XPS analysis suggested that the surface concentration of calcium increased with increasing conditioning temperature up to 600 °C. Results obtained using Energy

Dispersive X-ray spectroscopy (SEM-EDX) showed an increase in the concentration of potassium in the near surface region when fibres were heat treated in excess of 600 up to 700 °C. Significant physical changes at the fibre surface were also observed following heat treatment between 600 – 700 °C. Results of AFM analysis showed that the RMS surface roughness approximately doubled and features became visible by SEM.

Across the entire temperature range 200 – 700 °C, over which both roughness and retained fibre strength were investigated, a general trend of increasing surface roughness and decreasing fibre strength was found; however, there was not a correlation between regions of most significant strength loss and large increases in roughness.

Contents

Acknowledgements ii

Abstract iii

Contents v

List of figures xii

List of tables xvii

Chapter 1. Introduction 1

1.1 Background 1

1.2 Aims and objectives of project 1

1.3 Outline of thesis 2

Chapter 2. Literature Review 4

2.1 Glass fibre 4

2.1.1 Glass fibre formulation 4

2.1.2 E-glass 6

2.1.3 Glass surface 7

2.1.3.1 Hydroxyl groups 7

2.1.3.2 Surfaces of E-glass systems 9

2.1.4 Interaction with water 10

2.1.4.1 Effect on tensile strength of fibres 10

2.1.4.2 Adsorption of water on E-glass 12

2.1.5 Orientation of structure 13

2.1.5.1 Bulk structural orientation 13

2.1.5.2 Anisotropy orientation and birefringence 14

2.2 Strength of glass fibre 15

2.2.1 Types of strength 15

2.2.2 Flaw theory 16

2.2.3 Flaw visualisation 19

2.3 Strength loss of heat treated glass fibre 20

2.3.1 Temperature and time effects 20
2.3.2 Temperature and mechanical damage....23
2.3.3 The effect of heating atmosphere....23
2.3.4 The effect of heat treatment under tensile stress 24
2.4 Physical changes following heat treatment....26
2.4.1 Thermal compaction or enthalpy relaxation....27
2.4.2 Anisotropy (birefringence) relaxation....30
2.4.3 Crystallisation 30
2.4.4 Ion exchange 31
2.5 Silanes and sizings....32
2.5.1 Bonding of silanes to hydroxylated surfaces 34
2.5.2 Effect of silanes and sizings on glass fibre strength 36
2.5.3 Temperature degradation of silane based surface coating 37
Chapter 3. Experimental....39
3.1 Materials 39
3.2 Heat treatments....40
3.2.1 Furnace heat treatments....40
3.2.1.1 Bundle heat treatment 40
3.2.1.2 Single fibre heat treatment.... 41
3.2.1.3 Heat treatment for X-ray Diffraction Spectroscopy (XRD).... 42
3.2.2 Vacuum system heat treatment....43
3.2.2.1 Bulk glass fibre samples 44
3.2.2.2 Heat treatment of single fibre samples 45
3.2.3 Heat treatments using thermal analysis equipment....48
3.2.3.1 Thermo-Gravimetric Analyser (TGA) – treatment of samples for XPS analysis 49
3.2.3.2 Thermo-mechanical Analyser (TMA) – treatment of samples for AFM and SEM imaging.... 49
3.3 Tensile testing....50
3.3.1 Tensile test settings 50

3.3.1.1 Analysis of tensile data 52
3.3.2 Fibre diameter measurement 53
3.3.2.1 Optical microscopy and image analysis 54
3.3.2.2 Scanning Electron Microscopy 54
3.4 X-Ray Diffraction Spectroscopy (XRD) 55
3.4.1 Fibre used in analysis 55
3.4.2 Experimental settings 55
3.5 X-ray Photoelectron Spectroscopy (XPS) 55
3.5.1 Fibre used in analysis 55
3.5.2 Experimental settings 56
3.5.3 Data processing 56
3.6 Atomic Force Microscopy (AFM) 57
3.6.1 Fibre used in analysis 57
3.6.2 Experimental settings 57
3.6.3 Data processing 58
3.6.3.1 Image flattening and cleaning 58
3.6.3.2 Roughness analysis 60
3.7 Thermal analysis 61
3.7.1 Thermo-gravimetric and Differential Scanning Calorimetry (TGA/DSC) 61
3.7.2 CATLAB degradation analysis 61
3.8 Fractography using Scanning Electron Microscopy 62
3.8.1 Experimental settings 62
3.8.2 Sample preparation 62
3.9 Scanning Electron Microscopy – Energy Dispersive X-ray spectroscopy (SEM-EDX) 63
3.9.1 Experimental settings 63
3.9.2 Sample preparation 63
3.10 Image analysis – surface of heat treated fibres 64
3.10.1 Fibre used in analysis 64

3.10.2 Image processing and analysis 64
Chapter 4. Strength of heat treated sized and unsized E-glass 66
4.1 Introduction 66
4.2 Bundle heat treatment 67
4.2.1 Untreated fibre strength baseline 67
4.2.2 Results – bundle heat treatment 68
4.3 Single fibre heat treatment 70
4.3.1 Motivation 70
4.3.2 Results – bundle versus single fibre heat treatment 71
4.4 APS degradation and its effect on retained strength 72
4.4.1 Direct measurements of APS degradation on E-glass fibre 73
4.4.1.1 XPS analysis 73
4.4.1.2 SEM observations 74
4.4.2 Indirect analysis of APS degradation using APS film 77
4.4.2.1 TGA/DSC results 77
4.4.2.2 CATLAB analysis of thermal degradation products 78
4.4.3 Discussion of thermal analysis results 82
4.4.3.1 Applicability of results 82
4.4.3.2 Initial mass loss region (room temperature → T = 220 °C) 82
4.4.3.3 Significant mass loss region (T > 300 °C) 84
4.4.4 Summary of results 86
4.5 Mechanical handling and thermal damage of heat treated glass fibre 87
4.5.1 Interpretation of bundle heat treatment results with APS degradation 87
4.5.2 Interpretation of single fibre heat treatment results with APS degradation 89
4.5.2.1 Room temperature to 300 °C 89
4.5.2.2 450 to 600 °C 90
4.5.2.3 Heat treatment beyond 600 °C 90
4.5.2.4 Trend across whole heat treatment range 92
Chapter 5. Effect of moisture during single fibre heat treatment of bare fibre 93

5.1 Introduction 93
5.2 Characterisation of water desorption under vacuum in TVA system 94
5.3 Heat treatment of single fibres under vacuum 96
5.3.1 Effects of variables in heat treatment process on retained fibre strength. 98
5.3.1.1 Effect of heating/cooling rate 98
5.3.1.2 Effect of heat treatment under vacuum 98
Chapter 6. Analysis of the surface of heat treated glass fibres 100
6.1 Surface chemical changes 100
6.1.1 Introduction 100
6.1.2 Results 101
6.1.3 Discussion 104
6.2 Surface physical changes 105
6.2.1 Surface roughness 106
6.2.1.1 Surface of non-heat treated E-glass 106
6.2.1.2 Surface of heat treated E-glass 108
6.2.2 SEM observations 112
6.2.2.1 Comparability of AFM and SEM images 112
6.2.2.2 SEM of fibres treated ≥ 600 °C 113
6.2.2.3 Image analysis of surface features on fibres treated ≥ 600 °C 117
6.2.2.4 Rinsing of fibres treated ≥ 600 °C 119
6.2.3 Chemical analysis of features by SEM-EDX 121
6.2.4 Discussion of physical surface changes 123
6.2.4.1 Links with strength loss 123
6.2.4.2 Known surface roughening effects 125
6.2.4.3 Potential sources of surface structure/roughness 126
6.3 Fracture and flaws in glass fibres 128
6.3.1 Introduction 128
6.3.2 Fractography of heat treated E-glass fibre 129
6.3.3 Comparison of flaw theory with observed AFM data 131
6.3.3.1 Topography data for non-heat treated bare fibre 131

6.3.3.2 Implications of AFM topography and fibre strengths 133
6.4 Crystallisation behaviour 135
6.4.1 Introduction 135
6.4.2 Results 135
6.4.3 Discussion 136
Chapter 7. Conclusions 138
7.1 Strength loss of heat treated fibres (chapter 4) 138
7.1.1 Degradation of surface coating 138
7.1.2 Mechanical handling damage 139
7.1.3 Thermal strength loss 140
7.2 Effect of the presence of water during heat treatment (chapter 5) 140
7.3 Glass fibre surface changes due to heat treatment (chapter 6) 142
7.3.1 Chemical 142
7.3.1.1 Surface calcium content (XPS) 142
7.3.1.2 Physio-chemical: K content increase with development of surface structure 142
7.3.2 Physical 142
7.3.3 Crystallisation 144
Chapter 8. Future work 145
8.1 Surface analysis 145
8.1.1 Further study of surface roughening due to heat treatment 145
8.1.1.1 Continuing AFM study 145
8.1.1.2 AFM analysis of vacuum heat treated fibres 146
8.1.1.3 Environmental AFM study 146
8.1.1.4 Investigation of potential phase separation at high temperature 146
8.1.2 Further chemical analysis by SEM-EDX 147
8.1.2.1 Extension of temperature range investigated 147
8.1.2.2 Wavelength Detection X-ray spectroscopy 147
8.2 Further heat treatment & strength loss experiments 148

8.2.1 Investigation of the influence of production parameters (axial drawing stress) on strength retention following heat treatment 148

8.2.2 Further investigation of the effect of water on the fibre surface during heat treatment 150

8.2.3 The effect of water on flaws in glasses 150

References 152

Appendix A : Principles of XPS 164

Introduction 164

Photoelectron effect 164

XPS instrumentation and analysis 165

Appendix B : Principles of AFM 167

Introduction 167

General principles of AFM 167

Intermittent contact AFM 168

List of figures

Figure 2-1: Molecular structure of silica 5
Figure 2-2: Uni-axially stressed plate with edge crack, taken from [57] 17
Figure 2-3: Energy balance for fracture with increasing crack length 'a', taken from [57] 18
Figure 2-4: Results on single fibre tensile strength of heat treatments on E-glass fibres, reproduced from Thomas [5] 20
Figure 2-5: Result of isothermal heating on fibre length contraction with time, from Otto [71].....28
Figure 2-6: Representation of the sizing process applied to continuously formed glass fibre (from [86]) 33
Figure 2-7: γ-aminopropyltriethoxysilane molecule 34
Figure 2-8: Hydrolysation and condensation processes of alkoxysilanes [89] 34
Figure 2-9: Reaction between self-condensed alkoxysilane and substrate surface [89] 35
Figure 2-10: Chemical structure of hydrolysed γ-APS on glass fibre surface [92]...36
Figure 3-1: Rig used for heat treatment of glass fibre bundles 41
Figure 3-2: Simplified flowchart showing the difference between the bundle and single fibre heat treatment procedures.....42
Figure 3-3: Simplified block diagram of single line TVA setup used for vacuum heat treatment of glass fibre 43
Figure 3-4: Schematic representation and photograph of single fibre mounting arrangement for vacuum treatment of single fibres in TVA.....46
Figure 3-5: Temperature vs. position measurements within TVA sample tube during isothermal (furnace set to 560 °C) 47
Figure 3-6: Approximate position of single fibre sample holder within TVA furnace48
Figure 3-7: Mounting arrangement for heat treatment of single fibres in TMA 49
Figure 3-8: Schematic of single fibre tensile test sample card.....51
Figure 3-9: Idealised load-extension graph for single glass fibre tensile test 52
Figure 3-10: Schematic of single glass fibres mounted on microscope slide for AFM analysis 57
Figure 3-11: Edge effect of change in tip direction on AFM topography plot.....59
Figure 3-12: Example of streaks appearing on AFM topography plot that has been flattened.....59

Figure 3-13: Example of AFM plot from which streaks have been 'cleaned' 60
Figure 3-14: Typical area and points on line analysed using SEM-EDX of sites on a single fibre 63
Figure 4-1: Comparison between strength of untreated unsized fibre; (a) straight from roving and (b) after simulated bundle heat treatment procedure 67
Figure 4-2: Tensile strength of bare and APS sized fibres after bundle heat treatment for 25 minutes 68
Figure 4-3: Tensile strengths of bare and APS sized fibres after heat treatment for 25 minutes 72
Figure 4-4: quantification of nitrogen surface content from N1s peak (from survey scan).....74
Figure 4-5: SEM image of typical unconditioned APS sized fibre 75
Figure 4-6: SEM image of APS sized fibre, single fibre heat treated at 450 °C for 25 minutes.....76
Figure 4-7: SEM image of APS sized fibre, single fibre heat treated at 300 °C for 25 minutes.....77
Figure 4-8: Simultaneous TGA/DSC of APS film, measurement performed under air 78
Figure 4-9: comparison of mass loss curves by TGA of APS film analysed under air or nitrogen 79
Figure 4-10: DSC of APS film analysed under air (red dotted) and nitrogen (grey and black solid).....80
Figure 4-11: CATLAB degradation profiles of (a) AMU 18 [water], (b) AMU 17 [OH-water fragment or NH_3], (c) AMU 44 [CO_2] and (d) AMU 28 [CO or C_2H_4]. Measurements carried out under helium atmosphere 81
Figure 4-12: CATLAB degradation profiles of AMU 28, C_2H_4 [black solid] and AMU 42, C_3H_6 [grey dotted]. Measurements carried out under helium.....85
Figure 4-13: Tensile strengths of bare fibres after single fibre heat treatment for 25 minutes.....91
Figure 5-1: % absorbance gas cell IR plots of bare fibre samples heat treated to 500 °C for 15 minutes following vacuum drying for (a) zero hours, (b) 1 hour and (c) 2 hours 95
Figure 5-2: average tensile strengths of bare E-glass: (i) untreated, (ii) vacuum treated in TVA at 450 °C, (iii) furnace treated at 450 °C at approximately same

heating/cooling rate as TVA, (iv) furnace treated at 450 °C using standard single fibre heat treatment procedure.....97
Figure 6-1: Atomic percentages of Si at E-glass fibre surface with respect to heat treatment temperature. Measurements of 2 series of samples were carried out using XPS, at an interval of approximately 1 month 102
Figure 6-2: Atomic percentages of Al at E-glass fibre surface with respect to heat treatment temperature. Measurements of 2 series of samples were carried out using XPS at an interval of approximately 1 month 102
Figure 6-3: Atomic percentages of Ca at E-glass fibre surface with respect to heat treatment temperature. Measurements of 2 series of samples were carried out using XPS at an interval of approximately 1 month 103
Figure 6-4: average RMS roughness of E-glass fibre with respect to heat treatment temperature 107
Figure 6-5: 3D and 2D topography plots of a typical untreated unsized E-glass fibre 107
Figure 6-6: (a) phase contrast and (b) 2D topography plot of a typical untreated unsized E-glass fibre 108
Figure 6-7: 3D and 2D topography plots of a typical 200 °C treated unsized E-glass fibre 109
Figure 6-8: 3D and 2D topography plots of a typical 300 °C treated unsized E-glass fibre 109
Figure 6-9: 3D and 2D topography plots of a typical 400 °C treated unsized E-glass fibre 110
Figure 6-10: 3D and 2D topography plots of a 500 °C treated unsized E-glass fibre (1 of 2).....110
Figure 6-11: 3D and 2D topography plots of a 500 °C treated unsized E-glass fibre (2 of 2).....110
Figure 6-12: 3D and 2D topography plots of a typical 600 °C treated unsized E-glass fibre 111
Figure 6-13: 3D and 2D topography plots of a typical 700 °C treated unsized E-glass fibre 111
Figure 6-14: Images of 700 °C heat treated glass fibre obtained using (a) SEM [8000x magnification] and (b) AFM 112
Figure 6-15: SEM image of fibre surface following heat treatment at 600 °C.....113
Figure 6-16: SEM image of fibre surface following heat treatment at 625 °C.....114

Figure 6-17: SEM image of fibre surface following heat treatment at 650 °C.....115
Figure 6-18: SEM image of fibre surface following heat treatment at 675 °C.....115
Figure 6-19: SEM image of fibre surface following heat treatment at 700 °C.....116
Figure 6-20: larger scale SEM image of fibre shown in Figure 58; heat treated at 700 °C 117
Figure 6-21: Examples of segments (2 x 2 µm) of SEM images of bare glass fibre heat treated between 625 – 700 °C and their counterparts following image conversion to black and white. Images captured at 8000 – 9000 times magnification 117
Figure 6-22: Average percentage coverage of surface features formed due to high temperature heat treatment, calculated from analysis of binary images.....118
Figure 6-23: SEM images of bare E-glass fibres; (a) untreated (b) TMA heat treated to 700 °C and rinsed in still deionised water for 1h.....120
Figure 6-24: (a) 2D topography and (b) phase contrast plot of a typical 600 °C heat treated unsized E-glass fibre 120
Figure 6-25: (a) 2D topography and (b) phase contrast plot of a typical 700 °C heat treated unsized E-glass fibre 121
Figure 6-26: weight percentages (normalised) obtained by SEM-EDX of bare glass fibre following various heat treatments.....122
Figure 6-27: Tensile strengths of bare fibres after single fibre heat treatment for 25 minutes. Data are divided into a low temp and high temp zone either side of 450 °C and linear best fits for each of these zones are shown.....124
Figure 6-28: O-C unsized E-glass fibre; average fibre tensile strength and fibre surface RMS roughness against 25 minute heat treatment temperature.....125
Figure 6-29: AFM topography, 2x2 µm images of: (a) $12.5Na_2O$. $87.5SiO_2$ heat treated at 650 °C for 160 minutes, taken from reference [118]; (b) bare E-glass fibre heat treated at 600 °C for 25 minutes 127
Figure 6-30: fracture mirror and mist regions (a) and (b) of the same 450 °C vacuum heat treated fibre with strength 1.23 GPa, with approximate fracture origin indicated 130
Figure 6-31: fracture origin of a 450 °C vacuum heat treated fibre with strength 1.2 GPa 131
Figure 6-32: X-ray diffraction patterns for unsized E-glass fibre: untreated (blue) and heat treated to 800 °C and furnace cooled (red) 136

Figure A-1: From left to right; emission of kinetic electron due to incident photoelectron, internal transition to fill core hole, ejection of Auger electron due to transition energy 164
Figure A-2: Concentric Hemispherical Analyser (CHA) present in many XPS instruments 165
Figure B-1: Schematic of AFM probe showing cantilever and tip 167
Figure B-2: Feedback loop electronics for AFM working in intermittent contact mode 168

List of tables

Table 2-1: Typical formulations of E-glass, taken from [12] 6
Table 2-2: Typical formulations of boron-free E-glass, taken from [12] 7
Table 2-3: Characteristic temperatures of incumbent and boron-free E-glass, taken from [12] 7
Table 2-4: Composition by weight of spun basaltic wool fibres (SWFs) as reported by Lund and Yue [51] 24
Table 3-1: XRD settings used in analysis 55
Table 3-2: XPS settings used in analysis 56
Table 3-3: AFM settings used in analysis 58
Table 4-1: summary of principle findings regarding degradation of APS film and APS on surface of glass fibres 87
Table 6-1: Results of surface and bulk analyses of boron-free E-glass fibre from Chapter 6, presented alongside comparable compositional data taken from the literature. No heat treatments (HT) applied unless explicitly stated. All values given in atomic percentage (At%) 101
Table 6-2: number of areas analysed by AFM at each temperature condition 106
Table 6-3: Calculated E-glass fibre failure stresses with change in flaw depth according to (6.1), for straight (Y=1.12) and circular (Y=1.29) edge crack 132
Table 6-4: measurements (all in nm) in z-direction for individual bare E-glass fibres analysed by AFM. Approximately 3 µm squares were analysed for each sample .133
Table 6-5: comparison of measured average strengths of heat treated fibres, with calculated strengths based on z-ranges taken from AFM topography of heat treated fibres 134
Table 6-6: comparison of measured average strengths of heat treated fibres, with calculated strengths based on z_{min} values taken from AFM topography of heat treated fibres 135

Chapter 1. Introduction

1.1 Background

Glass fibres are used extensively in the composites market, constituting the most widely used reinforcement fibre by a significant margin. They are a versatile material possessing numerous advantageous properties such as high specific strength and stiffness as well as hardness and resistance to chemical and biological attack.

In the current climate there are significant environmental concerns, and in many cases accompanying legislation, regarding the recyclability of glass fibre composites. This issue has become an important challenge facing the industrial and academic composites community. Around 60 % of glass fibre composites are based on some form of thermosetting matrix and these materials are particularly difficult to recycle in an efficient manner [1]. Thermal recycling routes have been investigated in the past and are relatively technologically advanced [2, 3]. However, they are all subject to a fundamental problem: the strength of the recycled fibres obtained is always extremely low in comparison with newly manufactured fibres, with typical strength reductions of 80 – 90 %.

The significant decrease in the strength of glass fibre following exposure to elevated temperature is a phenomenon that has been known for in excess of 50 years [4–6] but the reasons for this strength loss are still not sufficiently understood. The phenomenon represents a limiting factor on what could otherwise be a relatively straightforward route of thermal recycling of glass fibres. Understanding the strength loss of glass fibre that occurs following exposure to elevated temperatures represents a potentially important step in the process of improving inherent recyclability of glass fibre composite materials.

1.2 Aims and objectives of project

The studies presented were carried out using a boron-free formulation of E-glass supplied by Owens Corning-Vetrotex. Fibre rovings of identical glass composition were provided with one of two surface coatings applied during manufacture. A 1 % γ -aminopropyltriethoxysilane (APS) hydrolysed solution or no coating other than

water which was used as a cooling spray was applied; the latter therefore referred to as bare, unsized or water sized fibre.

Using these materials possible causes of strength loss due to heat treatment were investigated. The aims of the study were:

- To investigate the effect of heat treatment procedure on retained fibre strength
- To study the effect of the presence of water during heat treatment on retained fibre strength
- To investigate possible bulk changes occurring in heat treated fibres which may be related to fibre strength
- To examine the surface region of fibres both before and after heat treatment, investigating any changes in physical and/or chemical properties

Glass fibre strength was measured by making extensive use of single fibre tensile testing. Various heat treatment procedures were carried out utilising a range of equipment depending on the requirements of the treatment atmosphere or heating rate.

Strength loss of APS coated fibres was attributed in part to degradation of the coating. Typical thermal analysis techniques such as Thermo-Gravimetric Analysis and Differential Scanning Calorimetry were used to study this degradation; further chemical analysis of degradation products was performed using a CATLAB system which combined a furnace and Mass Spectroscopy.

The study of changes at the surface of heat treated fibres was carried out using various techniques: these explored changes in chemistry (XPS, SEM-EDX, XRD) and physical appearance (SEM, AFM).

1.3 Outline of thesis

Chapter 2 presents an in depth discussion of the literature as relevant to the studies undertaken which are reported in this thesis. The discussion is broken down into 5 main sections of varying lengths, namely: Glass fibre, Strength of glass fibre, Strength loss of heat treated glass fibre, Physical changes following heat treatment and Silanes and sizings.

Chapter 3 describes the experimental details of the work undertaken, including the preparation or treatments applied to samples. Testing procedures or analytical studies performed are explained as well as relevant information regarding data analysis. Full details of the principles of some analytical techniques are given in the Appendices.

Chapter 4 outlines the findings of an investigation of the strength loss of APS sized and bare E-glass following heat treatment in air. The application of a novel single fibre heat treatment was used extensively in order to separate mechanical and thermal sources of strength loss. The majority of the data presented in the chapter formed the basis of a publication in Journal of Materials Science [7].

Chapter 5 presents the investigation of the effect of the presence of water on the strength loss of heat treated bare E-glass fibre using a Thermal Volatilisation Analyser (TVA).

Chapter 6 investigates the surface of heat treated glass fibres. Chemical and physical changes to the surface of bare E-glass fibres following heat treatment were investigated using various analytical techniques such as Atomic Force Microscopy (AFM), X-ray Photoelectron Spectroscopy (XPS), X-ray Diffraction Spectroscopy (XRD) and Scanning Electron Microscopy – Energy Dispersive X-ray Spectroscopy (SEM-EDX).

Chapter 7 summarises conclusions of the experimental results presented in chapters 4-6.

Chapter 8 presents future work that is proposed based on the results and conclusions presented in previous chapters.

Chapter 2. Literature Review

2.1 Glass fibre

Glass is one of the most ancient of all manufactured materials. Although a more recent development, glass fibre was used hundreds of years ago by the Venetians as a decorative material [8]. Its history as a material relevant to composite reinforcement began in the 1930's when it was first mass produced by Owens-Corning. Glass fibre has since become a technologically important material due to its many desirable material properties, and is today used in numerous applications such as structural composites, filtration systems and printed circuit boards (PCBs) [9]. Today the glass fibre (and glass yarn) production industry is huge: a 2010 estimate is that total fibre and yarn production was around 4.7 million tons [10] and global production of glass fibre has continued to increase since.

Glass fibre is a versatile material as it possesses many advantageous properties. First and foremost it has excellent strength due to a high surface to volume ratio and associated reduction in the density of flaws of critical dimension according to Griffith's theory [11]. Furthermore, glass fibres possess stiffness, hardness and resistance to chemical and biological action, in addition to other generally desirable properties such as transparency and thermal and sound insulation.

2.1.1 Glass fibre formulation

Glass fibres are produced using a large selection of naturally occurring minerals, mixed together in various ratios. Many of these fibre types contain a large weight percentage of pure silica (SiO_2), with the addition of other oxides; the balance between these constituents is altered in order to control the desired properties of the final product. The simplest glass system of all, pure silica fibres are amorphous polymers based on tetragonal SiO_4 groups with a silicon atom at their centre (Figure 2-1). The silicon atoms form a network by sharing the oxygen atoms at the corners of these tetrahedrons.

Amorphous silica has no true melting point but softens from 1650 °C. To enhance the ease of production of glass fibres numerous other minerals containing non-

siliceous species are added to silica sand. Some additives producing oxides in the melt such as Al_2O_3 and B_2O_3 are referred to as network formers as they become incorporated into the silica network. The effect of this is to reduce the processing temperature. Other oxides, known as network modifiers, are created in the glass mixture; examples of these are CaO, Na_2O or K_2O.

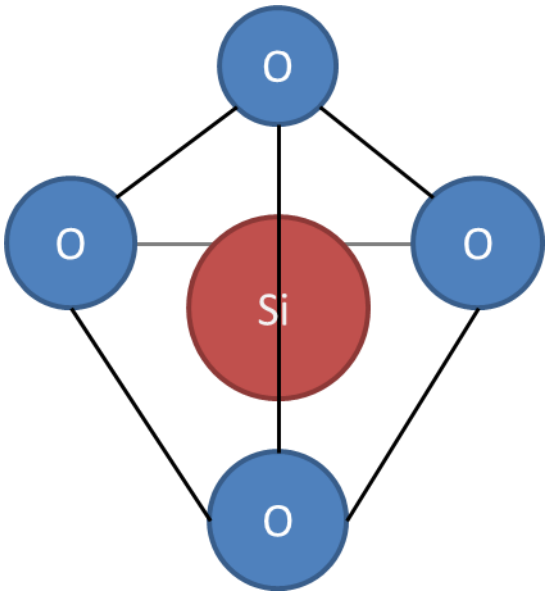

Figure 2-1: Molecular structure of silica

The purpose of network modifiers is to balance the charges associated with oxygen ions within the network, due to the incorporation of network formers other than silicon. These modifiers are found in the interstices of the glass network. Some further oxides known as intermediates are also used, MgO and TiO_2 for example, which can act as either network formers or modifiers.

Many different formulations of glass fibre exist, their chemical compositions being tailored towards an array of various practical uses [12, 13]. ECR glass is an acid, and to a lesser extent alkali, resistant glass. It is similar in composition to a boron-free E-glass (which is discussed in detail in 2.1.2) but with the additions of ZnO and extra TiO_2 which increases the cost significantly. Used in some PCB applications, D-glass has a very low dielectric constant which is achieved due to its very high B_2O_3 content.

Numerous high-strength glass fibres exist on the market: examples include S-, R- and Te-glass. These fibres have higher maximum working temperatures when compared to E-glass making them useful in certain applications. However, this

comes with an associated cost penalty during manufacture as the forming temperatures required are also higher. These glasses tend to be free of both boron and alkali metals.

2.1.2 E-glass

E-glass is the most widely produced of all the formulations of mechanical reinforcement glass fibres, due to the overall balance of desirable properties that it possesses [13]. Although unsuitable for some specialist applications, it is a suitable general purpose fibre formulation. There are broadly two types of E-glass: the incumbent (Table 2-1) and more recent boron-free formulation (Table 2-2). With respect to both of these types of E-glass two formulations, (a) and (b), are reproduced. In both cases the weight percentages used in production mixtures are quoted as typical ranges; this is an outcome of global variations that exist in composition of the oxides that are available to manufacturers. In some cases smaller weight fraction components may be left out altogether.

Table 2-1: Typical formulations of E-glass, taken from [12]

	Typical composition of E-glass (wt%)								
Component [X]	SiO_2	Al_2O_3	B_2O_3	CaO	MgO	$Na_2O + K_2O$	TiO_2	Fe_2O_3	F_2
Formulation (a)	52-56	12-16	5-10	16-25	0-6	0-2	…	…	…
Formulation (b)	52-56	12-15	4-6	21-23	0.4-4	0-1	0.2-0.5	0.2-0.4	0.2-0.7

E-glass originally contained a significant content of B_2O_3, and in some cases also fluorine. The trend recently has been to remove these components from the glass melt due to health concerns surrounding the volatilisation of these materials.

Table 2-2: Typical formulations of boron-free E-glass, taken from [12]

	Typical composition of boron-free E-glass (wt%)								
Component [X]	SiO_2	Al_2O_3	CaO	MgO	TiO_2	Na_2O	K_2O	Fe_2O_3	F_2
Formulation (a)	59	12.1	22.6	3.4	1.5	0.9	…	0.2	…
Formulation (b)	60.1	13.2	22.1	3	0.5	0.6	0.2	0.2	0.1

Typical production mixtures for boron-free E-glass are shown in Table 2-2. Compared with the incumbent E-glass, these formulations have a higher SiO_2 content and therefore slightly higher characteristic temperatures, as indicated in Table 2-3.

Table 2-3: Characteristic temperatures of incumbent and boron-free E-glass, taken from [12]

	Characteristic temperatures (°C)				
	Forming	*Liquidus*	*Softening*	*Annealing*	*Straining*
E-glass	1160-1196	1065-1077	830-860	657	616
Boron-free E-glass	1260	1200	916	736	691

2.1.3 Glass surface

2.1.3.1 Hydroxyl groups

In reviewing glass fibre and its strength it is of the utmost importance to discuss the fibre surface, as this is considered to be directly linked to fracture behaviour [11]. Some research into the surface of E-glass has been conducted in the literature, but a greater volume exists for pure silica. This is a useful place to begin the discussion as the complexities introduced by adding or altering even one component in a silica or glass system can significantly alter its state and complicate analysis of the surface [14, 15]. The study of pure silica systems began many decades ago [16] and has continued since [15, 17, 18].

Unless it has been treated under certain specific conditions the surface of silica can be assumed to be covered to some extent with hydroxyl (OH) groups; when these

hydroxyls are bonded to a silicon atom they are known as silanols. These silanols exist in one of two states: they are either free (isolated) or they are hydrogen bonded with a neighbouring silanol [16]. The overall coverage of hydroxyl groups on a surface is expressed by the hydroxyl number α_{OH}. This value was calculated for many types of silica with a range of specific surfaces by Zhuravlev [19]; for a fully hydroxylated silica he produced the so-called Kiselev-Zhuravlev constant, $\alpha_{OH} = 4.6$ nm^{-2}. A similar value of between 4.2 – 5.37 nm^{-2} was also reported by Bakaev and Pantano [18] using a hydrogen/deuterium exchange method. The Kiselev-Zhuravlev constant appears to be generally accepted, however differing values for fully hydroxylated silica have been reported; for example $\alpha_{OH} = 1.33$ nm^{-2} [15] and $\alpha_{OH} =$ 8.2 – 9.8 nm^{-2} [17]. Significant differences in the materials and methods for which these values were obtained may explain the disagreement in α_{OH} values.

The silanol coverage on a silica surface has been shown to be variable, depending on the application of heat and/or vacuum treatments. Zhuravlev [19], again, presented perhaps the most extensive data, regarding dehydration of physically adsorbed water, the dehydroxylation of surface silanols and the rehydroxylation of treated samples. Mass thermograms of a standard silica were presented, showing the intensity of water evolved against sample temperature using a heating rate of approx. 5 °C/min. Prior to the measurement, however, samples were pre-treated simultaneously under vacuum and at various temperatures. A key temperature of 200 °C was identified with respect to surface water; after vacuum treatment below 200 °C physically adsorbed water remained on the silica surface. However, following treatment at 200 °C or above the surface was fully dehydrated. Further heating led to further evolution of water, due to dehydroxylation of the surface. Two regions of dehydroxylation were found, one between approx. 200-450 °C and the second above 450 °C. The lower range was attributed to the removal of hydrogen bonded hydroxyls, the coverage of which halved by 450 °C. Above 450 °C only free hydroxyls remained; a temperature in excess of 1000 °C was required to fully dehydroxylate the surface.

Although it is more complex than simple silica, the surface of E-glass fibre has been shown using angle-resolved XPS [20] to be populated with silanol groups whose concentration is greater than in the bulk of the fibre. Values for the surface hydroxyl coverage of glass samples, rather than silica, obtained using contact angle measurements have also been published. The hydroxyl number of heat cleaned

laboratory glass slides was reported as α_{OH} = 2.5 nm^{-2} [21]. For slides of boron-free E-glass, once again carefully cleaned and fully hydrolysed, a value of approx. α_{OH} = 2.4 nm^{-2} was obtained [22]. In both cases it is clear that hydroxyl coverage is significantly lower than that of the idealised fully hydroxylated silica system.

2.1.3.2 Surfaces of E-glass systems

E-glass, like silica, is considered to an amorphous material whose surface is populated with hydroxyl groups. Nonetheless, they cannot be considered directly analogous, as suggested by the significant difference in hydroxyl number. Differences between the surface hydroxyl coverage of silica and more complex glass systems are perhaps not surprising given the changes to the molecular network caused by the additions of various network formers and modifiers in glasses. It has been shown [14] that the addition of one extra glass forming component, in this case boron, to silica significantly alters the surface state as demonstrated by a change in the interaction with adsorbate molecules; its effect on surface hydroxyl coverage has also been demonstrated [23].

The surface of E-glass has been studied by numerous researchers and in a few studies it has been shown that there are differences between the surface and bulk of glass fibres in terms of composition at an atomic level. Wong [24] used Auger Electron Spectroscopy (AES) to compare the elemental compositions of E-glass fibre surfaces with the bulk (obtained by analysis of fracture surfaces). His results suggested that the fibre surface is rich in silicon, a result also reported by Thomason and Dwight [25]. Wong also reported an enrichment of aluminium at the surface, but to a lesser extent compared with silicon. Conversely, the surface of the fibres studied appeared to have significantly lower concentration of calcium and magnesium compared to the fibre bulk. The conclusion of a calcium-depleted surface was also reported by Nichols et al. [26]. Using X-ray Photoelectron Spectroscopy (XPS) they measured the Ca/Si peak ratio and showed that the calcium concentration at the surface was lower than the bulk value. In addition, they heat treated E-glass fibre samples for 3 hours at temperatures up to 720 °C and found that the surface concentration of Ca increased, suggesting that diffusion to the surface occurred during thermal treatment. Similar results – of a silicon- and oxygen-rich and calcium-depleted surface – have also been reported by Wang et al. [27] but using thin glass slides of E-glass composition rather than fibres directly. The results of Wesson et al. [20] conflict somewhat with the aforementioned studies, as

they suggest an E-glass fibre surface which has lower concentration of oxygen than the bulk and is comparatively enriched with Ca and Al. Nonetheless, the suggested aluminium surface enrichment is in agreement with the finding by Wong [24]. It is clear from these various studies that investigation of the E-glass surface is particularly difficult and reproduction of results can be challenging. Studies using plate-glass of E-glass composition, rather than fibre, can simplify measurements due to their flat surface but they cannot be assumed to be analogous to E-glass fibres in their chemical molecular structure [28].

2.1.4 Interaction with water

2.1.4.1 Effect on tensile strength of fibres

From the moment they are drawn, the strength of glass fibres begins a downwards trajectory. At the first instant a fibre will be at close to the intrinsic strength (Section 2.2.1) associated with the formulation it is manufactured from, but exposure to both mechanical and chemical attack causes a decrease in tensile strength over time. The effect of atmospheric moisture on the development of E-glass fibre strength was investigated by Martin et al. [29] using freshly drawn fibres aged in controlled relative humidity. Exposure to moisture caused a decrease in strength with time; the authors postulated that this was related to an increase in the surface area of so-called macropores, which they defined as pores with a radius $r_p > 10$ nm.

In the literature the reduction in strength of glasses exposed to water has been a field of research in and of itself for a long time, primarily because the effect is so clear but the exact explanation of the mechanism responsible is a challenging research question. To simplify the problem analyses have focussed on pure silica which, due to the nature of E-glass fibres and particularly their surface (Section 2.1.3.2), remains pertinent in this discussion. Fatigue behaviour of glasses, including silica, under a constant tensile load and exposed to moisture or liquid water is a known phenomenon [30]. In glasses already containing surface cracks a process of crack growth occurs, ultimately leading to failure when it reaches the critical dimension. The general term for this mechanism is stress corrosion, and numerous different explanations for what it entails at a fundamental level have been proposed in the literature. Orowan [31] proposed a decrease in the surface energy of cracks facilitated by water. More involved models have also been suggested. One such

model is based on the dissolution of silica by water, leading to the breaking of Si-O-Si bonds in the vicinity of the crack tip. An investigation by Ito and Tomozawa [32] showed that dissolution of a silica sample increased with increasing hydrostatic pressure. Expanding on this, Tomozawa [33] commented that the glass volume too increases with higher values of hydrostatic pressure and compressive stress. This result suggests that the opposite would be expected in a sample subjected to tensile stress; in other words the application of tensile stress would reduce dissolution, rendering it an unlikely explanation for the stress corrosion reaction. Some additional evidence to this conclusion was also provided [34] using glasses with different fictive temperatures. The Si-O-Si bond angle in samples was varied by controlling fictive temperature and dissolution measured. Glasses with smaller Si-O-Si bond angle had a higher dissolution rate; Tomozawa reasoned that as tensile stress would tend to increase this bond angle this was further evidence that dissolution was not a satisfactory explanation for stress corrosion.

Another model published by Michalske and Freiman [35, 36], which could be termed hydrolysis, outlined a three-stage reaction whereby a water molecule could break a siloxane bond leaving two silanols behind. They suggested that this reaction was possible with water due to its structure; proton-donor sites at one end of the molecule and lone-pair orbitals at the other. Evidence of corrosion reactions using other molecules of similar structure was presented. Further results [37] led Michalske and Bunker to conclude that the strain of Si-O-Si bonds was also an important parameter: the hydrolysis rate of bonds with a smaller angle was more rapid because they were in a more strained state. In a review Tomozawa [33], however, interpreted this differently. He reasoned that the Si-O-Si bond angle decreases in tandem with a volume reduction, and this reduction is also associated with hydrostatic pressure or compressive stress – contrary to the stress corrosion reaction which is enhanced by tensile stress.

Instead of dissolution or hydrolysis, a diffusion model is suggested. Diffusion of water into silica was shown to be increased by application of tensile stress and retarded by compressive stress or hydrostatic pressure [38]. This diffusion was followed by a relaxation of the glass (particularly of surface over the bulk [39]) which could be interpreted as the stress corrosion reaction.

Whatever the mechanism causing glass stress corrosion, with respect to glass fibre it is most influential during the early stages of aging, immediately following fibre

forming. Unless working with laboratory-drawn glass fibres that are thereafter handled under very careful conditions, all fibres are subsequently exposed to various processes which are mechanically damaging. The effect of such processes causes further degradation of the fibre strength. When working with bare fibre produced on a commercial fibre bushing, as this project does, a significant degree of fibre damage from both moisture [29] and mechanical sources has occurred before any experiments using the material have been carried out. The tensile strength of the fibres tends to be stable over time. However, as outlined in Section 2.1.4.2, water remains on the surface of fibres. There may no longer be a stress corrosion reaction acting to further reduce the strength of the fibres, but the possible influence of this water during heat treatment is an area that has not been explored in the literature.

2.1.4.2 Adsorption of water on E-glass

The adsorption behaviour of water on E-glass has been investigated by various researchers. Akinc and Martin [40] used gravimetric methods to study fibres that they drew into a 'moist' laboratory air environment. Their results suggested a hydrophilic E-glass surface; BET water adsorption increased with increasing partial water vapour pressure. The adsorption kinetics over time showed that multi-layers of water formed over time. This idea of water multi-layer formation has been reported in other papers too [41, 42]. Carman and Pantano [41] presented results for water adsorption on fibres that were just drawn, compared with those that had first been aged in either moist air or water. These results showed that greater water adsorption occurred on fibres that had been aged in some way, suggesting that already adsorbed water molecules act as sites to promote further adsorption. They suggested multi-layer adsorption as a reasonable conclusion based also on the shape of adsorption isotherms observed which were similar to a Type II or Type III, i.e. monolayer then multi-layer. Additional results reported in this work suggested that the specific surface of E-glass fibres was changed by exposure to water; an increase in specific surface was found which they correlated with an increase in surface roughness or microporosity.

Multi-layer adsorption of water was reported by Nishioka and Schramke [42] based on evidence gathered using Temperature Programmed Desorption (TPD). They suggested that 3 layers of hydrogen-bonded water were present on the surface of E-

glass fibres, and that these were removed during the TPD process between temperatures of 55 – 200 °C.

2.1.5 Orientation of structure

2.1.5.1 Bulk structural orientation

The question of whether or not glass fibres possess an oriented structure – and, further, whether this may or may not help explain their superior strength compared to bulk glass – is one which has been investigated at length. However, before addressing the evidence and points of view it is important to first clarify what is meant by orientation of structure. Brannan [43] comments very succinctly on the matter. When molten glass is mixed prior to fibre drawing a perfectly homogenous melt should lead to the formation of homogeneous fibres. However, if any heterogeneities persist in the melt they will unavoidably be drawn out extremely long and thin along the length of the fibre. This is an orientation, but not of structure. An orientation of structure means that, on a molecular scale, the bonds within the material are formed with some preferential direction. In the case of glass fibre, if orientation were present, the assumption is that the 'strong' bonds would be along the longitudinal direction of the fibre.

Some evidence for the presence of oriented structure within glass fibre systems has been presented for the sodium metaphosphate system [44, 45]. Bartenev [46] reported that fibres of an alkali-silicate composition containing tin oxide were anisotropic while bulk glass of the same composition was isotropic in structure, following investigation by nuclear resonance. As per Stockhorst and Brückner [47], he also suggested the concept of an oriented fibre surface with isotropic bulk structure.

In the 1950's Otto and Preston [48] concluded that E-glass fibres are isotropic in structure based on measurements of density and length change (contraction) of fibres under elevated temperature. Their calculations based on this work suggested an equal contraction of the fibre in both longitudinal and transverse directions. They further argued against the theory that, rather than of structure, an orientation of Griffith flaws caused the high longitudinal strength of the fibres after comparing the breaking stresses of fibres in both tension and torsion. Brannan [43] added to the argument against orientation by measurements of Poisson's ratio; these showed

that single glass fibres had identical Poisson's ratio in their untreated state and following a 2.5 hour treatment at 510 °C. Later, further comparison of fibre failure in tension and torsion by Kroenke [49] led him to agree with Otto and Preston's conclusion that – due to their isotropy of mechanical strength – glass fibres are likely to possess an isotropic molecular structure.

2.1.5.2 Anisotropy orientation and birefringence

A reasonable volume of evidence, largely collected using mechanical methods, suggests that the structure of E-glass fibres is isotropic. There is, however, a separate discussion regarding a different type of orientation in glass fibre. In the literature this may be referred to as axial or optical anisotropy and it is quantified by measuring birefringence. If a material is birefringent its refractive index is different depending on the polarisation or direction of light passing through it. This property is imparted to glass fibres due to straining during the fibre drawing process [50]. Stockhorst and Brückner [47] measured birefringence (Δn) of E-glass fibre bundles drawn from a constant melt, but varied production parameters such as nozzle temperature, drawing speed and drawing force. The birefringence of fibres was shown to increase with increasing drawing speed and drawing force. For a constant birefringence, fibres drawn from a hotter nozzle required a smaller stress but, conversely, a greater drawing speed. From a structural point of view the authors suggest that the glass melt structure is more "open" after flow through the nozzle, and a higher nozzle temperature leads to a more open structure. It is therefore easier to deform and polarise which is why the birefringence is higher at constant axial pulling stress for higher nozzle temperatures. It is noted by the authors that their results indicate that glass fibres consist of two "portions" – an isotropic one due to thermal history and quenching of the melt (as discussed Section 2.1.5.1), and an anisotropic portion in the fibre longitudinal direction due to the drawing stress. Birefringence of E-glass fibres has been confirmed by numerous other researchers [51–53].

A link between orientation of anisotropy of E-glass fibre was investigated [51] using bare fibres that were formed using a range of drawing stress. The strengths of continuous fibres were shown to be higher than those of both the bulk glass and (E-glass) spun wool fibres, whose axial drawing stress was estimated to be around 1 MPa. However, continuous E-glass fibres drawn with stress between 10 – 70 MPa

showed no significant difference in their average tensile strengths all of which were in the range 2.5 – 3 GPa.

2.2 Strength of glass fibre

2.2.1 Types of strength

The theoretical maximum strength of glass has been calculated by various researchers, as summarised by Sugarman [54], to within a range between 10 – 30 GPa. Experimental values approaching this range are not possible in reality even when dealing with strong glass fibres; bulk glasses perform even worse with strengths in excess of 50 MPa seldom achieved. Theoretical strength is not of interest in this work; rather when discussing the strength of glass fibres it is crucial to make the distinction between the intrinsic and extrinsic strengths.

It is common knowledge that the range of strengths that may be measured for glass is vast, from very weak massive glass to high-strength fibres. However, it is possible in the context of glass fibres that, for a given composition, there is a maximum *intrinsic* strength that is measureable. Early research using E-glass fibre [5, 55] showed that very high values of strength (greater than 3.5 GPa) were achievable. These values were also repeatable with a low coefficient of variation. To achieve such results it was necessary for the experimenters to carefully control the manufacture and testing procedure to eliminate sources of damage to the fibre. Thomas, for example, only took fibre samples from between the bushing and winding drum, and went to great lengths to avoid the occurrence of any contact between the fibre surface and any other surfaces. In this way he measured the intrinsic strength for the particular glass composition and testing conditions utilised.

Extrinsic strength is controlled by the presence of flaws, and their severity. This general term ‘flaws’ may refer to numerous features such as surface scratches and cracks, devitrified regions or unintended inclusions in the bulk material (flaws affecting intrinsic strength may also be discussed: in such cases this refers to molecular-level defects such as substitutional or interstitial impurities, dislocations etc.). Unlike intrinsic strength, extrinsic strength is therefore dependent on both the diameter and length of a tested fibre sample. It is this type of strength that is of

interest in any practical applications, and indeed in the scope of the research work presented herein.

In addition to intrinsic and extrinsic strengths, the difference between inert and fatigue strength must also be addressed. Gupta [56] describes inert strength as that measured in the absence of fatigue. The most proven method of doing so is by performing tensile tests at liquid nitrogen temperature where the rate of the fatigue reaction may be neglected. Conversely fatigue strength is measured at a higher temperature (room temperature for example) and at some known level of humidity. A constant and moderate strain rate should be used.

The phenomenon of fatigue is induced by the presence of stress and by environmental conditions such as moisture and temperature, becoming generally more severe as their respective magnitudes increase. Extrinsic fatigue strength is complicated: humidity, temperature, geometry of (and stress at) the crack tip all affect it. Despite these complexities, established empirical models exist for the description of slow crack growth, as summarised by Gupta [56]. The type of strength measured in this body of work is extrinsic fatigue strength: however the intricacies of the fatigue model are not the subject of study of this work and thus are not covered here.

2.2.2 Flaw theory

In the discussion of extrinsic failure of glass fibre, flaws are the features of key importance – specifically cracks. A theoretical crack is a 2-dimensional flaw across whose boundary the atomic bonds of the material are broken. Around this flaw stress will be concentrated at the crack tip, which is assumed to be infinitely sharp (although in reality it must have atomistic dimensions). Cracks are considered the most important type of flaw as only they can grow under the application of tensile stress [56].

The issue with the above-mentioned infinitely sharp crack tip is that when considering a highly brittle material like glass (where no crack tip blunting occurs) any externally applied stress immediately translates to an infinitely concentrated stress at the crack tip. In reality this makes no sense as it would suggest the material would fail almost immediately under any load. The seminal work of Griffith

[11] addressed this mathematical issue by considering the problem using a different approach – the energy balance.

If one considers a uni-axially stressed plate with an edge crack (shown in Figure 2-2) some equations regarding energy can be given.

The strain energy – that which is stored in the body due to deformation – can be stated as;

$$U_0 = \int \sigma d\varepsilon \tag{2.1}$$

For glass, the linear constitutive equation σ = Eε holds, thus:

$$U_0 = \int E\varepsilon d\varepsilon = \frac{E\varepsilon^2}{2} = \frac{\sigma^2}{2E} \tag{2.2}$$

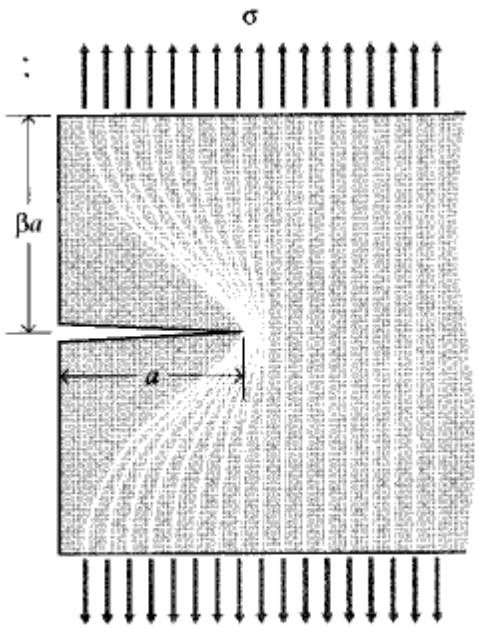

Figure 2-2: Uni-axially stressed plate with edge crack, taken from [57]

Taking the plane stress loading case, and given a unit distance perpendicular to the x-y plane, we can equate the parameter β=π. The strain energy released due to a crack of length 'a' is represented in Figure 2-2 by the two unloaded triangular regions on either side of the crack. Mathematically the expression for this released strain energy is;

$$U = -\frac{\sigma^2}{2E}\pi a^2 \tag{2.3}$$

Simultaneously, the formation of the 2 new surfaces of the crack has an associated required energy input – the surface energy.

$$S = 2\gamma a \tag{2.4}$$

In (2.4) γ is the material surface energy in J/m^2. A balance between these two energies describes how the crack will behave with growing length (and also with changes in stress, but it is assumed here that it is fixed). The effect of increasing 'a' is shown in Figure 2-3.

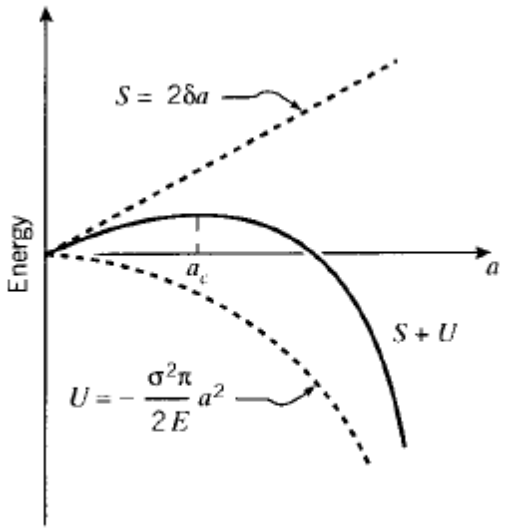

Figure 2-3: Energy balance for fracture with increasing crack length 'a', taken from [57]

The linear dependence of surface energy is dominated by the quadratic equation of strain energy release beyond a critical crack length a_c. In practice when a crack of length $a>a_c$ is present sudden failure will occur, but below this critical length, an externally applied stress is needed to grow the crack length.

From Figure 2-3 it is clear that differentiation of the sum of the two energies can provide information about failure stress, σ_f, as the sudden failure region begins at the turning point a_c.

$$\frac{\partial(S+U)}{\partial a} = 2\gamma - \frac{\sigma_f^2}{E}\pi a = 0$$

Rearranged gives;

$$\sigma_f = \sqrt{\frac{2E\gamma}{\pi a}} \tag{2.5}$$

Although very simple, (2.5) can be acceptably used to describe the behaviour of glass due to its highly brittle nature. In materials with greater ductility a proportion of the released strain energy is dissipated around the crack tip due to plastic flow in the material.

A further mathematical modification to (2.5) comes in the form of the Griffith-Orowan-Irwin Equation (2.6).

$$a = Y^2 \frac{E\gamma}{\sigma^2} \tag{2.6}$$

In the form presented, (2.6) may be used to calculate the dimension ‘a’ of some surface or volume flaw with circular or elliptical shape. Proper use of the equation however demands knowledge of the general dimensions of this flaw by some method (such as observation) so that the correct value of the geometric constant Y is chosen. Some values of parameter Y may be obtained in ASTM C1322-05b [58].

2.2.3 Flaw visualisation

Despite countless mentions in the literature, micro or nano dimensioned flaws have never been visualised in an un-fractured glass fibre. Lund and Yue [59] have attempted to systematically correlate strength levels of fibres with flaw types by fractographic analysis of single fibre fracture surfaces. However this is still an area where there remains work to be done.

2.3 Strength loss of heat treated glass fibre

2.3.1 Temperature and time effects

Investigations into the combined effect of temperature and time on the room temperature strength of glass fibre began a number of decades ago. Sakka [4] was one of the very first to report results on a laboratory-produced fibre with high silicon, boron, sodium and potassium oxides content. Fibres were heated for one hour, cooled in air to room temperature then tensile tested. The results showed that for the fibre composition used heat treatment beyond 200°C led to a significant and mostly linear drop in retained strength.

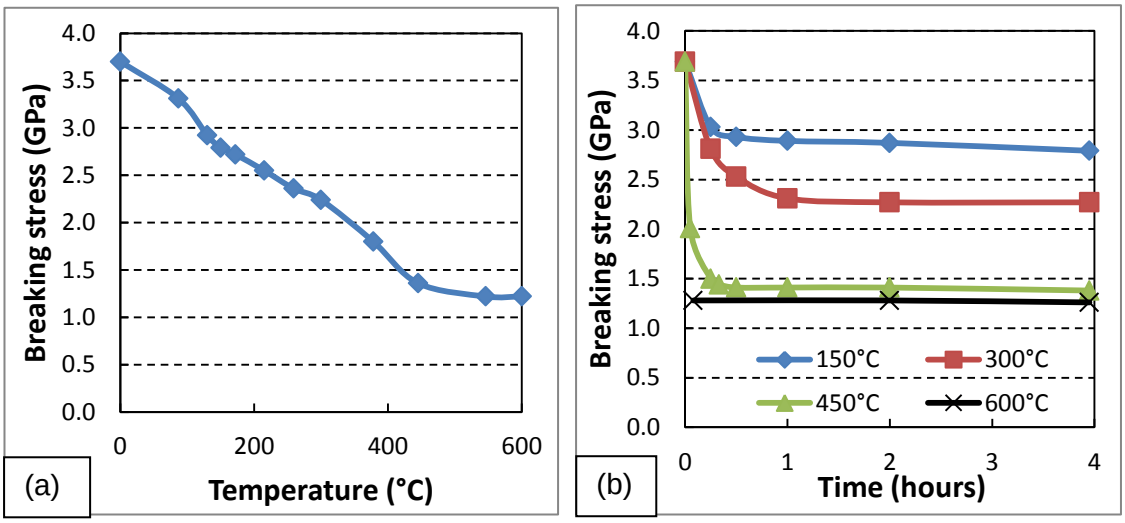

Figure 2-4: Results on single fibre tensile strength of heat treatments on E-glass fibres, reproduced from Thomas [5]

In the UK, Thomas [5] took a systematic approach to both the manufacture and testing of E-glass fibres. In one experiment he measured the effect of a 4 hour heat treatment procedure at a selection of temperatures between approximately 100 – 600°C. A fairly consistent decrease in strength was shown, with a suggestion that the slope becomes steeper between 300 – 400 °C (Figure 2-4a). More than a 60% loss compared to the strength of virgin fibre was found when treating beyond 400°C. Additionally, further work suggested that strength loss proceeds with length of furnace soak time until a constant minimum value is reached, but at higher conditioning temperatures this minimum value is reached within a very short time (Figure 2-4b). Small sample sizes in these experiments prevented statistically significant conclusions from being drawn but the trends observed were further researched.

Cameron, also working with E-glass fibres, presented curves showing the strength of heat treated fibres asymptotically approaching a minimum value with time [55]. Similar to the phenomenon shown by Thomas the minimum value of retained strength decreased with increasing treatment temperature. Cameron did not utilise such high temperatures – at the highest of 273°C he presented strength loss of anywhere between 25 – 40%. For a similar 4 hour treatment Thomas also measured a 40% strength loss.

In a further piece of work [60] Cameron showed that when working with production E-glass fibres (rather than pristine fibre) the effect of heat treatment on room temperature strength was equally significant. Using heating times of 40-60 minutes he measured approximately a 50% drop in strength after conditioning at around 300°C. In addition, during this work Cameron heated in atmospheres with greatly varying levels of contamination, but found this had no effect on these non-pristine fibres (which could be safely assumed to have incurred some damage since production).

Other early research – while not directly comparable to that mentioned above – added to the body of evidence regarding time and temperature effects. Examples include the work of Brearley and Holloway [61] on soda-lime-silica glass rods or Piggott and Yokom's [62] study of fine silica fibres. Similarly, the work of Aslanova [63] showed the weakening effect of time and temperatures of up to 600°C on several types of glass fibres.

More recently Dorzhiev et al. [64], working with high-strength Magnesium Aluminosilicate fibre, conducted heat treatments for 5 hours in the temperature range 100-700°C. Upon tensile testing they found very little loss of strength in samples treated at 350°C and below. Beyond this temperature, however, some threshold was crossed and a rapid deterioration in strength was observed, progressing to a maximum loss of 75% of the initial untreated value. Similar experimental data on E-glass fibre, fitted with curves, have also been reported by Feih et al. [65]. The strength loss curves reported by Feih et al. are particularly interesting; the trends in strength loss with coupled temperature and time are remarkably similar to those produced by Thomas [5]. The differences in material used between these two investigations are, however, significant. Although both E-glass, in Thomas' research the fibres were bare and, due to the method of production, exhibited an untreated strength close to the magnitude of the intrinsic

strength of the glass. Conversely, in the investigation by Feih et al. the fibres were commercially produced and coated with an industrial silane-based sizing.

Fibre tensile strength data for unsized heat treated fibre tend to be quite rare in the recent literature. Some findings were reported in [51] for laboratory produced E-glass; the nature of these samples meant that the room temperature strength of untreated fibre was very high at approximately 3 GPa. Interestingly and, despite performing long 3 hour heat treatments, no significant strength loss was reported until a temperature in excess of 300 °C was used. Rigorous explanations for the physical change(s) in glass fibres that can account for the strength loss measured are often absent. The same might be said about this work, but some interesting observations may be made based on the measurements of enthalpy (2.4.1) and anisotropy (2.4.2) relaxation that are reported alongside the tensile strength data. Firstly, the critical temperature above which strength loss and relaxation of enthalpy both begin to occur is around 300 °C. Secondly, however, some links might be drawn between heat treated fibre strength and anisotropy relaxation. The same E-glass formulation was used to produce both standard drawn fibres and a spun wool fibre (SWF), the production of which is described in [66]: without fully detailing the SWF production process it is important to note that it is less controlled than fibre drawing, which could allow greater fibre surface damage to occur . These E-glass spun wool fibres produced with minimal axial stress, and hence very low anisotropy, had a measured tensile strength of approximately 1.5 GPa. The anisotropy of continuous E-glass fibres was found to decay to approaching zero after treating at 500 °C for 3 hours; this treatment also caused a decrease in strength from around 3 to 1.5 GPa. Taken individually, either of these correlations could be used to postulate that either:

i. Strength loss is related to enthalpy relaxation, or
ii. Strength loss is related to anisotropy relaxation (neglecting the possibility that greater fibre damage during production, rather than low anisotropy, explains the lower strength of untreated SWF).

The authors themselves do not claim causation with respect to either of these observations of fibre relaxation. Heat treated fibres are still brittle materials and as such their fracture is tied to the existence of critical surface flaws or cracks. Whether relaxation of either enthalpy or anisotropy could affect this fracture behaviour is not definitively understood.

2.3.2 Temperature and mechanical damage

In contrast to these tightly controlled laboratory experiments discussed in Section 2.3.1, Kennerley et al. [67] showed tentative results for single glass fibres recovered from both heat-cleaned cloth and composites processed in their Fluidized Bed Combustion (FBC) rig. Although some of the average values reported were based on far smaller sample sizes than preferable for brittle glass, the inverse relationship between retained strength and temperature was observed. Crucially, in this work fibres were exposed to elevated temperatures for short times (20 minutes or less) yet significant strength loss was still measured. In the case of fibres that were FBC processed at 650°C only 5% of the measured virgin strength remained. Extreme mechanical damage was reported as the most likely cause for this very low strength retention.

2.3.3 The effect of heating atmosphere

The reduction of room temperature strength of glass fibre following treatment at elevated temperature is well established, and has been for decades. The effect of the atmosphere in which heating was conducted was also considered and this variable was studied in detail by Cameron during the 1960s. Some of his early thesis work [6] tentatively suggested that there was no difference between the retained strengths of E-glass when heating was performed under either air or argon. Later, though, he reported data comparing heating in an oven with vents closed (to air particle contamination) or open [55]. Some of these results seemed to show that after lengthy heating times (greater than 10 hours) more strength was retained in fibres heated in the ‘vents closed’ furnace. A possible explanation of dust particle contamination being a strength-reducing factor, also postulated by Brearley and Holloway [61], was later shown to be unlikely by Cameron himself [60] when he performed shorter duration heat treatments on E-glass under either laboratory air or argon with a very high purity (and exceptional dryness). Up to a temperature of 300 °C no significant differences in retained strength were measured between the two atmospheres.

Modern reinvestigation of the heating atmosphere effect has generally yielded similar negative conclusions about this effect. In work on spun basaltic wool fibres

(discontinuous-at-formation vitreous fibres, with a composition as presented in Table 2-4) Lund and Yue [51] found no difference in the retained strength of fibres heat treated for 3 hours in either air or nitrogen. Feih et al. [65], in work using silane coated E-glass, similarly reported no difference between treatment in ambient air or nitrogen in most cases. However, when heat treating fibre at 450 °C for only 30 minutes they observed greater strength retention when using a nitrogen atmosphere compared to both dry and ambient air (which showed no difference between themselves).

Table 2-4: Composition by weight of spun basaltic wool fibres (SWFs) as reported by Lund and Yue [51]

Oxide	**SiO_2**	**Al_2O_3**	**TiO_2**	**FeO**	**Fe_2O_3**	**CaO**	**MgO**	**Na_2O**	**K_2O**
Wt %	47.1	15.3	1.6	9.1	2.1	7.3	7.2	3.6	0.9

It appears from this body of research that – for uncoated fibres – neither dust contamination nor atmospheric moisture attack during heat treatment can be effectively used to explain the strength loss measured in glass fibres. What is less certain is what happens when a protective layer of surface coating has been applied to the fibre (be it silane based or other). The data of Feih et al. [65] suggest that over shorter time-scales (those of interest when considering recycling applications) an unreactive nitrogen atmosphere may lead to greater fibre strength retention. One of the possible mechanisms suggested is a reduction of degradation of the organic sizing material, and indeed in the same work a TGA comparison using both nitrogen and air shows a small but measureable difference, with less mass lost above 300 °C under the nitrogen atmosphere.

2.3.4 The effect of heat treatment under tensile stress

The effect of temperature, time and heating atmosphere on the strength of glass fibre in a stress-free state has been outlined above. A far less often investigated phenomenon, however, is the effect of heating fibres while under some induced tensile stress.

Bartenev and Motorina [68] published some early results on fine glass fibres of both alkaline and non-alkaline compositions. Of particular interest are the outcomes of

the tests on the alkaline fibres as these were benchmarked against values for fibres that were heat treated in a stress free state. With a fairly low initial strength of little more than 1 GPa the authors presented a roughly linear decrease in strength with stress free heating. On the other hand, fibres heated under stress showed improved strength retention. With an application of load equalling 2% of ultimate strength a moderately higher strength was measured throughout the temperature range. Application of 70% of ultimate pre-stress, however, produced further improved results: up to 100% extra strength was retained when compared to the stress free heating values and, following the 100 °C treatment, an increase beyond the initial untreated room temperature value was reported.

Cameron also conducted some experiments on the heating of tensioned fibres, but working with largely flaw-free E-glass [55]. The difference in fibre condition – virgin versus the aged fibres of Bartenev and Motorina – has a significant effect on the strength values obtained. Cameron heat treated his fibre for 2 hours, stress-free and under a pre-load which he estimated to equal between 2-20% of the fibre's room temperature strength (in this case around 3.8 GPa). All heat treatment led to a decrease in retained room temperature strength. However, beyond 250°C, and particularly at the maximum investigated 450°C, there appeared to be a significant trend for the tensioned fibres to retain more strength than those that were conditioned stress-free. At most the difference appeared to be approximately 0.75 GPa.

In the discussion of results of both of these pieces of work the retarded weakening, or strengthening, effect was attributed to alterations to the geometry around cracks or flaws on the fibre surface. Bartenev and Motorina discussed elastic and plastic deformation, and Cameron 'inelastic flow', of material in the vicinity of cracks. In both cases they assumed that this stress-forced flow leads to a less critical crack geometry and hence reduced stress concentrations developed when tensile testing was conducted.

More recently, Lezzi et al. [69] reported on work using silica glass fibre, of approximate diameter 125 µm. Single fibres were loaded in tension at stresses of up to 60 % of the breaking stress value and, while in tension, treated for 60 seconds with a hot gas stream at temperatures between 100 – 500 °C. After heat treatment the fibres were unloaded and tensile tested at room temperature and humidity. They reported that fibres heat treated while under tension retained more strength than

those treated in a stress-free state. The degree of improvement of strength retention was related to the applied stress during the heat treatment. For example after 60 seconds at 500 °C in stress-free state the strength was approx. 1.3 GPa, but when a 1, 2 or 3 GPa applied stress was applied the retained strengths were 1.8, 2.5 and 3.5 GPa respectively. The explanation given for this phenomenon is that a thin residual compressive stress layer forms on the surface of fibres when they are heated under stress while exposed to water vapour. The investigation of this phenomenon was extended to E-glass [70]; 100 µm diameter fibres were conditioned under stress and humidity for various times. Stress was induced by placing fibres in a two-point bending configuration inside silica tubes and testing was correspondingly carried out using a two-point bending method. Holding fibres under bending loads of 1 and 2 GPa led to an increase in the failure strain of fibres beyond that of the as-received value. Again, the explanation given for this observed strength increase was surface residual stress formation by surface stress relaxation.

What implications this work may have for glass fibre recycling concerns is certainly unclear. The primary concern is that these experiments were all carried out using uncoated fibres – whereas in practical applications it is likely that some silane-based sizing (such as Aminopropyltriethoxysilane, abbreviated to APS) will be present on the fibre surface. It cannot be said for certain that physical cracks or flaws within the glass fibre surface are always the source of critical stress concentrations leading to failure of heat treated glass fibres – although it seems plausible that they may be. For example agglomerations of sizing or matrix material, or some foreign particles that have become bonded to the fibre surface, could act as sufficient stress raisers to cause fibre failure. Whether or not this further layer of complexity regarding the surface coating would affect the ameliorating conditioning-under-tension effect described is unknown.

2.4 Physical changes following heat treatment

The precise mechanism, or mechanisms, that contribute to the strength loss of heat treated glass fibre are not acceptably established in the literature. There are, however, changes that occur during heat treatment that have been established. In some cases these phenomena are well understood; in others observations are

reported but the explanations presented may require further study to fully justify them.

2.4.1 Thermal compaction or enthalpy relaxation

Physical changes occurring in heat treated glass fibre tend to be separated into two discussions; either of surface, or bulk, phenomena. One phenomenon which may be considered a bulk change is thermal compaction.

A volume of early work, concerning bulk changes in E-glass fibre, was conducted by Otto [71]. The phenomenon 'thermal compaction' was first noted by Otto and Preston [48] in 1950. Later, using very fine fibres (less than 10 µm) Otto applied various heating regimes and measured changes in properties. The main conclusion was that the previously observed densification process – which he called thermal compaction – occurred when heating was carried out using suitably high temperatures or long time scales. As might be expected thermal expansion occurred at lower temperatures (between room temperature and 300 °C); however beyond this temperature the phenomenon of thermal compaction (with associated length reduction) dominated over thermal expansion. Subsequently holding the fibre at around 500 °C caused a contraction to below the starting fibre length. Furthermore, under isothermal heating (see Figure 2-5) even a temperature as low as 300 °C led to measureable contraction in fibre length given sufficient time; the process occurring much quicker at higher temperatures. Alongside this compaction Otto also showed other bulk changes such as an increase in density and, indirectly, in Young's modulus. These property changes also related directly to heating temperature. Although other experimental results were not presented, the author noted that the phenomenon was not unique to this glass formulation and similar exploratory results were obtained for other glasses.

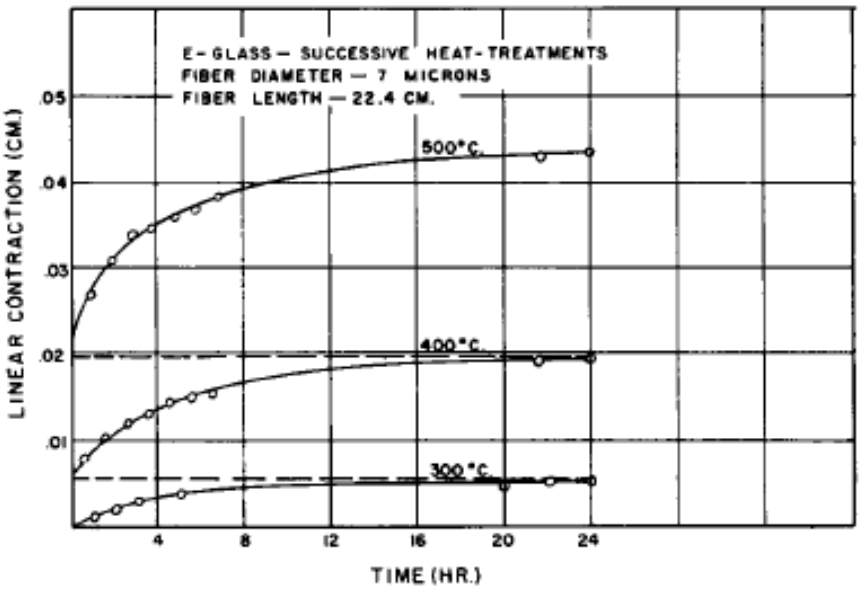

Figure 2-5: Result of isothermal heating on fibre length contraction with time, from Otto [71]

Aslanova et al. [72] published experimental data on glass fibres of numerous compositions and at many diameters, which were tested using a low frequency torsion pendulum under vacuum and over a range of temperatures. Changes with temperature in both internal friction and shear modulus were reported, and numerous explanations suggested for various observed effects. Particularly interesting comments on the behaviour of an aluminoborosilicate glass were made: with increasing temperature its relative shear modulus initially decreased but at around 300 °C a turning point occurred and it started to increase again. Exactly as Otto [71], they explained this effect as being due to compaction of the glass structure. They further stated that this can occur because of the relaxation of deformations within the fibre structure that are formed during drawing. Results showing contraction of fibres in both the longitudinal and radial directions have also been reported [47].

In some more recent studies [51, 52, 73–75] the relaxation of glass fibres was studied using Differential Scanning Calorimetry (DSC). The release of energy from fibre samples during temperature scans was measured over a wide range of times and temperatures. Different types of fibre were analysed within these various works, the most relevant of which for the purposes of this thesis were E-glass with a boron-containing composition [51, 52, 75]. Results for these, as well as calcium metaphosphate and basaltic fibres, demonstrate that heating close to, but below, T_g allows the release of what the authors term excess enthalpy from the fibres. The

phenomenon is thus called enthalpy relaxation. It is demonstrated [74] that the enthalpy relaxation is related to the quenching of the glass during its production; a larger amount of energy (excess enthalpy) is stored within the glass structure when quenching is performed at a higher cooling rate. The explanation offered for this phenomenon is a “cooperative rearrangement of the frozen-in isotropic network”. With respect to E-glass, this rearrangement occurs only once the heat treatment temperature surpasses around 300 °C and its rate increases significantly at higher temperatures.

Recent results published by Yang and Thomason [76] provided further evidence on this phenomenon by investigation of thermo-mechanical properties of single fibres. Single boron-free E-glass fibres were heat treated using a Thermo-Mechanical Analysis (TMA) machine; length changes were monitored and in-situ tests to measure the Young’s modulus of fibres were performed. The results agree with those obtained by DSC, as previously discussed [51, 52], and with those of Otto [71]. A small contraction in fibre length was found at an isothermal treatment of 300 °C but the effect was far more significant at higher temperatures (400 – 500 °C). Furthermore, the room temperature Young’s modulus of fibres was tested after isothermal heat treatments; an increase of almost 20 % compared to the original value was measured when treating to 600 °C. Once again, this effect initiated when a treatment temperature of approximately 300 °C or greater was used.

From the results of Otto [71] and Yang and Thomason [76] it is quite clear that thermal compaction of glass fibres occurs when they are heat treated above approximately 300 °C, and an effect of this is a corresponding increase in the room temperature Young’s modulus of the fibre. The temperature range over which this phenomenon acts agrees closely with that over which enthalpy relaxation of glass fibres by DSC has been shown in numerous works [51, 52, 73–75]. It seems reasonable to conclude that these works demonstrate the same phenomenon; the conclusions that long-range relaxation or reorganisation of the glass network is responsible appear justified. Although this is the case, an explanation of exactly what is happening within the fibre structure during the process has yet to be reported. A link between thermal compaction/enthalpy relaxation of fibres and the decrease in fibre tensile strength of heat treated fibre is also absent.

2.4.2 Anisotropy (birefringence) relaxation

Evidence for the presence of an axial anisotropy in fibres was presented in Section 2.1.5.2. This property is attributed to the fibre drawing process and is dependent on several parameters such as bushing nozzle temperature and drawing stress and speed. In many of the studies that have reported measurements of the birefringence of glass fibre, experiments were also conducted to analyse the effect of heat treatment [47, 51–53]. Lu et al. [53] suggested that anisotropy relaxation was temperature dependent; complete relaxation occurred if samples were heated to T_g but lower temperature annealing led to incomplete relaxation. Ya et al. [52] carried out birefringence measurements on E-glass after heat treating for various times over the range 300 – 550 °C. The anisotropy relaxation index, $\Delta n/\Delta n_{max}$, was introduced to describe the remaining anisotropy in a fibre sample ($\Delta n/\Delta n_{max}$ = 1 means zero relaxation has occurred). It was shown that a relatively low temperature treatment, 300 °C for 3 hours, was sufficient to reduce $\Delta n/\Delta n_{max}$ approx. 0.7. Full anisotropy relaxation was achieved when heating at 550 °C, or at a lower 400 °C but for a time of around 10 hours. Lund and Yue [51] reported further experiments using an identical glass composition. Their results showed anisotropy relaxation for a 3 hour treatment at as low as 200 °C; $\Delta n/\Delta n_{max}$ approached zero well below 500 °C. The differences between the two works are likely explained by the differences in fibre drawing temperature.

2.4.3 Crystallisation

Crystallisation of glass fibre has been proposed as the source of strength loss following heat treatment. Aslanova [63] reported on an electronographic study conducted using a non-alkaline glass fibre, in which the diffraction of slow moving electrons passing through the material was studied. In its standard form the glass fibre produced electronograms showing a weakly diffracted picture but after heating to 400 – 600 °C rings or points appeared in the pictures obtained. These are attributed to the growth of a modified form of cristobalite, with a tetragonal lattice. The levels of glass fibre crystallisation reported in this work do not seem to have been replicated since. However, a recent study of stone wool fibres [77] has shown evidence of a surface nano-crystallisation phenomenon. Whether these findings have relevance to the thermal recycling of E-glass fibres is unknown. There are

reasons to suppose that it may not: firstly nano-crystallisation was only observed after treatment times at close to the glass transition temperature (T_g). Secondly, and more crucially, the mechanism by which the process occurred relates to the significant iron oxide content of stone wool fibres. In the fibres, oxidisation of ferrous to ferric ions and the movement of electron holes caused a movement of divalent MgO towards the fibre surface. As E-glass contains zero to trace quantities of iron oxide, and small amounts of MgO (Table 2-1, Table 2-2), the same process would seem unlikely to be possible. Crystallisation of other glass systems (Na-Si, Si-B-Na-ZrO_2) has also been demonstrated [78, 79] but, once again, these findings followed heating of the samples for relatively long periods of around a day. Potential crystallisation of the E-glass system remains, to the author's knowledge, unexplored.

2.4.4 Ion exchange

In the literature, ion exchange is generally discussed (for example by Gy [80] and Varshneya [81]) as a method by which glasses may be strengthened – in a similar way to tempering. Unlike tempering, however, which is applicable to massive glass (with large internal stresses and potentially flaws on the millimetre scale) ion exchange can potentially deliver a strengthening effect to fine glass fibres.

When considering the movement of ions through the glass network, one must have an idea of the appearance of the network structure. In general terms, by its nature the structure is vitreous and disordered but the chemical makeup is important also. The composition of boron-free E-glass has been described previously (Table 2-2). The main component is silicon dioxide; however there are also significant concentrations of compounds whose metallic ions have valences of 2 or 3. In the glass network the Si-O bonds have the highest bond energy hence they are the strongest – the nature of the bond is more covalent (rather than ionic) compared to the other ion-oxygen bonds present. Kistler [82] suggests that the bonding of trivalent atoms (like aluminium, which is present) will be less strong but that those ions which are di- or monovalent are the most likely to be able diffuse through the glass network given the necessary potential to do so. The findings of Yue et al. [77] regarding magnesium oxide migration in SWFs would appear to be concurrent with this. Changes in surface concentrations of Mg, Al and Si following sub-T_g treatments

magnesium aluminosilicate fibres have been reported [64]. Some evidence suggests that a change in surface concentration of Ca occurs when E-glass fibre is heated close to the glass transition temperature [26].

In the context of this work the source of potential allowing diffusion is heat. In that case, the critical temperature is the annealing temperature T_{ann}, above which tempering of massive glass to remove internal stresses is carried out. Molecular diffusion may occur below this temperature assuming the straining temperature T_{strain} at least has been surpassed but the time taken will be greater. For boron-free E-glass these two temperatures can be given as approximately T_{ann} = 740°C and T_{strain} = 690°C (Table 2-3). Pugh et al. [83] reported that only monovalent alkali metal ions (K and Na) possessed any significant mobility through semiconductor fibres which were held at high temperatures for relatively long lengths of time. These heat treatments were far longer than both those typically employed in any recycling process, and the heat treatments used when studying E-glass fibre strength loss in this work. The case for ion migration in glass is clear; however it appears to be limited primarily to monovalent ions. Further, long heating times at temperatures approaching T_g appear to be required. In the context of strength loss of E-glass fibre – with its very low content of monovalent ions – diffusion would seem a less likely candidate to play a significant role. Even once very high temperatures are reached there are most likely a combination of effects at play – ion diffusion may play a part then in strength loss but it is not known what the dominant effect might be.

2.5 Silanes and sizings

Any discussion of glass fibre necessitates a discussion of surface coatings or sizings. Glass fibre sizings generally consist of a water-based formulation containing a film former, a silane coupling agent and some additional auxiliary components [84]. The reasons for applying coatings to glass fibres are numerous; examples include surface protection against both contact and the ingress of water, to reduce fibre damage, to eliminate the occurrence of static and, finally, to enhance coupling with composite matrix materials [85]. The most common industrially used coupling components in fibre sizings are silanes. Coating is applied immediately following fibre formation, as it is pulled from the bushing but before it is gathered into a strand (Figure 2-6).

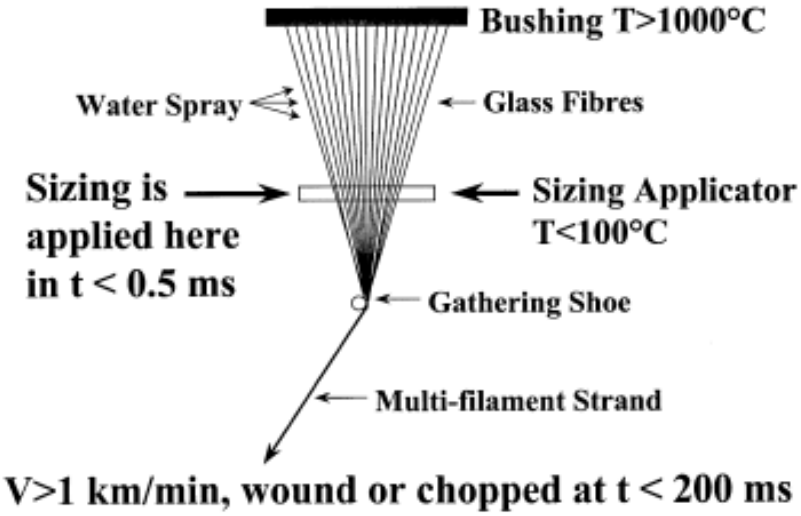

Figure 2-6: Representation of the sizing process applied to continuously formed glass fibre (from [86])

The term silane technically refers to saturated molecules (single bonds only) comprising only silicon and hydrogen atoms, the simplest of which is monosilane (SiH_4). In the context of fibre composites, silane is used as a shorthand for organo-silane. An organo-silane is a molecule made from a silicon compound which contains both organic and inorganic reactive groups and so can function as a coupling agent [87]. The general structure of the silane is [X-Si$(OR)_3$]. R is a hydrolysable group, often methyl (CH_3) or ethyl group (C_2H_5). X refers to a functional group which is generally selected to react with a desired matrix material; typically for glass fibre sizing applications one of just a few silanes will be selected [88]. The most widely used silanes are aminosilanes [85] due to a suitability for use with both thermoplastics and some thermosetting plastics. The aminosilane most relevant to the work presented in this thesis is γ-Aminopropyltriethoxysilane (γ-APS). As shown in Figure 2-7 the unhydrolysed monomer of γ-APS has 3 hydrolysable ethyl groups and one propyl chain which terminates with an amine (respectively R and X in general silane notation).

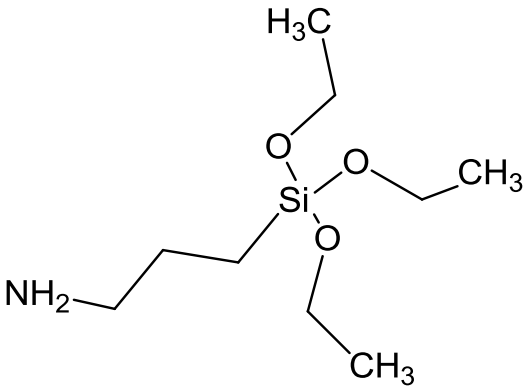

Figure 2-7: γ-aminopropyltriethoxysilane molecule

2.5.1 Bonding of silanes to hydroxylated surfaces

To bond γ-APS, or any silane, to a glass substrate the monomers must first be mixed in an aqueous solution in which a stepwise hydrolysis may occur, yielding the corresponding silanol. Following this a condensation reaction between silanols produces siloxanes; this is shown in Figure 2-8.

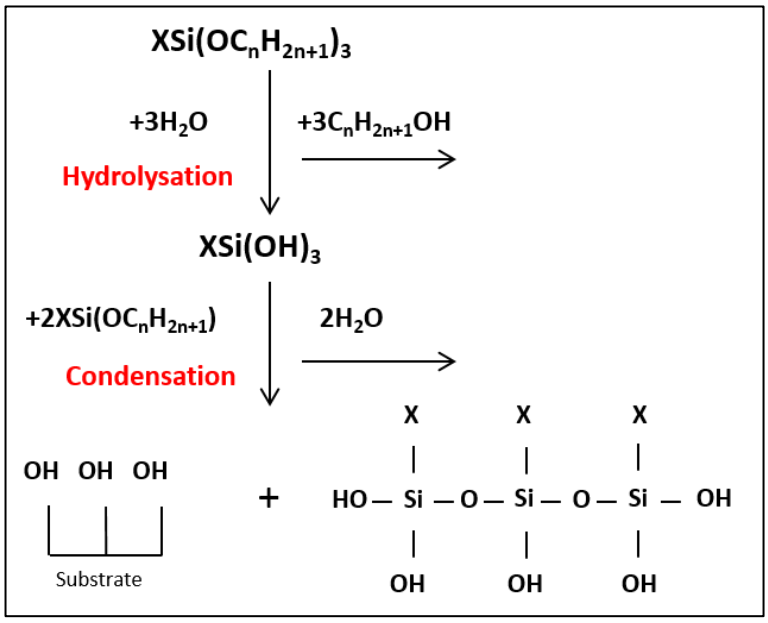

Figure 2-8: Hydrolysation and condensation processes of alkoxysilanes [89]

Once the hydrolysation and self-condensation reactions have taken place, the final step is a reaction between the remaining OH groups of the siloxane and those present on the surface of the substrate. This stage of the silane attachment process is shown in Figure 2-9; in this way a covalently bonded structure is formed.

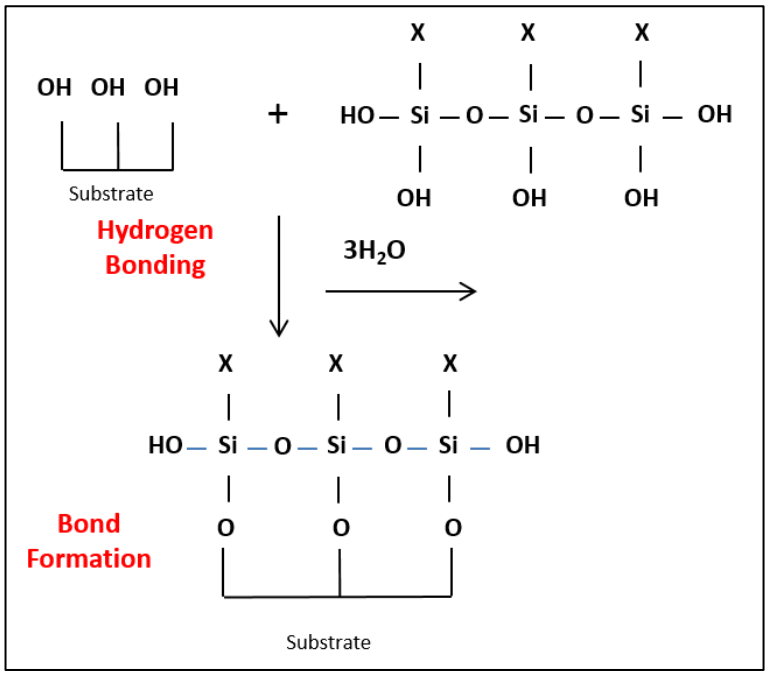

Figure 2-9: Reaction between self-condensed alkoxysilane and substrate surface [89]

In this simplified reaction model a monolayer of silane is bonded to the substrate surface. All of the functional groups X face outwards and would appear available for reaction with the matrix material. The reality of the reaction between organo-silanes and surfaces is, however, not as simple as depicted. A body of evidence against this simple model has been presented using aminosilanes and hydroxylated surfaces. It has been shown that amines are capable of forming strong hydrogen bonds with surface silanol groups [90], albeit with silica and triethylamine rather than glass and γ-APS. It was also demonstrated by Fowkes et al. [28] by XPS of γ-APS on E-glass fibre that the nitrogen in the first few nanometres was present in both a protonated and non-protonated form. From this they determined that the amine groups of the sizing were involved in bonding activity. Bellman et al. [91] also refer to the model reaction of γ-APS with a hydrolysed surface and they too note that this reaction may be influenced by numerous parameters which may prevent the functional amine groups being available at the surface for further reaction. In their work using streaming potential method they qualitatively analysed adsorption of γ-APS onto E-glass fibre surfaces, using detection of amino groups as evidence that adsorption had occurred.

Evidence against the existence of only a monolayer of γ-APS on E-glass surfaces was reported by Wang et al. and Liu et al. [27, 92]. Instead a three-dimensional graded network on the surface was proposed Figure 2-10, consisting of:

i. Interface: a chemisorbed surface layer that is resistant to hydrolysis, which is bonded primarily by Si-O-Si linkages
ii. Silane network: a chemisorbed three-dimensional layer of polysiloxane
iii. Silane oligomers: a physisorbed layer of γ-APS oligomers

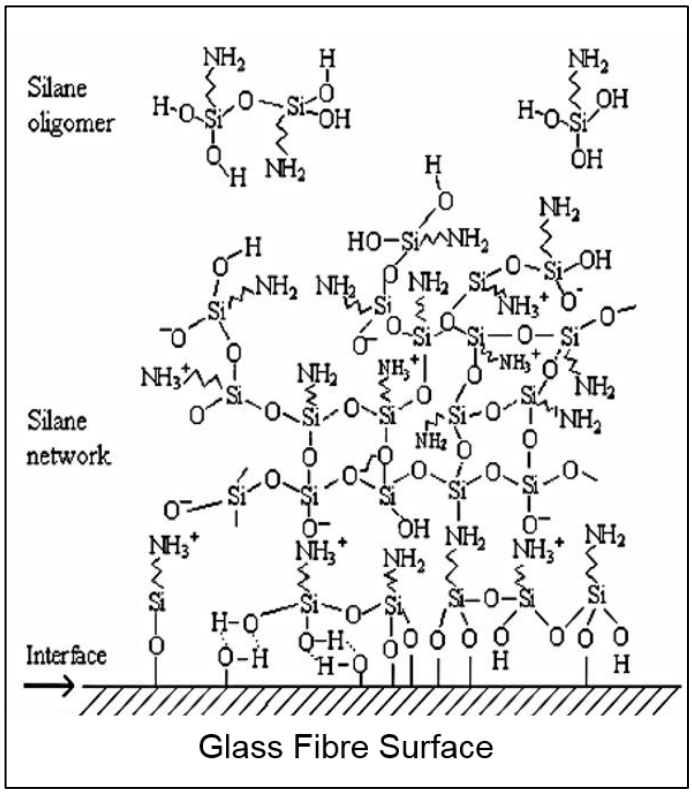

Figure 2-10: Chemical structure of hydrolysed γ-APS on glass fibre surface [92]

2.5.2 Effect of silanes and sizings on glass fibre strength

Glass fibre sizings are generally designed and applied with the intention of improving the ability to transfer stress across the interphase between fibre and matrix in some composite part that is to be produced. Also of great importance, however, is the capability of the sizing to protect the surface of the glass fibre so that it maintains the highest possible level of strength. As discussed in Section 2.1.4.1, the strength of glass fibres begins a downward spiral from the moment of drawing and this can generally be attributed to exposure of the fibre surface to moisture and mechanically aggressive processing. The application of an effective silane based sizing should therefore protect the fibre against these processes, from the instant they are applied and over time thereafter. The chemistry of the bonding reaction

discussed in Section 2.5.1 is important as the speed and simplicity with which the silane can attach to the surface and form a siloxane network will affect the potential for strength retention of fibres. In addition to protecting against the negative effects of moisture and mechanical damage, it has been suggested that silanes have the ability to heal fibre surface flaws, alleviating their negative effect on the fibre strength [85, 93–95]. A study by Zinck et al. [94] also suggested the possibility that adsorption of silane coupling agents on surfaces of already processed fibres could increase their strength, by a mechanism in which flaws of a critical size were healed.

2.5.3 Temperature degradation of silane based surface coating

In any glass fibre composite recycling process, relatively high temperatures will be involved, in order that the plastic matrix material may be removed, and these must be similarly replicated when carrying out controlled heat treatment of fibres. As an example Kennerley et al.'s Fluidised Bed Combustion process was operated at temperatures upward of 450 °C [67]. As a result the reinforcement is also exposed to an elevated temperature which will cause a corresponding loss of tensile strength (Section 2.3.1). Of equal interest is the effect of increasing temperature on the behaviour of silane-based sizings. In its pure form γ-APS has an atmospheric boiling point of 217 °C so volatilisation could potentially occur well within the range of thermal recycling temperatures. When a sizing is bonded to some substrate, however, the thermal behaviour will be more complex. Tiefenthaler and Urban [96] coated Nextel ceramic fibres with various different silanes. Mats of heat-cleaned cloth were coated and dried, then exposed to one hour of furnace heating at different temperatures. Their PA-FTIR study measured relative changes in intensity of the C-H stretching band as a method of analysing sizing loss. Consequently, their results were descriptive only of the degradation of the organic propyl chain of the γ-APS coupling agent. They showed by this method that, following a 200 °C treatment, almost 50 % of propyl chains were removed and by 300 °C none at all were detected. Feih et al. [65] presented data for E-glass fibres sized with a thermoset compatible sizing. Using Thermo Gravimetric Analysis (TGA) in air at 10 °C/min they measured a total mass loss of 0.5 % by 500 °C with the majority of mass loss occurring between 250 – 450 °C. Their results also showed that TGA under a pure nitrogen atmosphere caused slightly less weight loss than air. When analysing the strength loss of heat treated or recycled glass fibres upon which a

silane coupling agent or full sizing was present, it is necessary to consider the effect of the degradation of this coating as well as any changes in the glass fibre itself that may contribute to strength loss.

Chapter 3. Experimental

3.1 Materials

Boron-free E-glass (Advantex) fibres supplied by Owens Corning Vetrotex were investigated in this project. All fibre rovings were produced on the same pilot scale bushing and were received as 20 kg continuous single-end square edge packages. The rovings had a nominal tex of 1200 g/km and a nominal average single-fibre diameter of 17 µm. No sizing was applied to the bare fibres which had only been water sprayed using the normal cooling sprays under the bushing; these samples are referred to as water sized, unsized or bare (since it can be assumed that most water is removed during the subsequent drying step). Immediately following an identical cooling step by water spraying, the sized fibres were coated with a normal rotating cylinder sizing applicator containing a 1 % γ -aminopropyltriethoxysilane (APS) hydrolysed solution in distilled water. This silane only coating process produced fibres with significantly lower weight percentage coating compared to commercially available glass fibre products. All fibre packages were subsequently dried at 105 °C for 24 hours.

Pure APS, supplied by Sigma Aldrich, was used to make an APS film. A 1 vol% APS solution was produced in a polypropylene container with deionised water and oven-dried at a constant 105 °C. Once formed the film was stored in a desiccator containing silica gel.

When performing single fibre tensile tests, fibres were affixed to card templates using superglue. A 250 g/m^2 card and Loctite^{TM} gel superglue were used at all times. For the purposes of some experimental work it was necessary to secure or restrain fibres throughout processes in which they were exposed to very high temperatures. Restraining single brittle fibres using mechanical means is unsuitable, and glues degrade at elevated temperature, hence a ceramic cement was selected. Glassbond Saureisen Electrotemp Cement No. 8 was used. The reasons for selection were its resistance to thermal shock, very high maximum operating temperature and relatively long working time available between mixing and setting.

3.2 Heat treatments

A great deal of heat treatment of glass fibre was carried out in the work presented in this thesis. These treatments were performed using numerous different pieces of equipment depending on various requirements; for example volume of furnace, degree of temperature control possible or control of the furnace atmosphere.

3.2.1 Furnace heat treatments

A majority of heat treatments were carried out using a CSF1200 Carbolite electric furnace. Using this furnace it was possible to achieve sufficient temperature control over a large temperature range and with a large enough volume to allow the simultaneous treatment of large numbers of samples. A significant majority of the heat treatment carried out in this furnace was of fibres which were to be subsequently tensile tested.

All heat treatments were carried out for 25 minutes; ten minutes of re-heating were allowed to reach the target temperature and thereafter a 15 minute heat treatment period took place. This treatment time approximately reflects the length of some similar thermal recycling treatments found in the literature [67, 97]. After treatment, all samples were cooled immediately in room temperature air. Two different protocols were developed and used in the work: bundle heat treatment and single fibre heat treatment.

3.2.1.1 Bundle heat treatment

Lengths of fibre bundle were removed from the roving and attached to a metal rig (model shown in Figure 3-1) using a bolt and washer. After treatment at the desired temperature single fibres were then extracted for tensile testing.

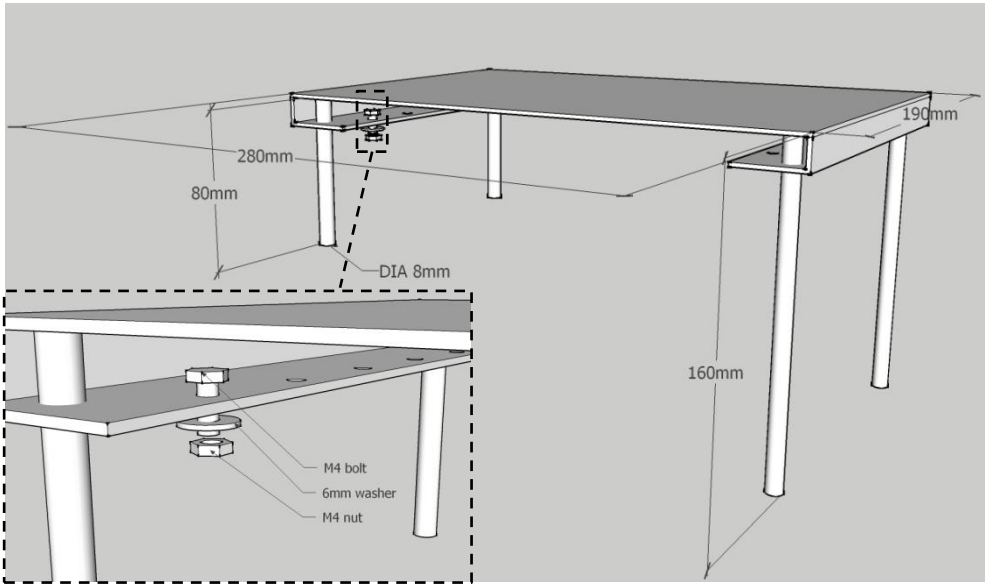

Figure 3-1: Model of rig used for heat treatment of glass fibre bundles

3.2.1.2 Single fibre heat treatment

In the single fibre heat treatment process, single fibres were extracted from a bundle prior to heat treatment. These were then attached to individual wire frames (model shown in Figure 3-2) using Glassbond cement and heat treated in batches of around 30 fibres.

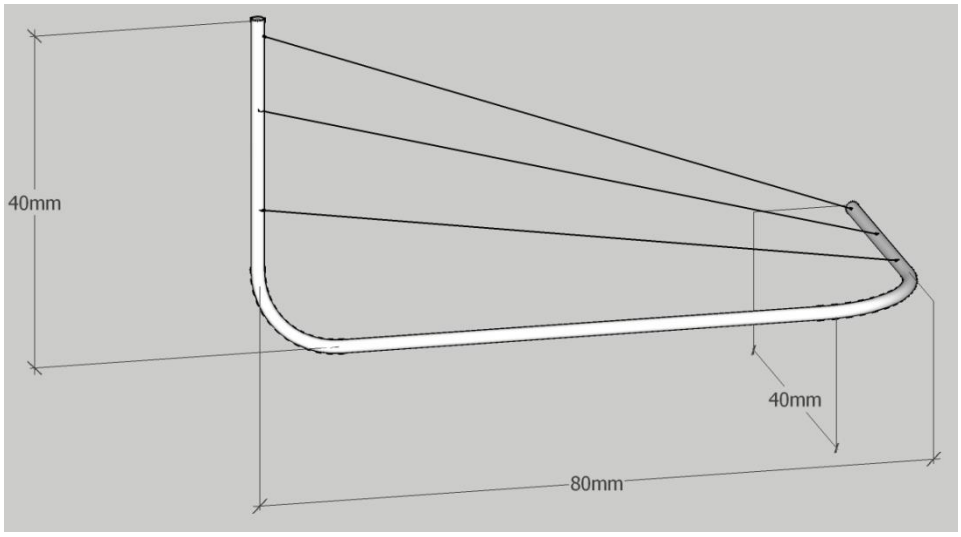

Figure 3-2: Model of wire frame used for heat treatment of single fibres (3 fibres represented by black lines)

In this, and the bundle heat treatment process, fibre or fibre bundles were supported at both ends so that no longitudinal tensile stresses were applied. Fibres were mounted with some slack along the length rather than being held tightly between the

two fixing points. This ensured that thermal expansion of the frame or rig would not induce longitudinal tensile stress. During single fibre heat treatment it was also possible for fibres to flex due to convective air currents; bending stresses caused by this were thus most concentrated at the fibre ends which did not form part of the tested gauge length.

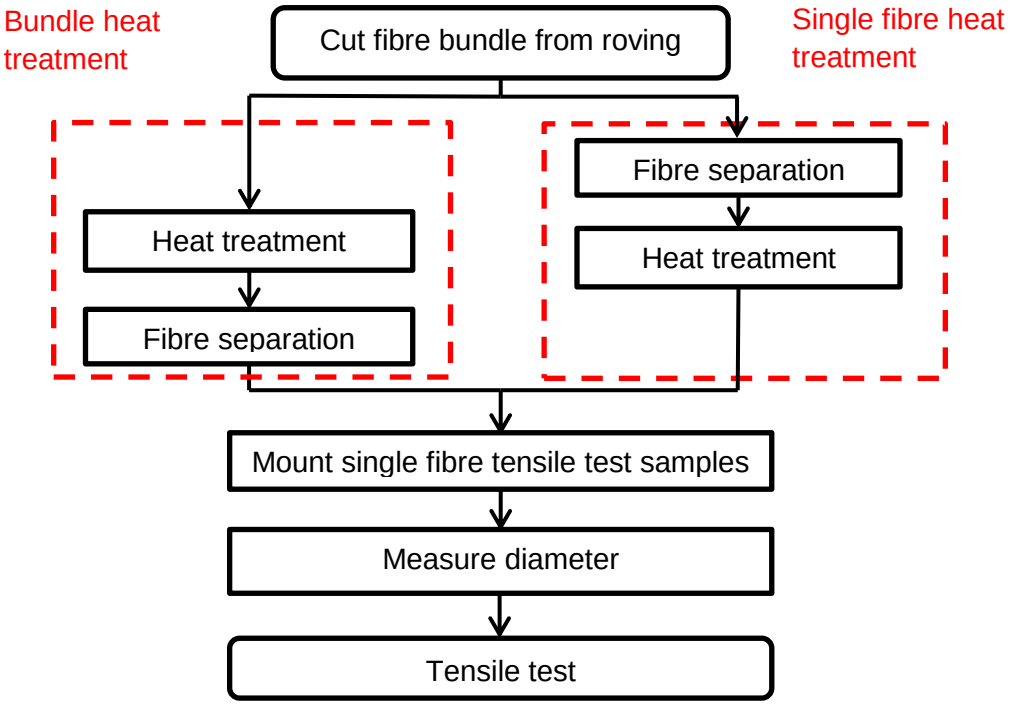

Figure 3-3: Simplified flowchart showing the difference between the bundle and single fibre heat treatment procedures

The only difference between the two methods developed – bundle and single fibre heat treatment – was the point of fibre separation from the bundle as indicated in Figure 3-3.

Some fibres, heat treated using the single fibre procedure, were also used for the purpose of studying their surface by SEM imaging.

3.2.1.3 Heat treatment for X-ray Diffraction Spectroscopy (XRD)

Fibres upon which XRD analysis was carried out were also treated in the furnace described, however a different treatment was applied. The furnace was pre-heated to 800 °C for over 1 hour. Bundles of fibre were inserted using the rig shown in Figure 3-1. Fibres were treated for a period of 2 hours after which the furnace was switched off. The fibres were then left to cool naturally to room temperature with the furnace door kept closed.

3.2.2 Vacuum system heat treatment

An investigation into the effect of atmosphere on the strength of heat treated glass fibre required the development of a method of treating fibres simultaneously under vacuum and at elevated temperature. A standard vacuum oven was not a suitable solution as it could not operate at high enough temperature. The method developed utilised an experimental setup called Thermal Volatilisation Analysis (TVA) which is most routinely used for investigations into the degradation of polymers [98, 99]. TVA systems are serial systems consisting of numerous elements, connected with vacuum rated glassware. In a standard analysis a sample is heated under vacuum (< 10^{-2} mbar) and the volatiles produced are collected using a liquid nitrogen trap. These volatiles can then be distilled off by allowing the trap to heat gradually to room temperature; depending on the material studied between 1 and 4 fractions may be distilled. The volatiles that are fractioned can then be transferred into cells for analysis by Fourier Transform Infrared spectroscopy (FT-IR). A simplified block diagram of the system used is shown in Figure 3-4. In this configuration the volatiles cannot be separated into multiple fractions.

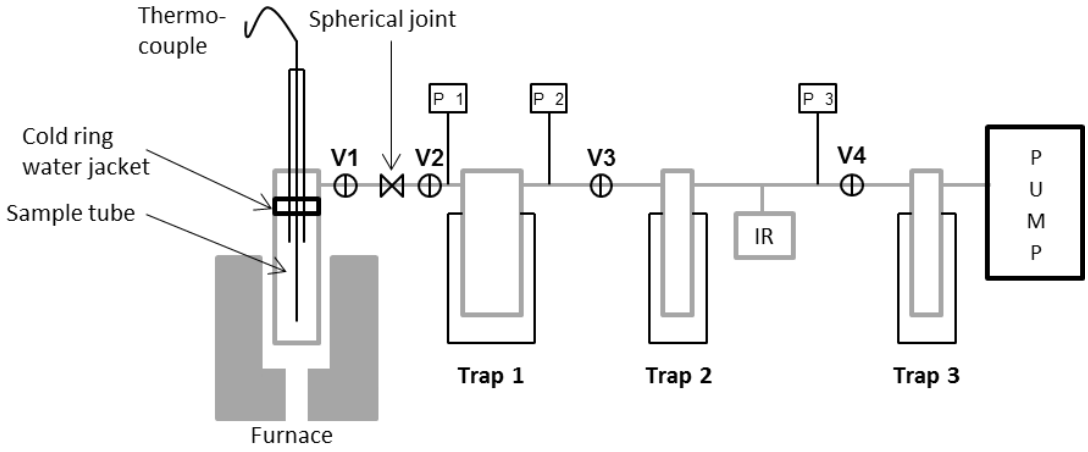

Figure 3-4: Simplified block diagram of single line TVA setup used for vacuum heat treatment of glass fibre

The sample is contained in a borosilicate glass or quartz tube of length 180 mm and outer and inner diameters approximately 35 and 30 mm respectively, on to which a tube head is fitted and sealed with grease. A cylindrical furnace is then placed around the tube to provide the necessary heat: its depth is less than the full length of the sample tube, as indicated in Figure 3-4. The temperature within the sample tube is directly measured by a thermocouple placed inside it. A cold ring water jacket

adjacent to the seal must be used to prevent the grease from melting at high temperature. At the opposing end of the system is a vacuum pump to provide the necessary negative pressure. Immediately preceding the pump is a cold trap (Trap 3); this must be chilled using liquid nitrogen (-196 °C) as a safety precaution to prevent any damaging volatiles entering the pump.

Volatiles leaving the sample tube can be captured by chilling Trap 1 with liquid nitrogen. If so, these volatiles are then moved to a second transfer trap (Trap 2) using a temperature differential. From there they can then finally be driven into a gas cell (marked as 'IR' in Figure 3-4) on which FT-IR analysis can be carried out.

The system used for the vast majority of the vacuum heat treatment work was a single line TVA; the volatiles contained in Trap 1 were transferred directly to an IR gas cell without fractioning. This was an acceptable method as relatively few volatiles were produced by the material studied. Using a simpler TVA system also reduced the total experiment time.

3.2.2.1 Bulk glass fibre samples

During initial assessment of the TVA as a means to conduct vacuum heat treatment it was desired to evaluate the volatilisation of water from a glass fibre sample. Bulk samples of chopped glass fibre weighing 1.3 g were used in these analyses. The sample tube was pre-dried by holding in an oven at a constant approximately 110 °C. Immediately after removal from the drying oven the fibre sample was inserted and pushed to the bottom of the tube, and the tube head attached. The sample assembly was inserted into the system and the vacuum pump started. Depending on the data being collected from the analysis the volatiles trap may or may not have been chilled with liquid nitrogen at this point. By leaving it un-chilled it was possible to allow volatiles to pass freely through the system and neglect them from gas cell analysis.

The entire system was left to pump down. Once again, depending on the data being collected for analysis the length of this period of time was variable. Regardless of the length of time allowed to pump down, before any heating was applied the approximate pressure of the sample, as measured by pirani gauge P1, was $< 10^{-2}$ mbar absolute. The furnace was programmed to heat the sample at a rate of 40 °C/min up to a (sample) temperature of 500 °C. This temperature was measured at the very bottom of the sample tube using a thermocouple as indicated in Figure 3-4.

To achieve this it was necessary to over-set the furnace temperature. Heating to the desired temperature took approximately 15 minutes, after which an isothermal period of 15 minutes was applied. Once the isothermal period ended the furnace was removed from the sample tube and it was left to cool back to room temperature under vacuum. Due to the use of glass components it was not possible to speed up the natural rate of cooling hence complete cooling to room temperature took around 1 hour.

The analysis of volatiles captured in gas cells was carried out using a Perkin Elmer Spectrum 100 Infrared (IR) analyser. The capillary tube of the gas cell was heated for approximately a minute before a measurement was taken to ensure that the volatiles were in the gas phase. Scans were performed at a resolution of 1 cm^{-1} and a background correction was taken before each measurement.

3.2.2.2 Heat treatment of single fibre samples

To perform vacuum heat treatment of glass fibres it was necessary to design a custom fibre mounting rig which was compatible with the dimensions of the TVA system and with the conditions to which it would be exposed. A photograph and schematic representation of the rig designed are shown in Figure 3-5. A hollow quartz tube was selected due to its low reactivity and very high melting point. As indicated in Figure 3-5 glass fibres were affixed around the circumference using Glassbond cement; approximately 25 – 30 fibres were mounted at once. This arrangement prevented contact between adjacent fibres, or between fibres and other surfaces, providing sufficiently careful handling was made. Once fibres were fixed to the rig the arrangement was left for approximately 24 hours to allow the cement to fully set. Once set, fibres were fully restrained at both ends; some flexibility along the length remained such that fibres would move with air currents but not so much that they could touch one another.

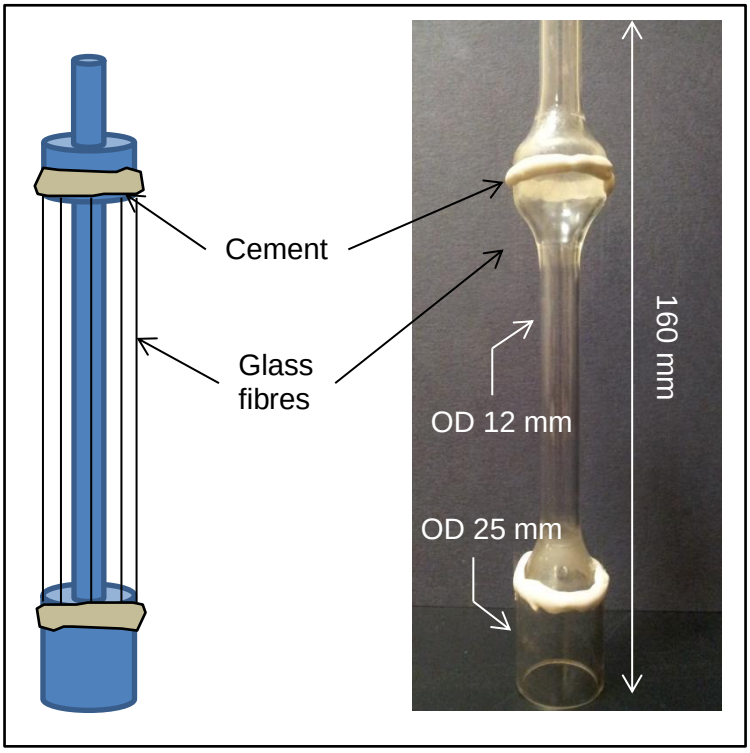

Figure 3-5: Schematic representation and photograph of single fibre mounting arrangement for vacuum treatment of single fibres in TVA

It was necessary, prior to carrying out single fibre heat treatments, to investigate the temperature performance of the TVA furnace and sample tube arrangement in terms of temperature gradients within the tube. It was already understood that there existed a difference in temperature between the value registered on the furnace controller and the actual temperature measured at the bottom of the sample tube, but this temperature difference could be corrected for using empirical data. In most analyses using the TVA system, the temperature at this position is the only concern as the material under investigation occupies this volume. When using the TVA for single fibre heat treatment, however, this was no longer the case. It was essential to know the treatment temperature to which a length of fibre of the order 50 mm was exposed. It was neither reasonable to assume that the temperature along this length would be constant, nor that it would be identical to the temperature at the bottom of the tube, therefore an analysis was carried out to quantify any gradients.

The temperature within the sample tube was measured by running the heat treatment, including sample mounting rig, several times while positioning the thermocouple at various heights. An identical program was run each time and it took approximately the same time to reach the steady state maximum temperature, the

values of which are indicated as (a) – (d) in Figure 3-6. A ramp rate of 40 °C/min was applied from room temperature up to 560 °C; this was empirically known to produce a sample temperature at the base of the tube of approximately 500 °C. A 15 minute isothermal at this temperature was applied, thereafter the furnace was removed and the sample allowed to cool back to room temperature.

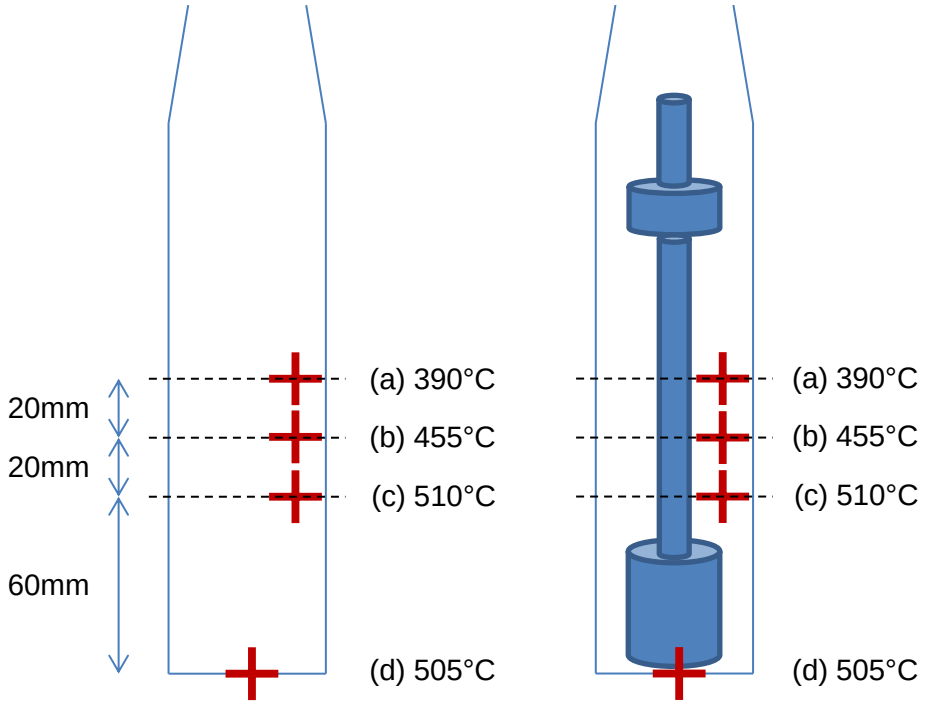

Figure 3-6: Temperature vs. position measurements within TVA sample tube during isothermal (furnace set to 560 °C)

Figure 3-6 shows four temperature measurements recorded at different positions within the sample tube. The standard position of the thermocouple was at (d) and this is where it was positioned during all bulk glass fibre work as outlined in Section 3.2.2.1. Also shown, in Figure 3-7, is the rough positioning of the tubular furnace in relation to the sample tube and mounting rig. The measurements (a) to (c) in Figure 3-6 clearly show that the temperature was not constant moving up the height of the sample tube. Point (a) was still well within the heating zone of the furnace but nonetheless was in the region of 100°C cooler than the desired temperature of 500 °C for which the furnace was set. The zone between (a) and (c) was crucial as it was intended that the lengths of glass fibre which would constitute the tested gauge length of tensile samples would be taken from this approximate region. By doing so the fibres would be as far inside the furnace as possible while still allowing a long enough portion at the ends to manipulate them on

to tensile test cards. From the temperature readings taken it was found that the average temperature in the region between (a) – (c) was around 450 °C, or 50 °C cooler than the very bottom of the sample tube. Thus, an empirical relation between the set furnace temperature and the treatment temperature of single fibre samples achieved was established.

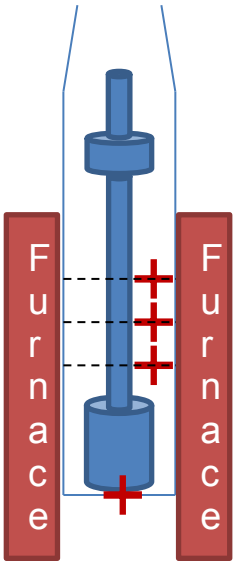

Figure 3-7: Approximate position of single fibre sample holder within TVA furnace

When conducting a single fibre vacuum heat treatment a clean sample tube was taken from a drying oven held at 110 °C. The fibre mounting rig was inserted into the tube using tweezers. Care was taken to ensure that the rig was placed into the centre of the tube and to prevent any contact between the tube walls and fibres. The sample tube head was put in place with a film of vacuum grease applied between them. Once the sample assembly was installed the vacuum pump was switched on and the system was allowed to pump down for 2 hours. After this 2 hour period the pressure of the sample, measured on pirani gauge P1 (Figure 3-4), was 10^{-2} mbar. The furnace program was initiated; the fibres were heated at a rate of approximately 40 °C/min up to 450 °C and held for a 15 minute isothermal period. The maximum pressure of the sample during the heating stage was of the order 0.5 mbar. Upon completion of the temperature program the furnace was removed and the assembly allowed to cool to room temperature under vacuum.

3.2.3 Heat treatments using thermal analysis equipment

In some cases it was elected to utilise the capabilities of thermal analysis equipment to perform heat treatments. This option was selected where only a small volume of sample was required for the analysis post-heat treatment. The advantages of the thermal analysis equipment over a large furnace in these cases were multiple:

- More accurate temperature control between room temperature to 1000 °C possible
- Smaller furnace guaranteed more uniform temperature experienced by all samples

- Significantly larger maximum heating rate possible
- Control of atmosphere (air or nitrogen flow control) possible within furnace chamber.
- Elimination of contaminant particles from the furnace volume

The details of the treatments carried out using two thermal analysis machines are outlined.

3.2.3.1 Thermo-Gravimetric Analyser (TGA) – treatment of samples for XPS analysis

A TA Instruments Q50 TGA was used for the treatment of APS sized fibre. A short length of bundled fibre was placed in the centre of a platinum pan. A ramp rate of 10 °C/min was applied from room temperature to the target temperature; once reached the program ended and the sample was allowed to cool naturally back to room temperature. A purge gas of either air or nitrogen was used at flowrate of 50 ml/min.

3.2.3.2 Thermo-mechanical Analyser (TMA) – treatment of samples for AFM and SEM imaging

A TA Instruments Q400 TMA was used for the treatment of glass fibres which were to be imaged thereafter using either Atomic Force Microscopy (AFM) or Scanning Electron Microscopy (SEM). During such treatments it was desired that single fibres were kept separate and were not in contact with either each other or any part of the furnace chamber. Under these conditions it subsequently made no difference which section of a fibre was imaged as it was assured that they were all heat treated under identical conditions. A suitable method of thermally treating single fibres was developed using a film/fibre stage which is a standard fitting for TMA. Several single fibres were embedded in a length of Glassbond cement (Figure 3-8). This assembly was then suspended using the slot in the TMA stage such that the fibres hung directly downwards.

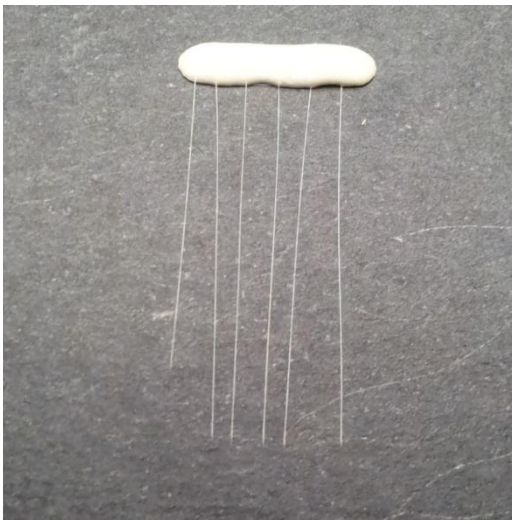

Figure 3-8: Mounting arrangement for heat treatment of single fibres in TMA

Heat treatment of fibres was performed across a temperature range of 200 – 700 °C. Regardless of desired treatment temperature, the control program was similar; the furnace equilibrated within 10 % of the desired temperature within the first minute and to exact temperature within approximately 5 minutes. Once equilibrated, a 15 minutes isothermal period was applied. Following this the program ended and the sample was left to cool to room temperature. This took approximately 10 minutes with the application of some chilling medium to speed up particularly the initial part of cooling. It was not possible to routinely use the cooling accessory existing for TMA as the temperatures used often exceeded its maximum operating temperature of 400 °C.

3.3 Tensile testing

3.3.1 Tensile test settings

A large volume of single fibre tensile tests were carried out as part of this work. For each test the fibre diameter was individually measured beforehand by microscopy (Section 3.3.2).

Tensile testing of both as-received and heat treated fibre was carried out. Single fibre tensile properties were obtained according to the method described in ASTM C1557-03. Tests were carried out using either of two tensile test machines:

i. Instron 3342 universal testing machine equipped with a 10 N load cell
ii. Testometric M250-2.5CT tensile machine equipped with a 5 N load cell.

All fibres were mounted at a gauge length of 20 mm. All tensile tests were performed at an extension rate of 0.3 mm/min, equivalent to a strain rate of 1.5 %/min.

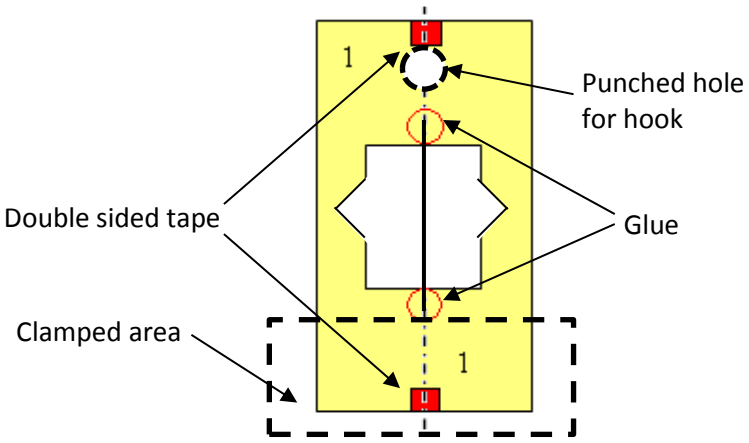

Figure 3-9: Schematic of single fibre tensile test sample card

The schematic of a typical (Instron) mounted tensile test sample is shown in Figure 3-9. Tape was used to position the fibre on the central vertical axis of the test card and it was secured with superglue. Samples were left for a minimum of 24 hours for the glue to fully cure. When testing, a hole was punched on the centreline of the card and used to hang the sample from a hook in the tensile machine; the load was then applied to the sample via this hook. The bottom portion of the card was clamped as indicated. It can also be seen in Figure 3-9 that the edges of the card were cut with a 'V' in order to improve ease of cutting once samples were clamped in the machine. This was particularly important when attempting to measure the strength of very weak fibres; because samples were not firmly clamped at the top some movement occurred when cutting the edges of the card and this could be sufficient to break weak fibres. Cutting through a smaller volume of card applies less shear stress to the system causing less unwanted rotation of the sample and thus reducing potential breakages.

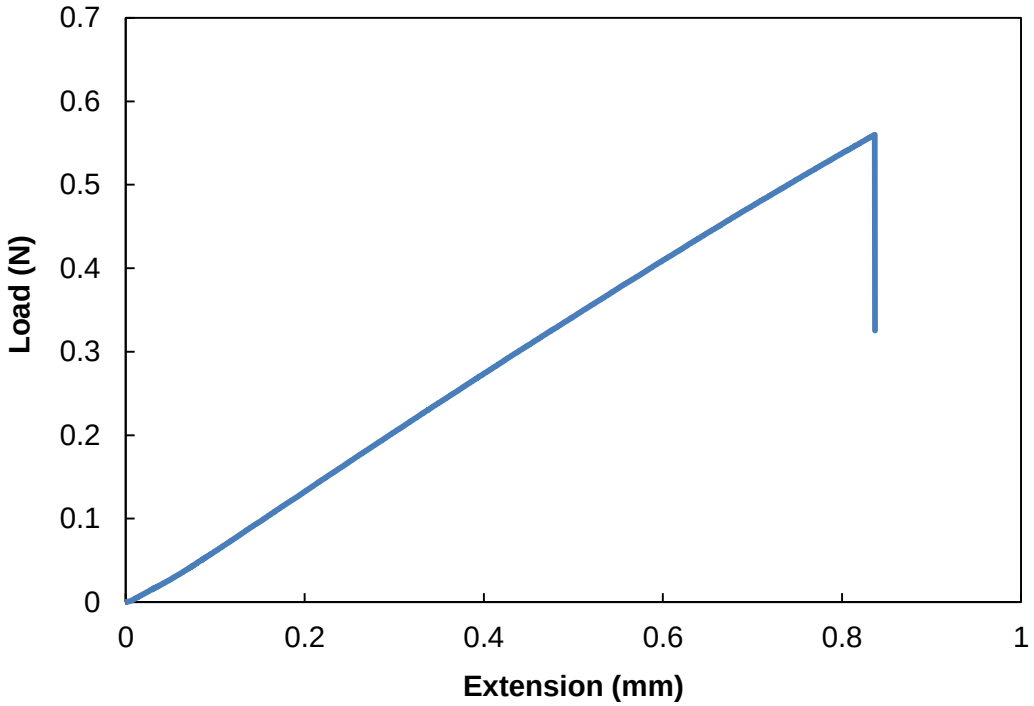

Figure 3-10: Idealised load-extension graph for single glass fibre tensile test

After cutting the edges of the card template the tensile machine column was manually raised to the point at which the fibre being tested was almost under strain. Following this method it was possible in an ideal case to produce a load extension plot similar to that shown in Figure 3-10. Pre-straining each fibre reduced the overall experimental time taken.

Preparation of tensile samples when using the Testometric machine was slightly different. The machine was configured to restrain samples with solid grips at both top and bottom; once installed samples were held rigidly and the chance reduced of weak fibres being broken before testing. It was not possible, however, to pre-strain samples before testing, increasing the experiment time.

3.3.1.1 Analysis of tensile data

Single fibre tensile strengths were calculated using cross sectional areas (A) from individually measured diameters and the load at failure (L) from tensile tests using equation (3.1).

$$\sigma = \frac{L}{A} \tag{3.1}$$

Following a set of tests of a fibre heat treated under some conditions a mean average strength was calculated. Some data were excluded from these calculations:

- Fibres broken at either edge of the card window were excluded from average strength calculations
- Fibres which fractured at a load of less than 0.1 N were not automatically detected by the tensile machine. In these cases the breaking force was manually estimated from the load-extension plot

In addition to the mean averages, sample standard deviations were calculated for each fibre dataset. The standard deviation was calculated using (3.2):

$$s = \sqrt{\frac{\sum(x - \bar{x})^2}{n - 1}} \tag{3.2}$$

Where $\bar{x}$ is the mean average, n is the sample size and x is one of the n values in the dataset.

The data averages presented graphically in this thesis are shown with confidence limits. In all cases the 95 % confidence limit is used, as calculated using (3.3).

$$95\%\ C.L. = 1.96\left(\frac{s}{\sqrt{n}}\right) \tag{3.3}$$

In addition, a statistical hypothesis test was used when comparing the significance of differences in the means of fibre test datasets. The Student's t-test was selected as a suitable test; the equation used to calculate this statistic is shown (3.4).

$$p = \frac{\bar{x}_1 - \bar{x}_2}{\sqrt{\frac{s_1^2}{n_1} + \frac{s_2^2}{n_2}}} \tag{3.4}$$

In all cases the p-value was calculated by specifying a two-tailed distribution and for two datasets with unequal variance. When analyzing tensile strength datasets, a difference in average strength was considered statistically significant if it had a p-value of less than 0.05 (i.e. significant in 95 % of cases).

3.3.2 Fibre diameter measurement

For every single fibre tensile test the fibre diameter was measured prior to testing. This was carried out using either an optical microscope or, in some cases, a Scanning Electron Microscope (SEM).

3.3.2.1 Optical microscopy and image analysis

Two inverted optical microscopes were used: a Nikon Epiphot and an Olympus GX51. An image of each fibre was captured and transferred to image processing and analysis software ImageJ. With use of a calibration scale marker the diameter of each fibre was measured and recorded. The potential error in the measurement of fibre diameter on average tensile strength was modest due to the large number of tensile tests carried out at each condition.

3.3.2.2 Scanning Electron Microscopy

Immediately after mounting each tensile specimen a part of the excess length, used to manipulate the fibre into position, was cut as close to the gauge length as possible. This length of fibre was affixed to a SEM stub using carbon tape. Once full, stubs were sputter gold coated to allow imaging. Images were captured using a Hitachi SU6600 Field Emission SEM (FE-SEM); aperture positions for high resolution, and consistent beam settings, were used:

- Accelerating voltage V_{acc} = 15.0 kV
- Extraction voltage V_{ext} = 1.8 kV
- Magnification = 4000x

The portions of fibre of which the diameter were measured were not part of the gauge length to be tested as this is not a feasible method for SEM observation (prior to testing). However, the measured length was taken from within a distance of ≤ 40 mm of the gauge length portion. For the fibres used in this work it is known that, along a single strand, there is some variation in diameter: however within a typical 1 m length of single fibre the variance of around 20 measured diameters is less than 0.1. It was therefore considered suitably accurate to assume that the diameter of the gauge length section could be equated with the diameter of the immediately adjacent portion that was possible to image. All diameter measurements were taken from image stills captured, using the measuring tool contained within the SEM software. An accuracy of ± 0.1 µm was achieved.

3.4 X-Ray Diffraction Spectroscopy (XRD)

3.4.1 Fibre used in analysis

Unsized fibre was used in the investigation using XRD facilities in the University of Strathclyde's Advanced Materials Research Laboratory (AMRL). An analysis of fibre heat treated using the method outlined in Section 3.2.1.3 was conducted and compared with an untreated fibre sample. In both cases the fibre was hand ground using a mortar and pestle before analysing.

3.4.2 Experimental settings

X-ray diffraction spectroscopy measurements were carried out using a Bruker D8 Advance instrument. The instrument settings used for analysis are presented in Table 3-1.

Table 3-1: XRD settings used in analysis

Voltage	40 kV
Current	40 mA
2-theta angle, 2θ	10-80°
Step size	0.05°
Step time	3 s
Radiation (wavelength, λ)	Cu (1.56 Å)

3.5 X-ray Photoelectron Spectroscopy (XPS)

3.5.1 Fibre used in analysis

Both sized and unsized fibres were investigated by XPS, using equipment at the University of Surrey's Surface Analysis Laboratory. Fibres were conditioned by either bundle heat treatment (Section 3.2.1.1) or using TGA (Section 3.2.3.1). Lengths of fibre bundle of approximately 20 mm were placed parallel to each other on the sample holder. As it was not possible to produce a perfectly flat sample 'surface' the longitudinal fibre axis was aligned with the electron analyser to minimise interference between exit electrons and the sample.

3.5.2 Experimental settings

XPS measurements were carried out using a Thermo Scientific™ Theta probe angle resolved XPS system. A monochromated Al Kα X-ray with an energy of 1486.6 eV was used. Analyses were carried out using the instrument settings outlined in Table 3-2.

Table 3-2: XPS settings used in analysis

Emission current	6.3 mA
Anode potential	16 kV
Spot size	400 µm

To achieve reasonable count rate and experimental time, survey scans were carried out using a pass energy of 300 eV with a step size of 0.4 eV. Re-scanning of the same sample at least 3 times was allowed to improve smoothing of the baseline. High resolution scans of some peaks were also carried out: a pass energy of 50 eV was used, with the exception of the N1s scans for which a pass energy of 100 eV was used. A step size of 0.2 eV was chosen in all cases. All measurements were taken at a take-off angle of 90° relative to the surface.

The insulating nature of the glass fibre samples required utilisation of charge compensation using an ion flood gun; the flood gun operating conditions were optimised for each sample individually. This caused the position of all peaks to move in relation to the amount of charge compensation applied. Further, because charge compensation was used, the operating pressure of the system was of the order of ≥ $5x10^{-8}$ torr, higher than the ideal value of approximately 10^{-9} torr.

3.5.3 Data processing

Analysis of data was carried out using Thermo Scientific™ Avantage software. All data were corrected regarding relative peak position because of the effect of charge compensation. The magnitude of correction was calculated by shifting the C1s peak to 285.0 eV.

3.6 Atomic Force Microscopy (AFM)

3.6.1 Fibre used in analysis

An investigation of unsized fibre was undertaken. Experiments were performed at University of Nottingham, in the Laboratory of Biophysics and Surface Analysis (School of Pharmacy). Untreated fibres were compared with fibres that had been heat treated to a temperature of between 200 – 700 °C inclusive. Analyses were carried out at 100 °C intervals. Fibres were mounted on glass microscope slides (Figure 3-11) and secured at both ends using glue. A consequence of this fibre arrangement was the potential for fibres to vibrate between the mounting points under the application of a force by the AFM tip, lowering the quality of the image captured. An alternative method of affixing fibres along their entire length using a fine film of adhesive was nonetheless rejected. Suitable control of fibres during mounting could not be assured and the possibility of fibres rolling slightly was a concern. If this occurred parts of the true fibre surface could be obscured by adhesive; moreover the analysis of heat treated fibre surfaces would be further complicated as there would be doubt regarding the source of observed surface features i.e. due to fundamental changes in the material or due to contamination from the adhesive.

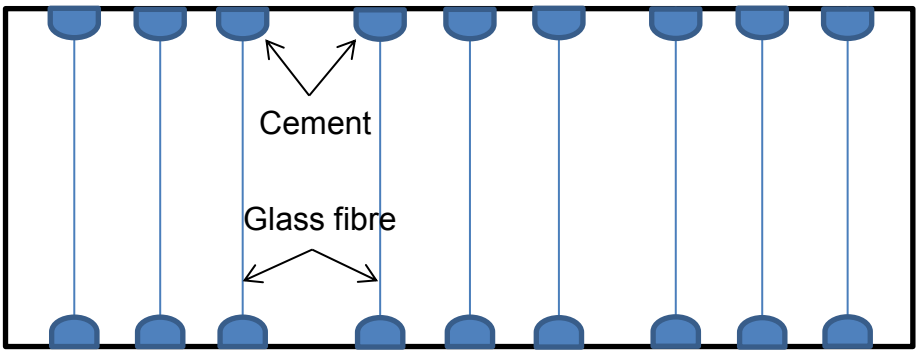

Figure 3-11: Schematic of single glass fibres mounted on microscope slide (of dimensions 80 x 25 x1 mm) for AFM analysis

3.6.2 Experimental settings

Imaging of fibres by AFM was performed using a Digital Instruments D3000 alongside a Nanoscope IIIa controller with phase extender. All images were

captured using tapping or intermittent contact mode. The details of the cantilever and probe used are presented in Table 3-3.

Table 3-3: AFM settings used in analysis

Probe designation	TAP150A (RTESPA-150)
Tip material	Si
Cantilever material	Al
Spring constant	5 N/m
Resonant frequency	~ 150 kHz

The selection of tapping mode and a cantilever with low spring constant were necessary due to the nature of the sample mounting method. Using the settings described, however, it was possible to avoid undesirable vibration of the fibre during analysis and achieve images of acceptable quality. Images were obtained with the fast scan direction being perpendicular to the longitudinal fibre axis. The rate of capture was 1.5 Hz and the scan size 3x3 µm.

3.6.3 Data processing

3.6.3.1 Image flattening and cleaning

Data processing was performed using Nanoscope Analysis. Images were flattened to remove the curvature of the fibre using 3rd order polynomial fitting. The edges of each image were excluded from analysis at this stage; this was necessary because of the presence of unwanted noise at the edges where the tip suddenly changes direction to scan the next line in the opposite direction. An example of this is shown in Figure 3-12.

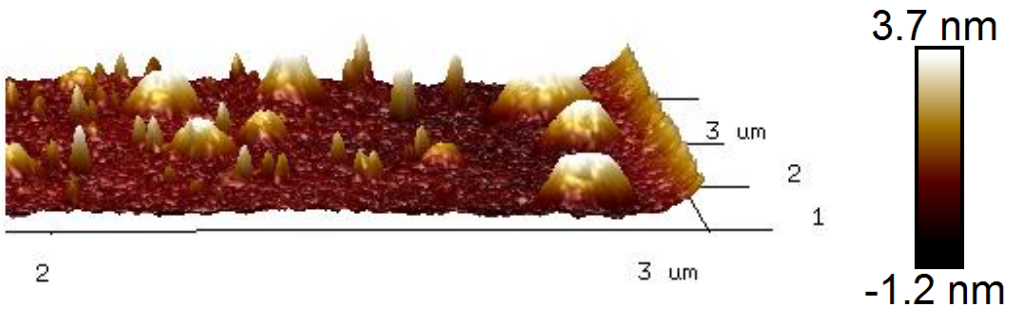

Figure 3-12: Edge effect of change in tip direction on AFM topography plot

This curvature at the edges of images did not always occur to the same degree, however for consistency all images were cropped to a size of approximately 2.7 – 2.8 µm square. It was then possible to perform roughness analyses.

A small amount of image cleaning was also carried out when necessary. It is important not to perform excessive image cleaning as it can have the effect of removing 'real' features on the surface which should be included in any surface analyses such as roughness analysis.

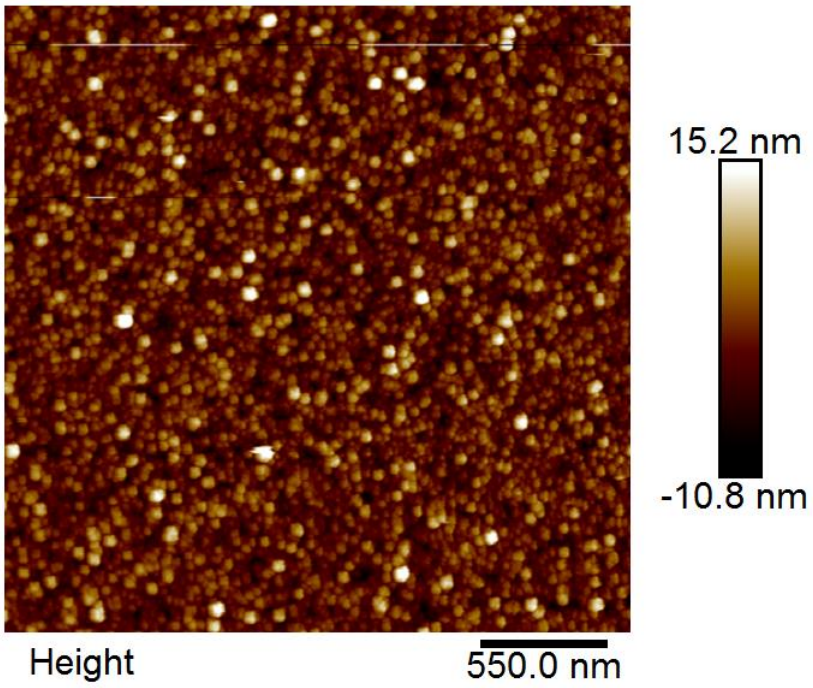

Figure 3-13: Example of streaks appearing on AFM topography plot that has been flattened

The image cleaning carried out was targeted to certain areas (for example where obvious streaks created during removal of fibre curvature were observed) rather

than applied across the whole image. Figure 3-13 shows an example of the streaks that can appear in AFM images of fibres following flattening.

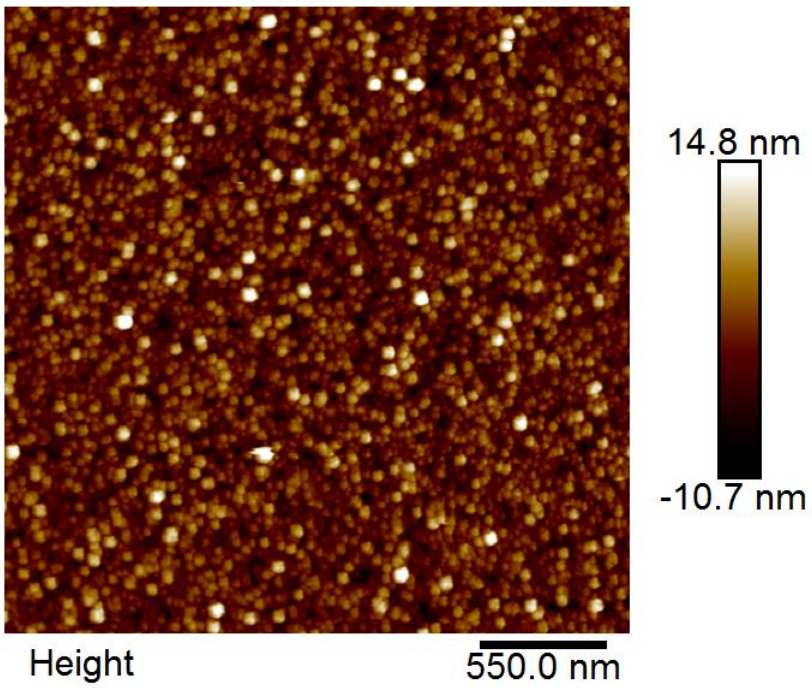

Figure 3-14: Example of AFM plot from which streaks have been 'cleaned'

Defects of this type were removed using the streak cleaning tool, targeted over only the problematic area. The effect of streak removal can be seen in Figure 3-14; the marks prominently visible in Figure 3-13 are completely removed but the rest of the image is largely unchanged.

3.6.3.2 Roughness analysis

Roughness analysis was carried out using images that had been acceptably cropped, flattened and cleaned to remove streaks. The parameter calculated was the RMS roughness.

$$R_q = \sqrt{\frac{1}{n}\sum_{i=1}^{n} z_i^2} \tag{3.5}$$

In (3.5) z_i is the z-height of a point i on the surface and n is the total number of z-heights measured in an image. The RMS roughness was suitable for the roughness analysis as it can account for both positive and negative values of z-height.

3.7 Thermal analysis

Thermal analyses were carried out using complimentary techniques. The analyses were performed using samples of APS film, as the weight percentage of APS on the sized fibres was very low and therefore challenging to detect using some techniques, for example TGA.

3.7.1 Thermo-gravimetric and Differential Scanning Calorimetry (TGA/DSC)

These analyses were carried out using a Netzsch STA 449 F1 Jupiter in the AMRL. Dedicated TGA was conducted in an alumina beaker while simultaneous TGA/DSC measurements were made using platinum pans. Approximately 100 mg of sample was analysed during TGA and 10 mg during TGA/DSC. The thermal profile applied in all cases was a ramp of 10 °C/min from room temperature to 1000 °C, following which the sample was allowed to cool to room temperature. Both air and nitrogen were used as the furnace carrier gas, each at a flowrate of 50 ml/min.

3.7.2 CATLAB degradation analysis

A Hiden CATLAB^{TM} was used to conduct thermo-chemical analysis. The CATLAB consists of a microreactor with temperature and gas flow control, coupled to a Hiden QIC-20 mass spectrometer, allowing temperature resolved identification of volatile species over the range 2 – 200 AMU.

Samples of APS film of the order of 1 mg were placed into a borosilicate glass cap; this was placed into a quartz reactor tube which was then inserted into the furnace. A ramp rate of 10 °C/min from room temperature to 550 °C was chosen, to reflect the TGA/DSC described in Section 3.7.1. The purge gas was helium at a flow rate of 40 ml/min.

3.8 Fractography using Scanning Electron Microscopy

3.8.1 Experimental settings

Examination of the fracture surfaces of some glass fibres following tensile testing was carried out using the Hitachi SU6600 Field Emission SEM (FE-SEM) at Strathclyde's AMRL. Aperture positions for high resolution, and consistent beam settings, were selected and Accelerating and Extraction voltages of 15 and 1.8 kV respectively were used. A magnification of between $4x10^3$ to $22x10^3$ times was employed to obtain images with sufficient resolution. Images were captured with the detector directly above the fracture surface by utilising the rotation and tilt functions of the SEM stage.

3.8.2 Sample preparation

The preferred samples for the manufacture of fractographic specimens were those for which both halves of the fibre were preserved following fracture, as it could be assured that the plane viewed under SEM was that in which the fracture occurred. As a consequence of this, the majority of the fracture surfaces imaged were those of fibres that fractured at a relatively low stress. Fibres with higher breaking stress would, in most cases, break at additional positions along the gauge length following the initial fracture and therefore could not be recovered for fractographic analysis.

Lengths of fractured single fibres were mounted along short lengths (approximately 25 mm) of copper tape such that all fibre ends protruded by about the same distance beyond the edge of the tape. Once secured the fibre and tape assembly was affixed to a SEM stub and the copper tape bent slightly such that the fibre ends pointed upwards. Samples were sputter gold coated; before insertion into the SEM the tape was bent further to ensure that the fibre fracture ends pointed almost directly upwards.

3.9 Scanning Electron Microscopy – Energy Dispersive X-ray spectroscopy (SEM-EDX)

3.9.1 Experimental settings

SEM-EDX was carried out in tandem with standard SEM imaging of fibre surfaces using a Hitachi SU6600; the settings utilised were identical to those outlined in 3.3.2.2. It was however necessary to adjust the aperture settings of the microscope: this is standard procedure as the settings best suited to collection of high resolution images differ from those required to perform the most effective EDX analysis.

The FE-SEM was equipped with Oxford Inca 350 with X-Max 20 mm^2 detector energy dispersive spectrometer (EDS) for elemental analysis. To improve the accuracy of the measurements, rather than performing only one scan of each fibre a minimum of 2 sites were analysed. Further, at each site multiple measurements were made. As indicated by Figure 3-15 the spectrum was captured over an area and 3 distinct points on a straight line.

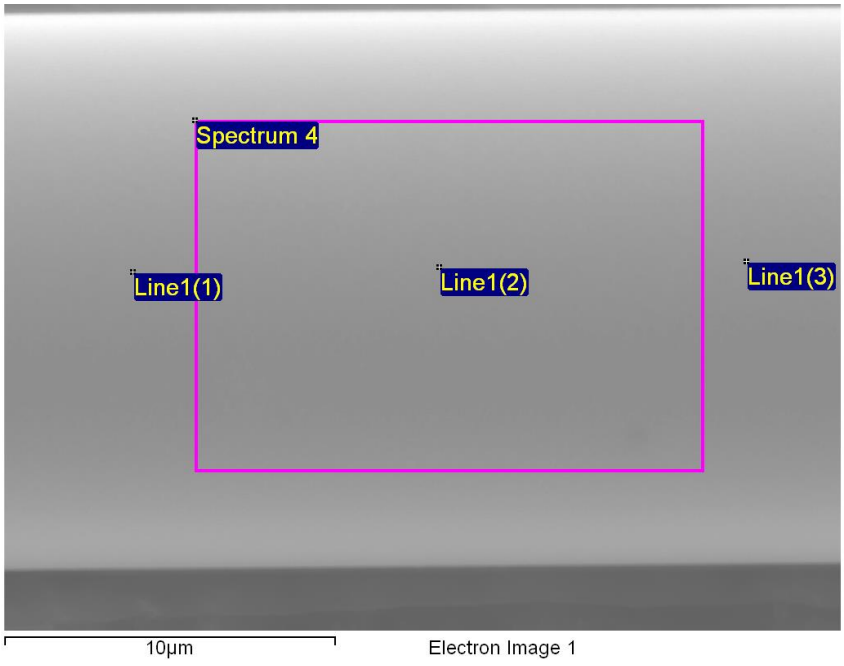

Figure 3-15: Typical area and points on line analysed using SEM-EDX of sites on a single fibre

3.9.2 Sample preparation

Samples analysed by SEM-EDX were prepared in the same manner as those which were simply imaged using SEM. A length of carbon tape was affixed to the centre of

1 inch diameter metal stubs. Upon the tape several lengths of glass fibre were arranged roughly parallel to one another and sputter coated with gold. The effect of this gold coating on the elemental analysis was removed automatically by the Inca software utilised.

3.10 Image analysis – surface of heat treated fibres

3.10.1 Fibre used in analysis

Bare glass fibres were heat treated at temperatures of 625 – 700 °C using the procedure outlined in 3.2.3.2. Imaging by SEM was performed in a similar manner as outlined in 3.3.2.2. The surfaces of these fibres were found to exhibit the development of some features which were further investigated by processing and analysing the images.

3.10.2 Image processing and analysis

ImageJ software was used to analyse the surface features which formed following heat treatment. The original SEM images selected were all captured at a magnification of approximately 8000 times. From these images small sections measuring 2 x 2 µm were cropped from the centre line of the fibre, where the curvature had the least effect on the perspective.

The original SEM images were captured in greyscale. A black and white image was created by adjusting the colour thresholding of the 2 x 2 µm areas in ImageJ. The output of the procedure produced a binary image: it was then possible to assess the image histogram for the number of black and white pixels present. Thresholding was performed such that, as closely as possible, the particles formed on the surface appeared as white while the spaces in between appeared as black. This procedure became more straightforward as the surface particles appeared to develop with increasing treatment temperature as there was an associated increase in the contrast produced in the original images. Production of representative binary images from the greyscale SEM originals was of importance as the relative area of surfaces occupied by the features which developed due to heat treatment was assessed directly using the ratio of white to black pixels in the binary images. By careful side

by side comparison of the greyscale originals and binary images during the thresholding conversion process acceptable representations were achieved.

Chapter 4. Strength of heat treated sized and unsized E-glass

4.1 Introduction

The strength loss of heat treated glass fibre has been investigated and reported in the literature for in excess of 50 years. Now, as then, single fibre tensile tests remain an effective and relatively simple method by which data can be obtained. Using these tests, a general trend of progressive strength loss with increasing heat treatment temperature has been reported, as summarised in 2.3.1. Although this general trend is well established, it is also the case that the strength loss behaviour of a fibre never previously studied cannot be fully predicted based on what is known about other fibres even if they are relatively similar in their composition, for example.

In this investigation, a full characterisation of the strength loss behaviour of both the APS sized and bare fibre was necessary, for several reasons. As noted in 3.1 all E-glass fibre investigated was produced using a pilot bushing of a commercial glass fibre manufacturer; however the surface coatings applied thereafter were significantly different to the normal application of a multi-component sizing. APS is commonly added to sizings as the coupling agent and studies of the strength loss of commercially sized fibre have been reported before [65, 100], but no data have been produced using fibre with only the silane coupling agent present on the surface. Data for commercially produced bare fibre are also scarce in the literature; in the vast majority of cases the bare E-glass which is heat treated has been produced using a custom laboratory scale bushing, for example in [5, 51, 55]. As such the processing history of these fibres is significantly different to a commercial E-glass. This particularly applies to physical handling and storage of the product, but there may also be significant differences in the thermal histories of the melt and drawn fibres.

As previously discussed in 3.2.1 a constant heat treatment time was used; 10 minutes to allow the furnace to re-equilibrate and a further 15 minutes heat treatment time.

4.2 Bundle heat treatment

4.2.1 Untreated fibre strength baseline

The most obvious baseline against which the strengths of heat treated fibres should be compared is obtained simply by testing a suitably large number of fibres taken straight from the roving. Using this value would, however, neglect a variable that is introduced by performing heat treatment, namely extra manual handling when attaching and removing fibres from the rig 3.2.1. Of the two heat treatments it was known that the bundle method had a greater potential for mechanical damage to be sustained: similarly the bare fibre would be more susceptible to damage than the APS sized. For these reasons a simulated run of the bundle heat treatment using bare fibre was carried out. The procedure detailed in 3.2.1.1 was followed but without switching on the furnace, therefore aiming to simulate any possible damage from physical manipulation of the fibres but without affecting the strength through heating. This represented the highest likelihood of surface damage that could occur due to handling during heat treatment.

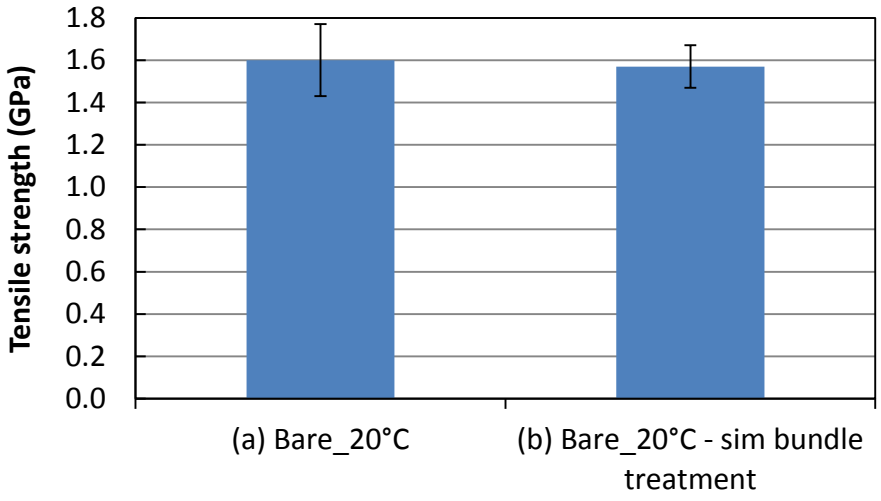

Figure 4-1: Comparison between strength of untreated unsized fibre; (a) straight from roving and (b) after simulated bundle heat treatment procedure

It was found that there was no significant difference between the strengths of the two samples of unsized fibre as indicated by Figure 4-1. This suggested that it was acceptable to use the strength of glass fibre taken straight from the roving and tensile tested, as a baseline to compare with the strength of heat treated fibre. It was assumed that this conclusion could be extended to results using the single fibre heat

treatment as it involved less, or more careful, handling, and to results using APS fibre as its surface was further protected from potential damage by the silane coating.

4.2.2 Results – bundle heat treatment

The average single fibre tensile strengths calculated using (3.1) measured at room temperature following bundle heat treatments are presented in Figure 4-2. In this and all other figures showing average fibre strength the error bars are 95 % confidence limits, calculated using Equation (3.3).

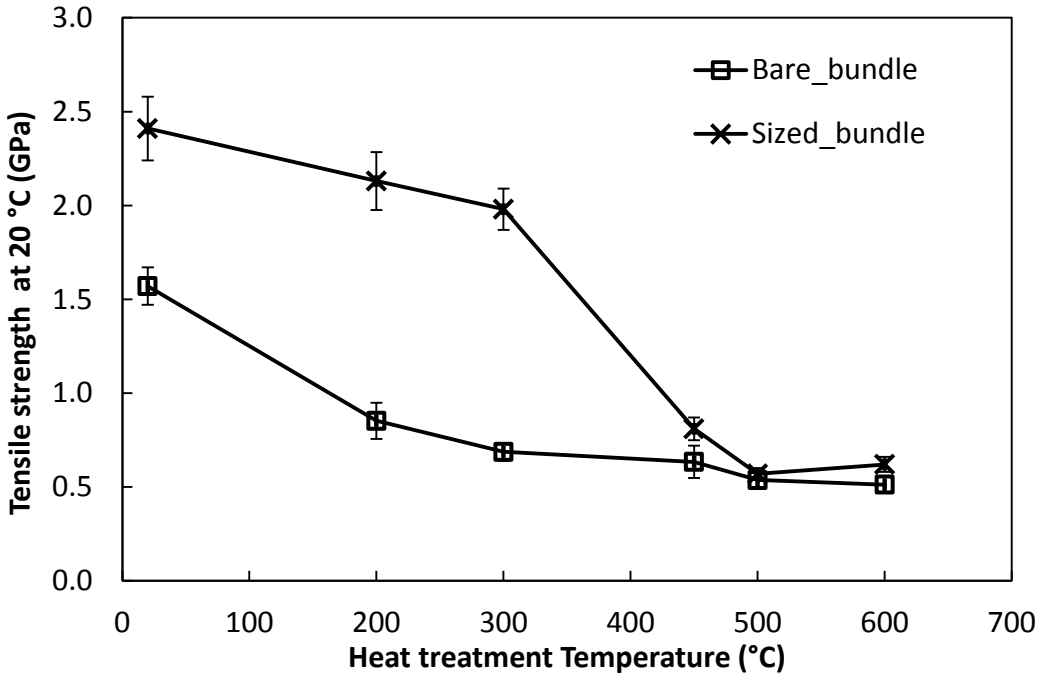

Figure 4-2: Tensile strength of bare and APS sized fibres after bundle heat treatment for 25 minutes

The APS sized fibre, before application of any heat treatment, has much higher room temperature strength than bare fibre, which is not surprising as it is protected from surface damage by the silane coating. For sized fibre, around 20 % of this strength had been lost after treatment at a temperature of 300 °C. The strength loss increased greatly above 300°C and became much less dependent on conditioning temperature beyond 500°C. The bare fibre, on the other hand, lost over half its original strength by 300°C and in fact much of this loss was also observed when treating to just 200 °C. At higher temperatures the bare fibre strength decreased

further but to a lesser degree; drops in strength between immediately adjacent temperature treatments were not themselves significant but a decrease of almost 200 MPa occurred between 300 – 600 °C. Conversely, the strength of the sized fibre decreased most significantly at higher temperatures. Following treatment at 450 °C it retained only one third its original strength and after 500 °C treatment just one quarter: approximately the same absolute magnitude as measured for the bare fibre.

The strength of sized and bare fibre tended to converge as the heat treatment temperature increased; statistically equal strengths were measured after treating at 500 °C. As the only difference between these two specimens is the presence of APS coating, it may be reasonable to state that strength retention resulting from the surface coating is compromised by heat treatment and can be completely dismissed when a temperature of 500 °C is applied. Further investigation on the degradation of APS is presented and discussed in Section 4.4.

It is interesting to observe that bare fibre was subject to significant strength loss due to the thermal treatment applied in this work, implying that some level of strength loss during heating could also be attributed to factors other than surface coating alone. It is widely accepted that loss of the protective sizing (for example at elevated temperature) is likely to contribute to strength loss but equally it is known that some other fundamental changes, independent of the sizing, occur in glass fibres at high temperatures [51, 71, 72, 76]. The use of both bare and sized fibre in this work helps to separate the variable of sizing effect from other strength loss mechanisms in the glass.

Comparison of these data with those published in the literature is somewhat problematic. Bare E-glass can often only be obtained by manufacturing it at a laboratory scale using custom fibre drawing apparatus [5, 51, 55]. Such manufacture methods tends to comprise the drawing of just one fibre at a time from a crucible with a single die. The processing of this fibre may be similar in terms of drawing temperature and quenching rate, but the handling of the fibre after drawing is significantly different. Where commercial production entails the immediate gathering of many hundreds to thousands of fibres into a roving, at the laboratory scale the single fibre length can be carefully wound on to a roller, minimising its mechanical handling. In some cases even this contact can be eliminated, by stopping the

production and removing for investigation the length of fibre held between the die and roller [5].

Studies of the strength loss of heat treated commercial E-glass with a full sizing (rather than just APS) have been conducted by Feih et al. [65, 100] and the data presented in Figure 4-2 are compared with their normalised fibre strength data in Figure 4-3 . They present normalised fibre strengths following heat treatment at similar temperatures and times to those used in this work. In all cases they report slightly higher normalised retained strengths than reported here: for example at 450 °C, a reduction of 50 – 55 % compared to 65 %, or 10 – 15 % at 350 °C where a loss of around 20 % at 300 °C was found. These differences are most likely attributable to the fact that the fibres used in this work had a lower weight percentage of coating applied to them, although differing glass compositions or thermal histories may also have had an effect.

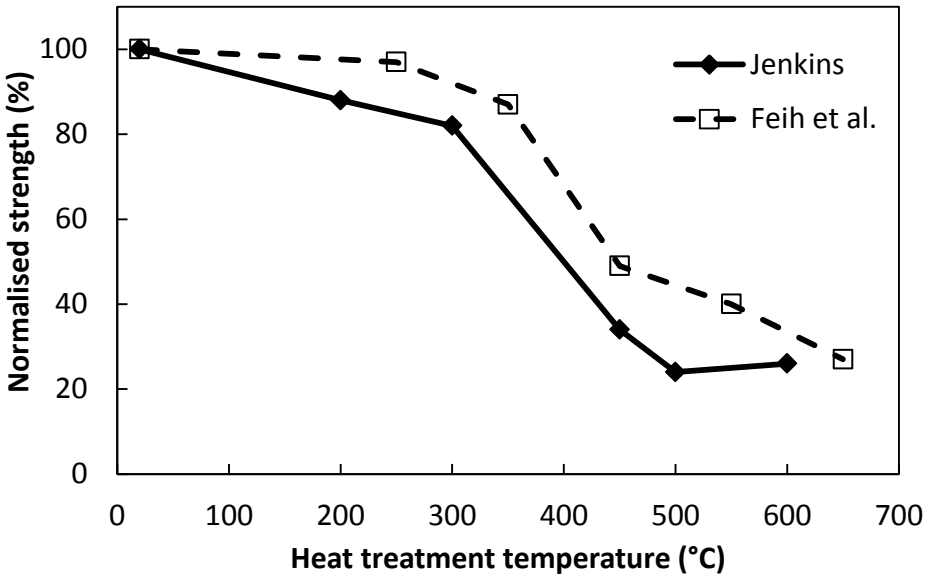

Figure 4-3: Comparison of normalised strengths of APS sized fibre (from Figure 4-2) with silane sized fibre reported by Feih et al. [65]

4.3 Single fibre heat treatment

4.3.1 Motivation

It was noted heuristically, during the mounting of single fibre tensile samples, that the separation of single fibres from a heat treated bundle became progressively

more challenging following heat treatment at higher temperatures. Consequently fibres broke more frequently during manual removal from the bundle despite the best efforts not to stress them in tension or bending. These observations led to the supposition that when a fibre is removed from a bundle that has been heat treated, even though it may not break, it may be subjected to some damage. This would weaken the fibre leading to an erroneous result, underestimating its true strength. To eliminate this potential source of error the single fibre heat treatment procedure was developed, as outlined in 3.2.1.2. This approach draws on the methods used by early researchers such as Thomas [5] and Cameron [6]; in their work heat treatments were naturally performed on individual fibres as their laboratory equipment produced these rather than multi-fibre rovings typical of commercial production.

4.3.2 Results – bundle versus single fibre heat treatment

The bundle heat treated data from Figure 4-2 are presented again alongside data obtained using the single fibre heat treatment procedure in Figure 4-4. Retained fibre strength decreased with an increase in heat treatment temperature; this was true generally for both fibre types and regardless of which of the two methods of heat treatment was used. Concerning the data produced using single fibre heat treatment, the difference in average strength between bare and APS sized fibre was reduced as the heat treatment temperature increased. Following treatment at 600 °C no difference in strength was measured. This differs from the bundle heat treatment data which converged at a lower temperature of 500 °C.

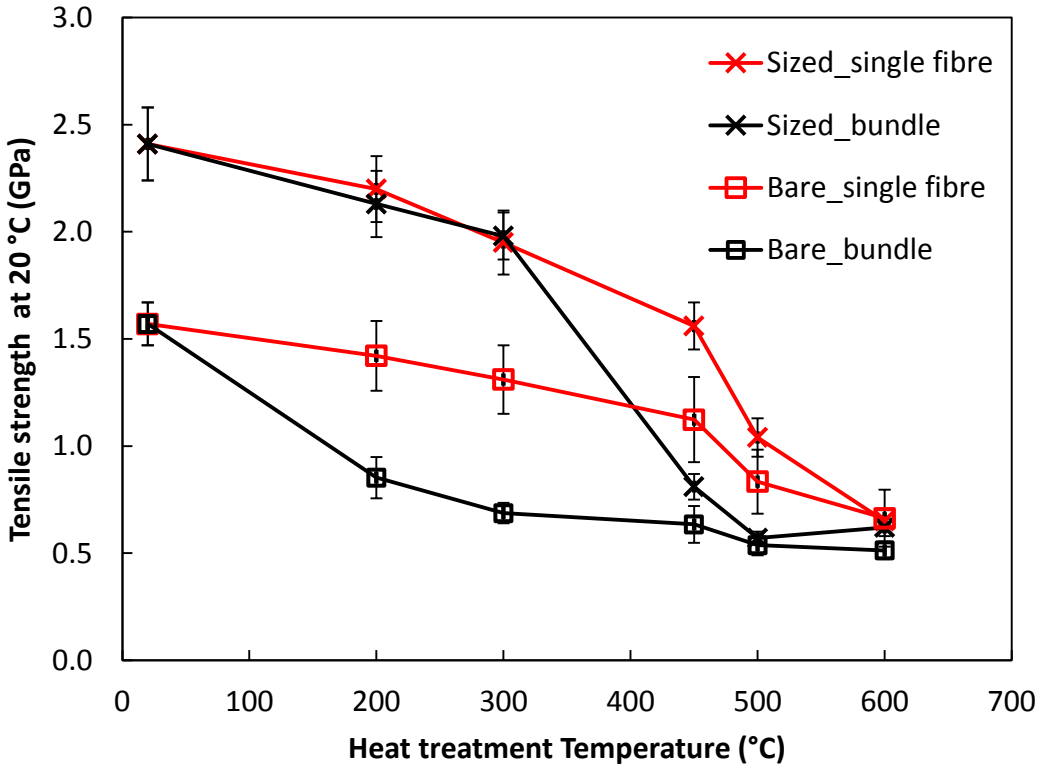

Figure 4-4: Tensile strengths of bare and APS sized fibres after heat treatment for 25 minutes

Both bare and sized fibre retained a significantly greater strength when heat treatment was carried out on single fibres rather than bundles. For bare fibre, this difference was evidenced at temperature as low as 200 °C, whereas for the sized fibres it occurred after heat treating above 300 °C. Considering only the data obtained using single fibre heat treatment (red lines) a similar trend in the data was observed. For both sized and bare fibre the most significant decrease in strength occurred upon increasing the conditioning temperature from 450 to 500 °C. In the case of bare fibre strength data, this was the only temperature step which caused a statistically significant decrease, i.e. from room temperature to 200 °C or 500 to 600 °C, for example, the difference between strengths was not significant.

4.4 APS degradation and its effect on retained strength

Even a cursory analysis of the data presented in Figure 4-2 and Figure 4-4 indicates that the APS surface coating has a significant effect on retained fibre strength following heat treatment. This is particularly clear in the data in Figure 4-2, generated using bundle heat treatment. Furthermore, comparing the effect of heat

treatment method used on the strength retention of sized fibre, Figure 4-4, the trends obtained were dissimilar. An investigation into the degradation of APS was carried out to provide further information to explain these observations.

4.4.1 Direct measurements of APS degradation on E-glass fibre

A common technique available when analysing silane degradation is Thermo-Gravimetric Analysis (TGA) which can be performed under air or nitrogen [65]. This may be feasible when working with glass fibre to which a full sizing has been applied. However, as noted (in 3.1) the fibre utilised in these investigations was coated with only the silane coupling agent (APS) rather than a multi-component sizing. This overall very small weight percentage (wt%) surface coating made TGA measurements extremely challenging, therefore other methods of generating information about the state of the surface coating of heat treated fibres were sought.

4.4.1.1 XPS analysis

Surface chemical analysis of heat treated fibre bundles was carried out using XPS. This technique is highly surface sensitive, generally allowing investigation of no more than the top 10 nm of a material, therefore any surface contamination present has a significant effect on the results. Such surface contamination is generally carbon based so the quantified results are often corrected against this. However, the APS molecule contains carbon atoms in the propyl chain connecting the amine group with the silicon atom; for this reason all of the carbon (C1s) signal measured by the instrument cannot be attributed to unwanted surface contamination. The quantified values for nitrogen content presented in Figure 4-5 have therefore not been carbon corrected. Changes in surface carbon content cannot be distinguished between those attributable to removal of carbon-based contamination or to degradation of the APS coating.

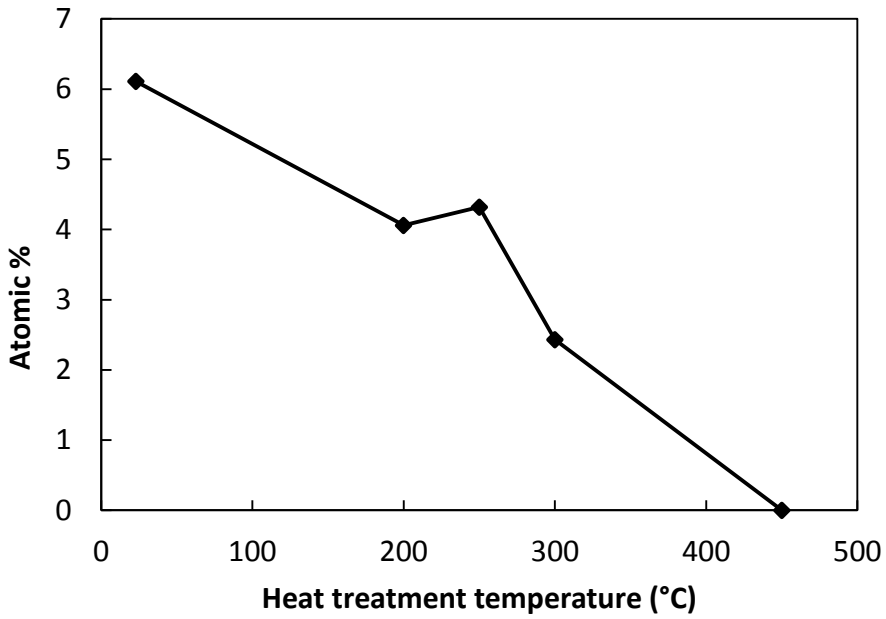

Figure 4-5: quantification of nitrogen surface content from N1s peak (from survey scan)

An immediate decrease in nitrogen content occurred following heat treatment at 200 °C; an almost linear decrease with increasing conditioning temperature was found with the exception of the result after 250 °C heat treatment. Most importantly, these results showed zero remaining nitrogen signal following heat treatment at 450 °C strongly suggesting that the amine component of the silane had been volatilised; based on these data alone it is not possible to assess the degree of degradation of the rest of the organic components. This value is higher than that reported by Tiefenthaler and Urban [96] who suggested that 300 °C was sufficient to remove γ-APS from Nextel fibres whose constituents were alumina, silica and boron oxide. A possible explanation for this difference is that in their study fibres were heat treated for 1 hour, more than twice as long as the samples in this work. However, their findings for fibres heated at 200 °C suggested that approximately 60 % of the coupling agent remained which is in close agreement with the result shown in Figure 4-5.

4.4.1.2 SEM observations

Direct observation of heat treated APS sized fibres was made using SEM (3.3.2.2). Attempting to draw conclusions on the basis of SEM images alone can be misleading; multiple explanations for observed features may be proposed with equal validity and in some cases they may be nothing more than an ambiguous artefact. For this reason tens of millimetres of fibres were inspected at each condition and

within these examined sections at least 20 images captured for record and close inspection. Lengths of fibre in between those selected for imaging were still inspected visually using the live view from the SEM. Only features with high frequency and repetition were considered as indicative of a trend; nonetheless, it is accepted that this type of evidence is not fully objective and rigorous. The surface of an untreated APS sized fibre is shown in Figure 4-6.

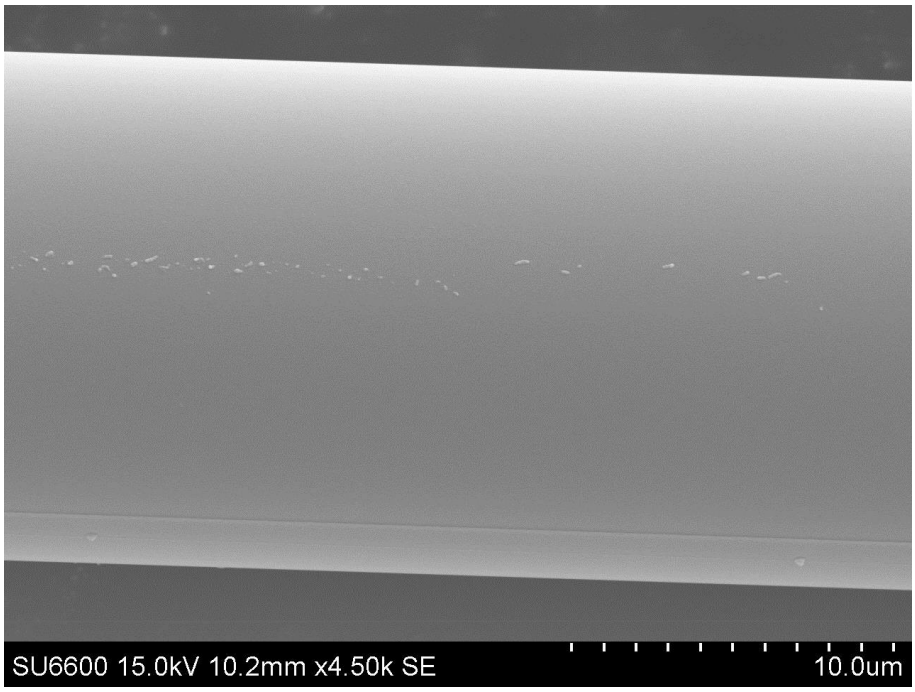

Figure 4-6: SEM image of typical unconditioned APS sized fibre

This image is representative of the unconditioned fibre surface. A small amount of surface contamination, white particles of less than 500 nm size, are commonly observed. Also visible on the vast majority of SEM images are bands running longitudinally along the fibre length, similar to the one near the bottom of Figure 4-6. These may well represent the points at which fibres within the roving were in contact with one another prior to separation.

A typical SEM image of a fibre heat treated at 450 °C is shown in Figure 4-7.

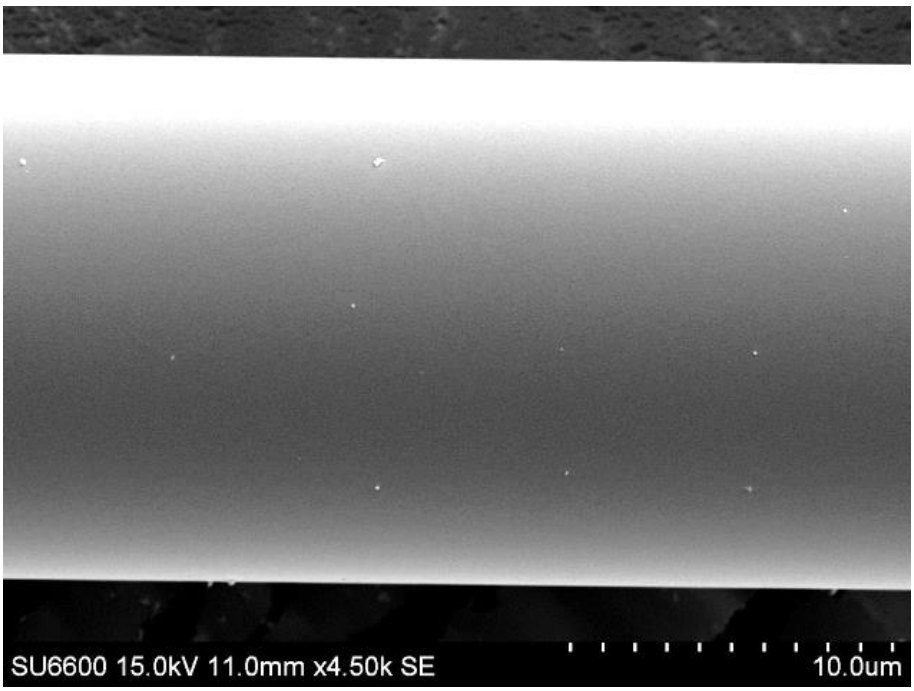

Figure 4-7: SEM image of APS sized fibre, single fibre heat treated at 450 °C for 25 minutes

The surfaces of fibre treated at 450 °C were predominantly featureless as shown. In general they appeared largely similar to non-heat treated APS fibres, with some small contaminant particles and the longitudinal banding possibly associated with fibre-fibre contact. Observations similar to these were made on fibres heat treated at all of the temperatures at which retained tensile strength was tested, with the exception of 300 °C. A representative image of a fibre heat treated at 300 °C is shown in Figure 4-8.

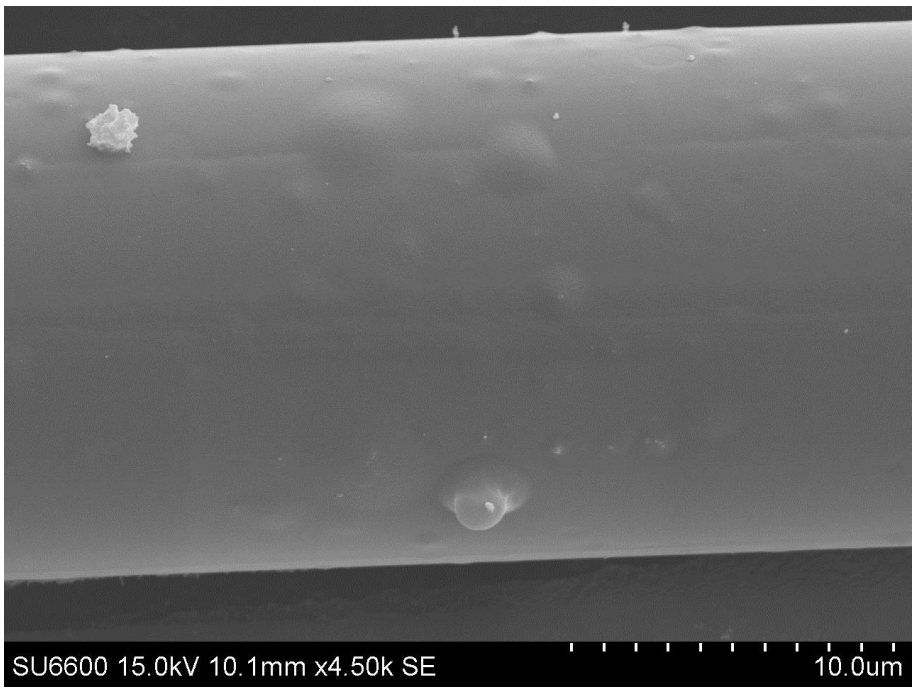

Figure 4-8: SEM image of APS sized fibre, single fibre heat treated at 300 °C for 25 minutes

Fibres treated at this temperature exhibited areas of what appear to be convex, dome-like, structures dispersed randomly across the fibres. It is suggested that the convex structures are created by the volatilization of the APS surface coating – much the same as might be observed on a painted surface that is subject to high temperatures. Correspondingly, a temperature of 300 °C would appear to be critical for the sized fibre under investigation; this is approximately the temperature at which most significant volatilisation of the silane coating may initiate (as suggested by mass loss curve in Figure 4-9), such that its ability to provide sufficient protection to the fibre surface begins to be compromised.

4.4.2 Indirect analysis of APS degradation using APS film

4.4.2.1 TGA/DSC results

In order to provide further evidence regarding the thermal degradation of APS, and its effect on retained fibre strength, thermal analyses were conducted using samples of a prepared APS film as described in 3.1. Results of simultaneous TGA/DSC, confirmed by repeat analyses, are presented in Figure 4-9. The shape of the mass loss curve alone was also confirmed by performing dedicated TGA using a larger sample mass in an alumina beaker.

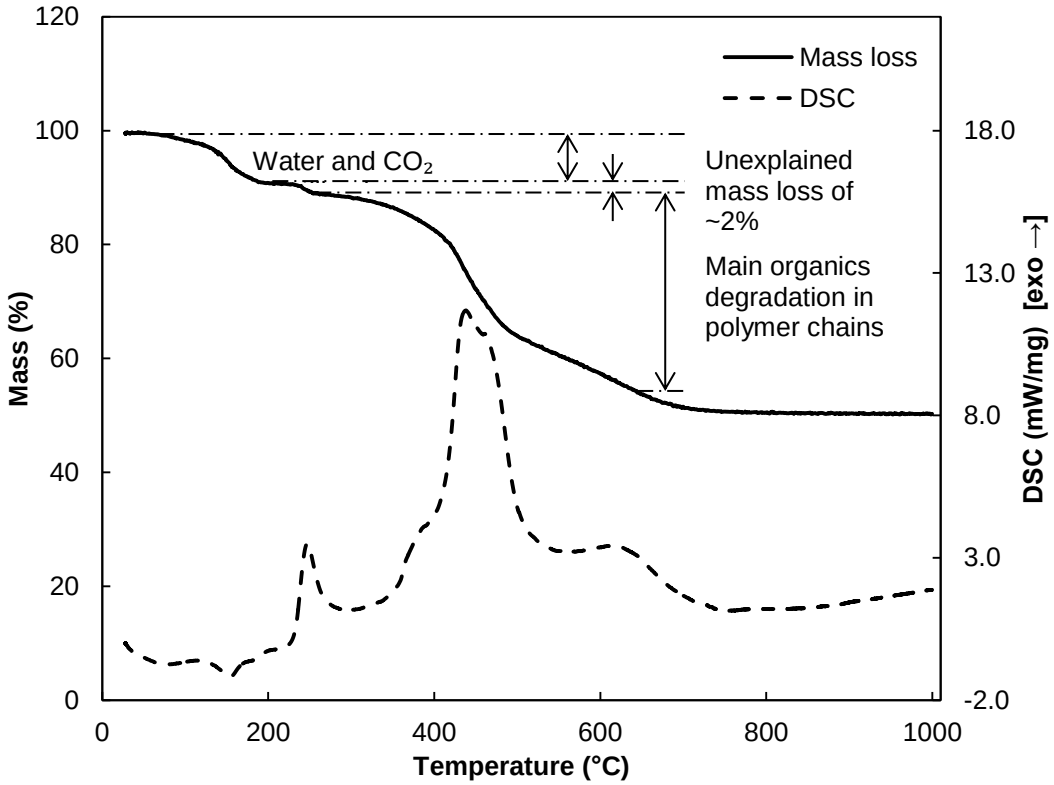

Figure 4-9: Simultaneous TGA/DSC of APS film, measurement performed under air

An initial endothermic process was found in the range 20-225 °C, during which a mass loss of almost 10 % occurred. The volatilisation reaction of the APS film became rapidly exothermic beyond approximately 225 °C and the lowest of three peaks occurred at 245 °C. The region of maximum mass loss of the film commenced at around 300 °C with the maximum rate of mass loss occurring at around 440 °C. This corresponded with the largest exothermic peak in the DSC data.

4.4.2.2 CATLAB analysis of thermal degradation products

In parallel with mass loss data obtained by TGA, chemical data regarding the thermal degradation products from APS film were generated using a CATLAB system as described in 3.7.2. One limitation of this system is the effect of the purge gas on collection of results: using air as the furnace carrier gas produces very strong signals in the mass spectrum at mass numbers 28 (N_2) and 32 (O_2) for example. Another potential issue is the presence of even very small amounts of water, which can complicate results at mass numbers 17 and 18. These signals can obscure the degradation products of the material under study; for this reason helium, with very

high purity and dryness, was selected as a suitable furnace carrier gas. The use of helium in the furnace chamber means that oxidative reactions cannot take place, unless oxygen is produced by thermal degradation of the sample. It was therefore necessary to first compare the oxidative and non-oxidative mass loss of APS in the TGA.

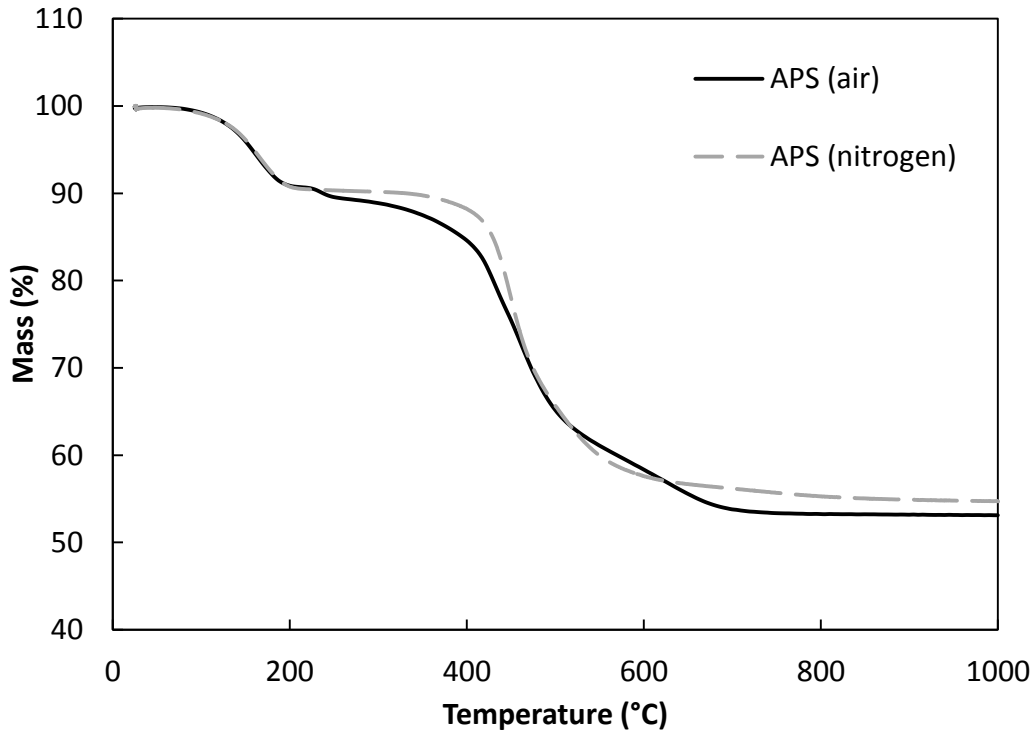

Figure 4-10: Comparison of mass loss curves by TGA of APS film analysed under air or nitrogen

In Figure 4-10 the mass loss curves of APS film analysed under both air and nitrogen are presented. A broadly similar trend was evident regardless of the furnace atmosphere used. Mass loss was identical up to approximately 220 °C; in the range 220 – 240 °C there was a mass loss of around 2 % in the air TGA data (noted in Figure 4-9) which was not seen in the analysis under nitrogen. The maximum rate of mass loss occurred between 400 – 500 °C in both cases, but the onset of this region of degradation occurred at lower temperature under air. Final mass loss upon reaching the maximum temperature of 1000 °C was greater by 1.5 % for the sample heated under air, although at this stage the nitrogen TGA mass was still decreasing while the air TGA signal had reached a steady state value.

The thermal behaviour of APS heated under air and nitrogen was also analysed by DSC. The data produced under air from Figure 4-9 are presented alongside those obtained under nitrogen, in Figure 4-11.

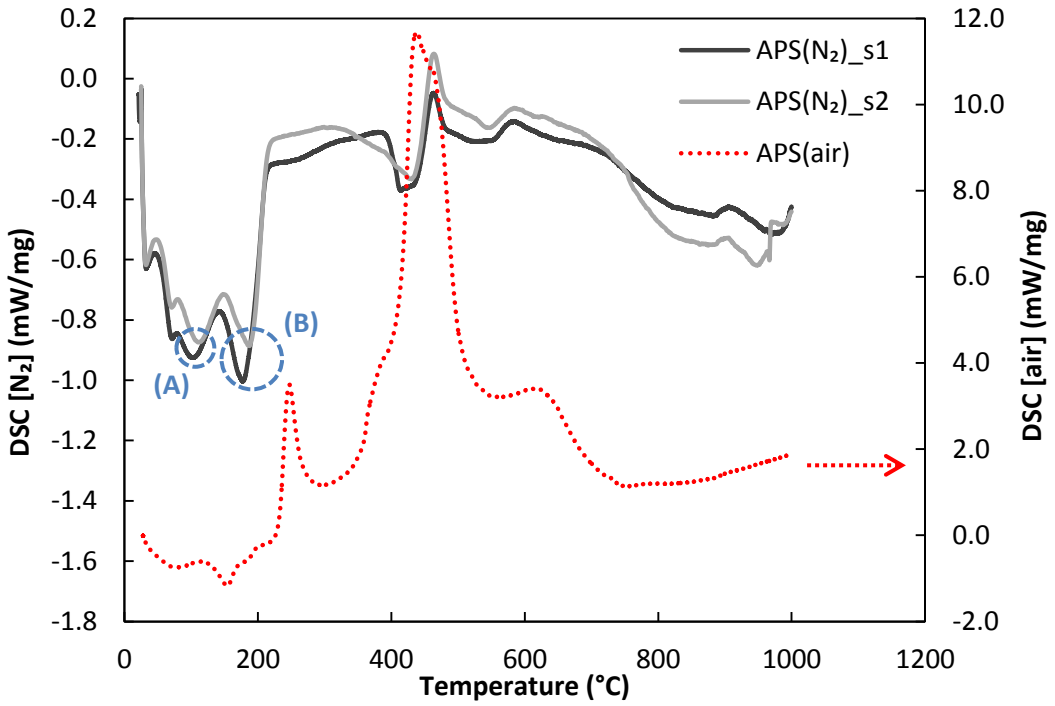

Figure 4-11: DSC of APS film analysed under air (red dotted) and nitrogen (grey and black solid)

Under both furnace atmospheres an endothermic region was found below 200 °C. The highest peak in all three datasets was between 430 – 450 °C, corresponding to the region of most rapid rate of mass loss (Figure 4-10).

Results of CATLAB degradation analysis for 4 mass numbers (17, 18, 28 and 44) are presented in Figure 4-12. The relative intensities of all mass numbers from 2 – 200 were analysed but those shown in Figure 4-12 represented the most intense signals over that range.

From room temperature to approximately 200 °C strong peaks in the data for AMU 44 and 18 were produced, with smaller peaks at AMU 17 and 28. There appear to be some correlations between endothermic peaks – labelled (A) and (B) in Figure 4-11 – and those obtained by CATLAB analysis. Peak (A) at 100 °C corresponded to the evolution of water from an APS film sample at the same temperature as indicated by Figure 4-12 (a). The second endothermic peak in this temperature range occurred between 165 – 185 °C; in this approximate range the latter part of a peak in the evolution of AMU 44, associated with CO_2, was found as indicated in

Figure 4-12 (c). Initiating at around 300 °C there was a sudden increase once again in the relative intensity of mass number 17. It peaked below 400 °C and thereafter rapidly decreased at approximately the same rate as the original increase. When a temperature of 350 °C was reached there was also a very significant increase in the intensity of mass number 28. An initial peak in these data occurred at approximately 400 °C; a second less defined peak also occurred between 450 – 460 °C. The relative intensity was greatest for AMU 28, in comparison with the other analysed molecular masses, from above 425 °C up to the maximum analysis temperature of 550 °C.

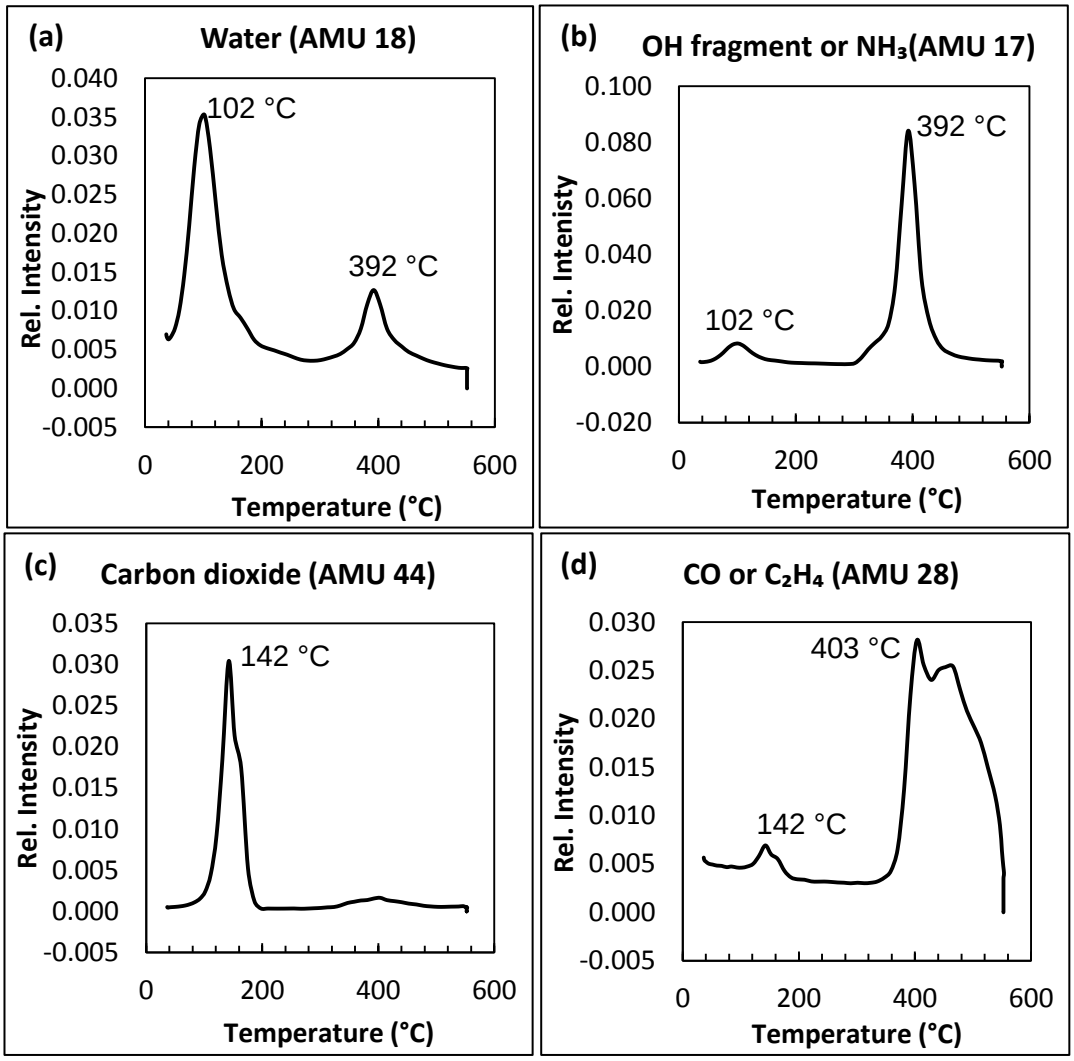

Figure 4-12: CATLAB degradation profiles of (a) AMU 18 [water], (b) AMU 17 [OH- water fragment or NH_3], (c) AMU 44 [CO_2] and (d) AMU 28 [CO or C_2H_4]. Measurements carried out under helium atmosphere

4.4.3 Discussion of thermal analysis results

4.4.3.1 Applicability of results

Results obtained using TGA, DSC and CATLAB were analysed alongside each other in order to attempt to explain the degradation behaviour of APS and, in turn, the strength behaviour of E-glass fibres with an APS coating following heat treatment. Clearly, the two cases of an APS coated fibre (or fibre bundle) and a sample of pure APS film are distinct; the weight percentage of APS on the surface of the fibre used in this work was orders of magnitude less than the pure APS film with which thermal analyses were carried out. However, one of the currently accepted models of the APS coated glass fibre surface suggests that the APS exists as a disordered, cross-linked polymeric network which is largely bonded to its own molecules, with only a thin layer also bonded to a glass surface [92]. The structures of APS film and coated fibre may therefore be relatively similar, so that experimental results obtained for one may be applicable to the other.

Distinctions between oxidative and non-oxidative degradation of APS are also pertinent in this discussion. Fibres (Figure 4-4) were heat treated in air, TGA/DSC was performed under air and nitrogen and CATLAB analysis was carried out under helium. It is evident from the TGA and DSC data (Figure 4-10 and Figure 4-11) that the heating atmosphere has an effect on APS thermal degradation, although the trends are broadly similar. TGA data are identical at lower temperature and the maximum rate of mass loss occurs in the same range. In addition, the DSC data show a maximum exothermic peak at similar temperatures, associated with high rate of mass loss. It is likely that the degradation reactions differ under air or inert gas but the mass loss is broadly similar; a maximum difference of 5 % occurs at approximately 430 °C (shown in Figure 4-10). In the context of the APS sized fibre heat treated under air, a similar amount of its protective surface coating would be removed if treatment was performed using a nitrogen filled furnace, although some discrepancies would occur in the range 350 – 440 °C. Non-oxidative degradation results obtained using CATLAB are considered nonetheless to remain informative in the discussion of APS degradation under air, in the cases of both APS films and APS coated fibres.

4.4.3.2 Initial mass loss region (room temperature → T = 220 °C)

The initial endothermic region in which approximately 10 % mass loss occurred was found to be largely attributable to the evolution of water from the APS film. In Figure

4-12 (a) a strong peak for water (AMU 18) is shown; a corresponding weaker peak for the common water mass spectrum fragment (AMU 17) was found at the same temperature. This water comes in small part from water trapped during the preparation of the film from aqueous solution and in large measure from the condensation reaction that occurs during the curing of the APS film as it forms a cross-linked polymer network [101]. Chemical degradation analysis also showed considerable evolution of CO_2 from the film below 200 °C, as indicated by Figure 4-12 (c), which may contribute along with water to the initial mass loss measured by TGA. The source of this CO_2 was not believed to be from the degradation of any part of the APS film but rather was due to the release of bound atmospheric CO_2. It has been shown by Culler et al. [102] that triamine coated E-glass mats dried under air will produce trapped CO_2 gas when subsequently heated above 100 °C.

A mass loss of approximately 2 %, initiating at 220 °C, was noted in Figure 4-9. The same phenomenon was not observed in TGA of APS carried out under nitrogen; therefore it is suggested that it is the product of some oxidative degradation reaction. The precise nature of this is not yet understood; however, there is evidence of a correlation between fibre heat treatment in this temperature range and an apparent loss of surface functionality [103]. This correlation, though, is somewhat problematic as the referenced work was carried out using glass fibres with an industrial surface sizing containing numerous chemical components of which only one is APS. The significant loss in composite tensile and impact strength due to treatment of the fibres at 250 °C may be an effect of other factors, other than degradation of the silane coupling agent.

Regarding the magnitude of mass loss, of around 1.5 – 2 %, it is assumed that as this occurred well above 200 °C – by which temperature all remaining water and adsorbed CO_2 was removed – it should be related to degradation of the APS itself. Following thermal degradation up to 1000 °C a residual mass of over 60 % remained (Figure 4-9) consisting of the inorganic Si-O-Si structure of the APS film; degradation of the propyl chain and terminating primary amine is therefore responsible for mass loss at lower temperatures. A model of the hydrolysed and condensed APS structure is given in Figure 2-10. Depending on the degree of condensation, each Si atom shares a certain number of its oxygen atoms with neighbouring Si atoms: for example oligomers as shown in Figure 2-10 may

possess 2.5 or 3 oxygens per silicon atom, whereas in the silane network it is significantly lower with only 1.5 oxygens per silicon.

The degree of condensation achieved within the APS films studied using TGA was not analysed, therefore the appropriate number of oxygen atoms per silicon can only be estimated. It is likely to be within the range 1.5 < O:Si < 3 as the structure consists neither of only isolated oligomers nor a fully condensed network. Using a value of 2 or 2.5 oxygens per silicon it is possible to calculate the atomic mass of an effective 'monomer' unit of for the APS film of 118.1 or 126.1 respectively. These values are close and, for either, a mass loss of 1.5 – 2 % as observed in the TGA data corresponds to a loss of around 2 atomic mass units. In the APS network this is only possible through the loss of 2 hydrogen atoms; from either the primary amine or the propyl chain. Whether this is in fact the explanation for the observed but unexplained mass loss would require further investigation, possibly using a combination of isothermal TGA experiments and chemical analysis of the APS film both before and after heating.

4.4.3.3 Significant mass loss region (T > 300 °C)

The region of most significant mass loss initiated at approximately 300 °C, based on TGA data obtained under air; under nitrogen a slight delay was observed to this decrease in mass until 350 °C was exceeded. The mass loss initiating in this temperature range progressed rapidly, regardless of atmosphere, as temperature was further increased. A consistent and significant mass loss over the wider temperature range 400 – 600 °C was clearly observed, with maximum rate between 430 – 450 °C. This corresponded to the degradation of the organic, non-chain forming, fraction of the aminosilane polymer chain. CATLAB data showed that, between 300 – 350 °C, the relative intensity of mass number 17 increased. Within this temperature range there was no significant change in the intensity of AMU 18; this suggested that the change in intensity at AMU 17 was not associated with the evolution of water fragments, as it was at low temperature (Section 4.4.3.2). A probable alternative is, instead, the volatilisation of protonated amine groups, NH_3^+. The relative intensity of AMU 17 decreased following its peak at 400 °C and returned to the baseline 'zero' value between 450 – 500 °C. This compared with XPS results (Figure 4-5) in which amine groups (at least at the surface) were shown to have been eliminated by treatment at 450 °C. The discrepancy in these results may be explained by differences in heating atmosphere (XPS on air heat treated

samples, helium during CATLAB analysis) and the dynamic heating rate used during CATLAB.

Moving above 400 °C into the region of maximum mass loss of APS film, another significant feature in the chemical degradation analysis was noted. In Figure 4-12 (d) a rapid increase in the intensity of AMU 28 in the mass spectrum was measured between approximately 350 – 400 °C; a strong signal was observed up to the maximum experiment temperature as described in Section 4.4.2.2. This was attributed to the volatilisation of C_2H_4, which was a product of the direct fragmentation of the propyl chains of the cross-linked APS polymer occurring once the temperature had exceeded 350 °C. Further evidence of this fragmentation of the propyl chains in the APS polymer is shown in Figure 4-13. The mass spectrum for AMU 42, attributed to the un-fragmented propyl chain C_3H_6, is presented superimposed with the data obtained for mass number 28. The peak at 140 °C for AMU 28 is not relevant in this discussion: as shown by Figure 4-12 it is paired with, but less intense than, the peak for AMU 44, associated with CO_2. It is therefore suggested that it is associated with the detection of CO rather than a fractured hydrocarbon chain.

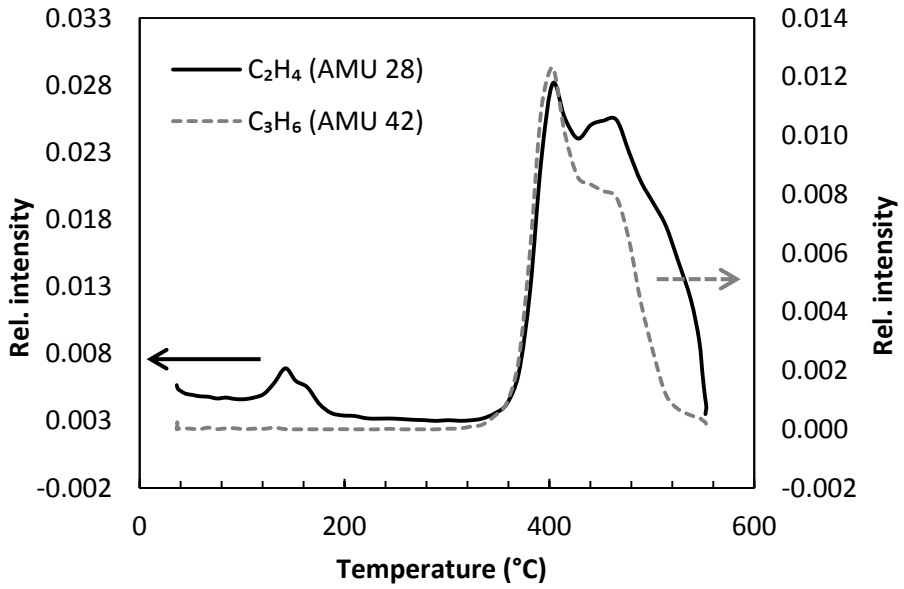

Figure 4-13: CATLAB degradation profiles of AMU 28, C_2H_4 [black solid] and AMU 42, C_3H_6 [grey dotted]. Measurements carried out under helium

The total relative intensity of AMU 42 is less than AMU 28, but they share an almost identical rapid increase at 350 °C and a narrow peak at 400 °C. At approximately 430 °C the data deviate significantly; the relative intensity of mass number 42

continues to decrease but there is a secondary increase in mass number 28. This may be explained by the effect of continuously increasing temperature; propyl chains are further fragmented creating a higher relative intensity of shorter chains such as C_2H_4.

From the data produced by both TGA and CATLAB it is evident that significant degradation of APS takes place at elevated temperature. This effect initiates at around 300 – 350 °C, depending on the nature of the treatment atmosphere (oxidative or non-oxidative). At above 400 °C, rapid and significant mass loss occurs and it has been shown that this is due to the volatilisation of the organic fraction of the APS polymer. With respect to APS sized heat treated fibres these conclusions indicate that their protective surface coating rapidly degrades once a temperature of approximately 300 °C is exceeded. The initial stages of this process may be what can be observed in the SEM image shown in Figure 4-8. The effect of this phenomenon on the retained strength of heat treated fibre is discussed in Section 4.5.

4.4.4 Summary of results

The significant findings of the results pertaining to the degradation of APS, both in film form and on the surface of glass fibres, are summarised in Table 4-1.

Table 4-1: summary of principle findings regarding degradation of APS film and APS on surface of glass fibres

	Temperature (°C)	Description of event	Experimental evidence
Fibre	300	Volatilisation of APS on glass fibres	SEM pictures (Figure 4-7 and Figure 4-8)
	450	Complete removal of nitrogen from APS	XPS data (Figure 4-5)
APS film	0 – 200	Loss of water followed by CO_2	TGA (Figure 4-9), DSC (Figure 4-11), CATLAB (Figure 4-12)
	400 – 600	Rapid and significant degradation of organics	TGA (Figure 4-9), DSC peak at 450°C (Figure 4-11), CATLAB (Figure 4-13)

4.5 Mechanical handling and thermal damage of heat treated glass fibre

4.5.1 Interpretation of bundle heat treatment results with APS degradation

The strength loss profiles of bundle heat treated fibre, both APS coated and unsized, were shown in Figure 4-2. The trends found can be understood by considering the evidence presented regarding the degradation of APS, on fibres and in its pure form. The presence of this aminosilane on the fibre surface enhances the ability of fibres to retain their tensile strength; unsized fibres by design have no such protective effect. When heat treated at a relatively low temperature of 200 or 300 °C, the unsized fibre strength decreased to around half of its original untreated value. By contrast the sized fibre strength was reduced by significantly less; a 12 and 18 % decrease was measured at 200 and 300 °C respectively. Following heat treatment at 450 °C the sized fibre strength dropped dramatically, however, to just a third of its

untreated value; only slightly greater than the strength of bare fibre. This difference disappeared entirely following heat treatment at 500 °C.

These results can be well reconciled with those regarding APS degradation, obtained by XPS and thermal analyses. At 300 °C the APS coating has undergone some degradation, as shown by SEM, XPS and TGA but it remains in the early stages of this process. After heating to 450 °C and above, however, significant degradation of the organic fractions of the silane has occurred. It is thus unable to provide protection to the glass fibre surface. Therefore, the most significant decrease in the strength of sized fibres occurs between 300 – 450 °C; while for unsized fibre the largest decrease is between room temperature and 200 °C. Both of these drops in retained strength are related to an absence of protective coating on the surface of heat treated fibres.

During sample preparation of both bare and APS sized fibre it was found that it became generally more difficult to extract single fibres from a heat treated bundle as the conditioning temperature used was increased. It has been shown for silica that the surface concentration of Si-O-Si bridges increases with temperature [19]. It is proposed that a similar process occurred at the surfaces between fibres within a roving, creating an inter-fibre bonding effect. Following heat treatment, fibres were separated from one another in the roving therefore any bonds formed with neighbouring fibres were broken. The breakage of these bonds introduced surface damage, or produced structures around which concentration of stresses could occur. Significant weakening of the fibre was attributed to this effect – referred to as mechanical handling damage – at treatment temperatures where the fibre surface was not protected by a coating: that is at all temperatures at which bare fibre was conditioned and at 450 °C and above for the treatment of APS fibre. The mechanical handling damage effect can obscure the strength loss that may be attributable to other thermal effects, such as those discussed in 2.3.1, and so the strength of fibres heat treated using bundle heat treatment can be significantly underestimated. Minimising mechanical handling damage by adopting the single fibre heat treatment procedure, and the implications to the discussion of fibre strength loss, are outlined in Section 4.5.2.

4.5.2 Interpretation of single fibre heat treatment results with APS degradation

4.5.2.1 Room temperature to 300 °C

A statistically significant decrease in fibre strength of approximately 20 % of the original value occurred following heat treatment to 300 °C, for both sized and unsized fibre. This strength loss of sized fibre at relatively low temperature is consistent with similar published data [65]. Results using pristine bare E-glass have also shown such a decrease in strength, but it is interesting that the commercial E-glass also experiences a strength drop at these relatively low temperatures.

The average strengths measured for APS fibre at both 200 and 300 °C were not affected by the change in heat treatment method from bundle to single fibre. This demonstrates that the introduction of mechanical handling damage to fibres does not occur when the silane surface coating remains largely intact; results presented in Section 4.4 strongly suggest that at 300 °C the degradation of APS is minimal in terms of total mass loss, although XPS results suggested a 60 % decrease in nitrogen at the surface based on the N1s signal. By contrast, the results obtained using bare fibre show that heat treating as single fibres facilitated a significantly greater strength retention; in the region of 70 – 90 % higher than when using bundle heat treatment. This difference in strength is revealed simply by separating single fibres prior to heat treatment, thereby minimising the degree of handling damage experienced.

This disparity in strengths, influenced by the heat treatment method used, is of critical importance with respect to investigation of glass fibre strength loss. When single fibre heat treatment is employed and great care is taken to avoid fibre surface damage, any changes in the single fibre strengths measured thereafter can be attributed to some thermally induced mechanism or mechanisms. On the other hand, fibres that are bundle heat treated may be subjected to an unknown degree of mechanical handling damage, in addition to the thermal damage process(es) that will act. The bundle heat treatment method is therefore insufficient as it may easily lead to erroneous strength measurements; specifically an underestimation of tensile strength after a given heat treatment temperature.

4.5.2.2 450 to 600 °C

The region of most significant strength loss using single fibre heat treatment was in excess of 450 °C. The explanation for this result may be at least partly found in the literature. A constant treatment time was utilised in all heat treatments; however it is known (2.3.1) that at lower temperatures a greater length of time is taken for the fibre strength to decrease to an asymptotic minimum value at that given temperature. In this case the strengths of single fibres heat treated at 200 and 300 °C (and potentially 450 °C) for sufficiently long are expected to be significantly lower than the values presented in Figure 4-4, following a 25 minute heat treatment. In the context of the investigation of the strength loss of heat treated glass fibres, and the thermal mechanisms involved, the time dependent minimum strength phenomenon is not problematic. A region of significant strength loss, due to only thermal effects, was identified. This finding informed all following experimental investigations into the fundamental mechanism(s) responsible for the strength loss. Using a consistent total heat treatment time of 25 minutes, a temperature in excess of 450 °C was necessary to cause the most severe thermal damage hence investigations into the underlying mechanisms focused most strongly on this temperature range.

4.5.2.3 Heat treatment beyond 600 °C

A maximum heat treatment temperature of 600 °C was utilised for the comparisons of both bare with APS fibre, and single fibre with bundle treatment. A similar maximum temperature of 600 – 650 °C has been used in numerous studies of the effect of heat treatment on fibre strength [5, 62, 63, 65] and of the effect of thermo-mechanical recycling on the strength of fibres extracted from composites [67]. Investigation of E-glass fibres treated to 700 °C are unusual but have been reported for lab-produced fibre [51]. An attempt was made to measure the strength of the commercial E-glass utilised in this work following treatment at 700 °C. This is within 10 % of the glass transition temperature of this formulation which has been reported as approximately 760 °C [76].

Unsized fibres were heat treated using the single fibre method. APS fibres were not studied; the strengths of both fibre types were shown in Figure 4-4 to converge at 600 °C and it was presumed that this would also be the case at higher temperatures. The strengths of bare single fibre heat treated samples over the range room temperature to 700 °C are presented in Figure 4-14.

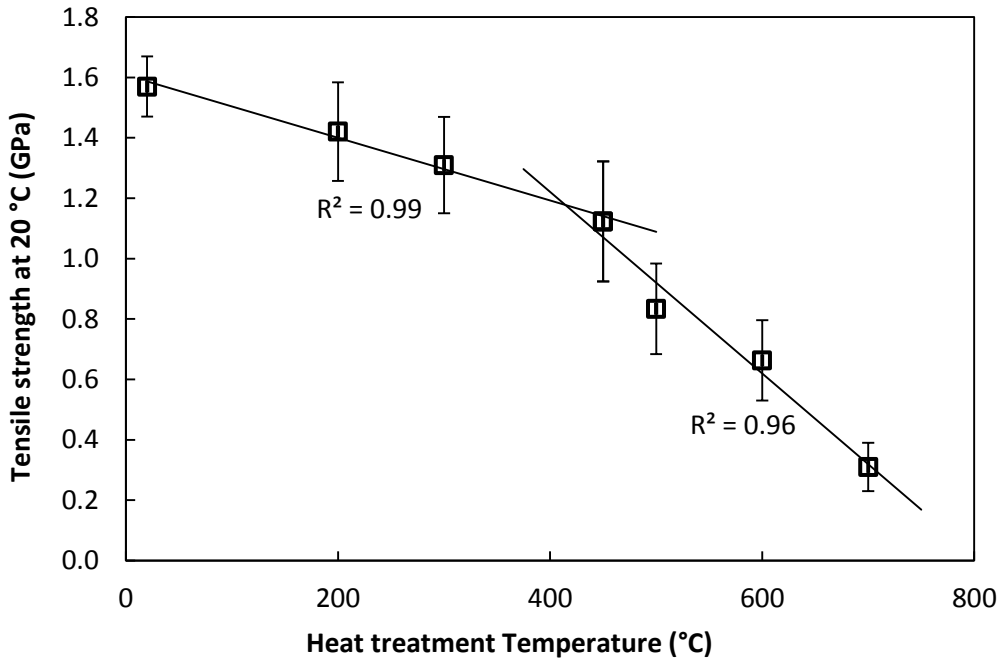

Figure 4-14: Tensile strengths of bare fibres after single fibre heat treatment for 25 minutes

Fibres heat treated at 700 °C were found to be extremely fragile, but through careful application of the single fibre heat treatment method 24 tensile specimens were manufactured. The survivability of these samples during the mounting phase of tensile testing was, however, very low and approximately half broke before testing. Of those that survived mounting, about 75 % fractured at the extreme edge of the gauge length where they were attached to the card tab. Following the acceptance criteria for fractured tensile test specimens outlined in 3.3.1.1 it was necessary to exclude these results from the calculation of average fibres strength. As a result only 2 acceptable successfully fractured single fibres were obtained, giving an average strength of 0.31 GPa. If the excluded single fibre strength values (of which there were 8) were included in calculation of a mean average strength, a value of 0.19 GPa was obtained. This suggests that it is correct to neglect these values from the analysis; the fibres failed at lower stresses, related to fibre bending or the influence of the glue used to affix them to the tabs. Inclusion of these values would thus give a significantly lower average not representative of the true fibre strength.

Although the sample size of only 2 is very low for a material subject to failure by brittle fracture, and is ten times less than the minimum in other strength measurements, the value of 0.31 GPa obtained fits the approximately linear behaviour of strength loss which can be observed between 450 – 700 °C in Figure

4-14. Furthermore, particularly between 500 – 700 °C, the strength loss of individually treated fibres occurs at its most rapid rate, such that the minimum fibre strength value will be obtained within the 25 minute heat treatment time. The continued decrease in strength suggests that the strength loss mechanism progresses with increasing temperature in this high temperature range.

4.5.2.4 Trend across whole heat treatment range

The use of single fibre heat treatment minimised the physical or mechanical handling damage to which some fibres were subjected during bundle heat treatment at the corresponding temperature. Results obtained using the bundle treatment method were shown not to be useful when attempting to examine the fundamental strength loss of glass fibres following heat treatment, in that mechanical handling damage was an uncontrolled variable contributing in part to strength loss. When changes in fibre strengths were measured following single fibre heat treatment, they could be reasonably stated to be an effect of a thermal damage mechanism.

The development of single fibre heat treatment, and its application over a temperature range 200 – 600 °C, revealed a characteristic strength loss profile for the commercial E-glass fibres used. The trend in strength loss was very similar for both APS coated and bare fibre; suggesting that the thermal source of fibre strength loss was not related to degradation of the surface coating. The thermal damage of fibres progressed most significantly at a temperature in excess of 450 °C. This reflects the understanding of glass fibre strength loss in the literature [5, 65] that at higher conditioning temperatures a minimum strength is reached more quickly. At a treatment temperature of 600 °C the strengths of both bare and APS sized fibre converged, suggesting the presence of a thermal based mechanism (or mechanisms) which was independent of fibre surface coating. Subsequent measurement of an even lower average strength following heat treatment at 700 °C proved that the convergence of strengths at 600 °C was not an artefact of a minimum measureable fibre strength due to the mechanical stresses associated with the testing procedures.

Chapter 5. Effect of moisture during single fibre heat treatment of bare fibre

5.1 Introduction

The ability of water to affect the strength of glass was discussed in 2.1.4.1; following fibre drawing, a stress corrosion reaction facilitated by water can cause a decrease in the tensile strength of glass fibres [29]. With respect to heat treatment of glass fibres, the effect of atmosphere has also been reported in the literature, as summarised in 2.3.3. Typically, heat treatment in air was compared with an inert gas. For bare fibres no effect on the retained tensile strength with change in the heat treatment atmosphere has been reported [51, 60]. Additionally, results for sized E-glass [65] showed no significant difference in strength following treatment for 2 hours at 450 °C under air or nitrogen; sufficient conditions that the protective effect of the sizing was likely neglected by either oxidative or non-oxidative degradation. In the same paper it was also reported that there was no effect on retained strength when treating under ambient or dried air. Together, these findings suggest that neither the moisture nor oxygen content of the atmosphere in which heat treatment is carried out have an effect on the retained strength of glass fibre.

An alternative method of minimising the oxygen and moisture content of the fibre treatment atmosphere is by conducting the experiment in a vacuum. Such an experiment has not previously been reported. A vacuum treatment environment also has the potential to facilitate an additional effect: it was shown by Zhuravlev [19] that the amount of physically adsorbed water on silica surfaces could be decreased by treating under vacuum at room temperature. It has been demonstrated that multi-layers of adsorbed water exist on the surface of bare E-glass fibres, as discussed in 2.1.4.1. In theory exposing such fibres to a sufficiently high vacuum could cause desorption of the physically adsorbed surface water. If a subsequent heat treatment was then performed in situ, the effect of the surface water on fibre strength loss could thus be investigated. Samples under vacuum would be treated in the absence of physically bound surface water, as opposed to furnace treatment where surface water is still present.

A system by which such a heat treatment could be achieved was developed utilising a Thermal Volatilisation Analysis (TVA) system. The details of the procedure developed are given in 3.2.2. These include the description of how fibres were mounted and how acceptable control of the temperature was achieved.

5.2 Characterisation of water desorption under vacuum in TVA system

Initial characterisation of the desorption behaviour of glass fibres under vacuum was carried out using manually chopped lengths of fibre, as described in 3.2.3.1. A relatively large mass of fibre in excess of 1 g was used such that a sufficiently high signal to noise ratio was obtained. Although a significant volume of data regarding vacuum pre-treatment and thermal desorption behaviour of water from samples was published by Zhuravlev [19] it was necessary to perform characterisation experiments using E-glass. Aside from the significant differences in material under study, details of the precise vacuum pressures used were not given in [19].

The capabilities of the TVA vacuum system used in this work were tested by altering the length of time for which samples were held at room temperature and a pressure of less than 10^{-2} mbar absolute. Samples were held for 0, 1 or 2 hours under vacuum at room temperature; in reality the 'zero' hour experiment was under vacuum for the minimum possible time between stabilisation of the pressure at approximately 10^{-2} mbar and switching on of the furnace program used. This time period was estimated as 40 ± 10 minutes. In the latter cases, once the aforementioned vacuum pressure was achieved they were left for a further 1 or 2 hours to 'pre-dry' under vacuum. During the pre-drying phase all volatilised products were allowed to pass through the system, eliminating them from analysis. Before beginning the furnace program, however, the sample trap was cooled with liquid nitrogen such that the volatiles produced during heating were retained for analysis. Heating the sample up to 500 °C under vacuum should be sufficient to remove any physically adsorbed water on the glass surface: in addition, this temperature is high enough to remove any hydroxyls that are bound through a hydrogen bond [19].

The volatiles captured from three manually chopped unsized glass fibre samples, pre-dried under vacuum for between 0 – 2 hours, were transferred to a gas IR cell

and analysed as outlined in 3.2.3.1. The results of the IR analyses are presented in Figure 5-1.

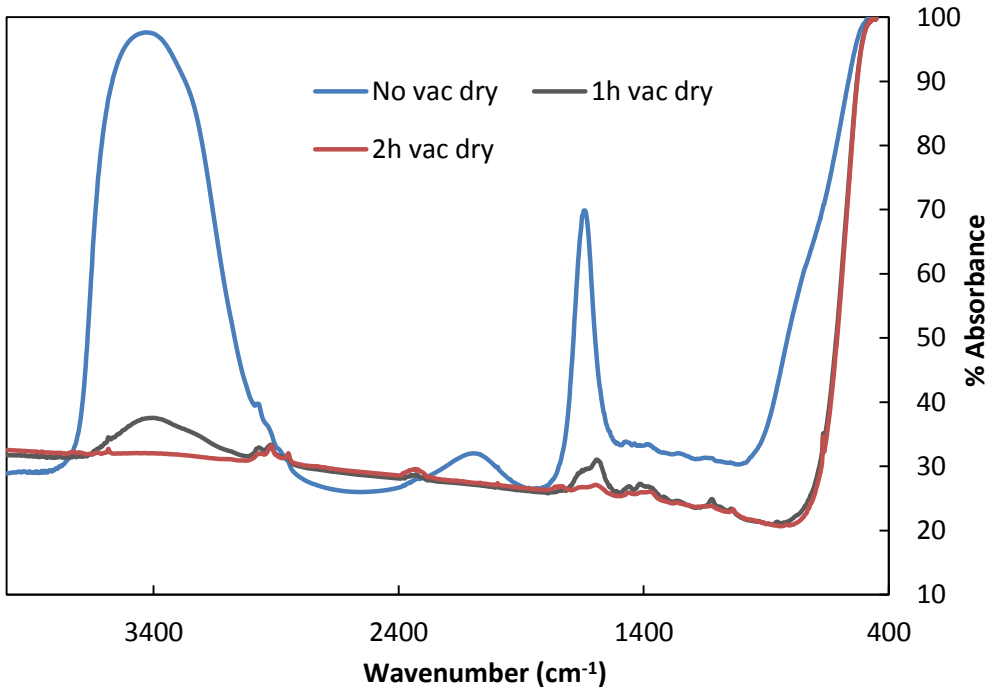

Figure 5-1: % absorbance gas cell IR plots of bare fibre samples heat treated to 500 °C for 15 minutes following vacuum drying for (a) zero hours, (b) 1 hour and (c) 2 hours

As the fibres used in this work were bare (or water-sized) the IR spectrum of the volatiles produced was expected to be relatively simple. Theoretically only water should be found in the spectrum; in reality, however, contamination of the fibre surface and from within the TVA system itself may cause additional peaks. A clear example of this phenomenon is found in Figure 5-1; in the region between 3000 – 2900 cm^{-1} there are several small peaks associated with various C-H bonds, typical of contamination by organic molecules. The levels of contamination of the three samples shown in Figure 5-1 appeared to be approximately the same based on the similar relative absorbance of C-H bonds in the region 3000 – 2900 cm^{-1}, although for the sample not vacuum dried the signal is convoluted with the very strong broad OH stretching band.

The blue curve in Figure 5-1 shows the IR spectrum for a sample which was not allowed to pre-dry under vacuum (‘0’ hours). This represents the maximum strength of water signal that it should be possible to measure using gas cell IR following TVA. Two clear peaks in this spectrum were visible: a broad peak from approximately 3700 – 3000 cm^{-1} and a narrow peak at about 1650 cm^{-1}. These are characteristic of

water; the broad band corresponds to the O-H stretching vibration and the narrow peak to the O-H scissoring vibration [104]. An apparent peak between 2000 – 2250 cm^{-1} is also visible, but does not correspond to an absorbance phenomenon. Rather it is a standard feature observed in spectra demonstrating a strong water signal [104].

The grey and red curve in Figure 5-1 show the spectra obtained from gas cell IR of samples that were pre-dried under vacuum for 1 and 2 hours respectively, before heating to 500 °C. It is clear that the intensity of both water peaks, compared with the non-pre-dried sample, was significantly reduced following vacuum drying for 1 or 2 hours. Following 1 hour pre-drying the maximum absorbance for the O-H stretching band decreased from approximately 97.5 % to around 37.5 % and for the O-H scissoring band from around 70 % to 31 %. This suggests that some water remained adsorbed to the sample after the first hour of vacuum pre-drying, but the quantity decreased significantly compared to the maximum possible value indicated by the blue curve.

The red curve in Figure 5-1 shows the spectrum obtained when a fibre sample was subjected to 2 hours of pre-drying under vacuum then heated to 500 °C. The spectrum was largely featureless, the strongest absorbance being due to C-H contamination. The broad peak associated with water between 3700 – 3000 cm^{-1} was almost completely eliminated and the O-H scissor peak barely greater than the background absorbance level. This suggested that 2 hours of pre-drying the fibres under vacuum removed all physically adsorbed water. Upon heating to 500 °C it is possible that remaining hydrogen bonded hydroxyl groups were removed from the sample, which would explain the very small O-H related absorbance that persists.

5.3 Heat treatment of single fibres under vacuum

Based on the water desorption results obtained using chopped fibre, a vacuum pre-drying period of 2 hours was selected for single fibre vacuum heat treatment experiments. In the single fibre treatment the volume of fibre placed in the sample tube was of the order of 1000 times less compared with the chopped bundle desorption experiments, and the full surface of each fibre was exposed making it theoretically easier for desorption of water to take place.

As discussed in Section 5.1 only bare E-glass fibres were utilised in this study; APS fibres were not investigated as the effect of surface water on the fibre was of interest and the degradation of APS under temperature and vacuum would complicate the analysis significantly. Average tensile strength results obtained for fibres heat treated under vacuum were compared with those of bare fibre treated using a standard air furnace. All of the heat treatments compared were carried out using single fibres separated before the application of any heat. The average tensile strength results of several treatments are presented in Figure 5-2.

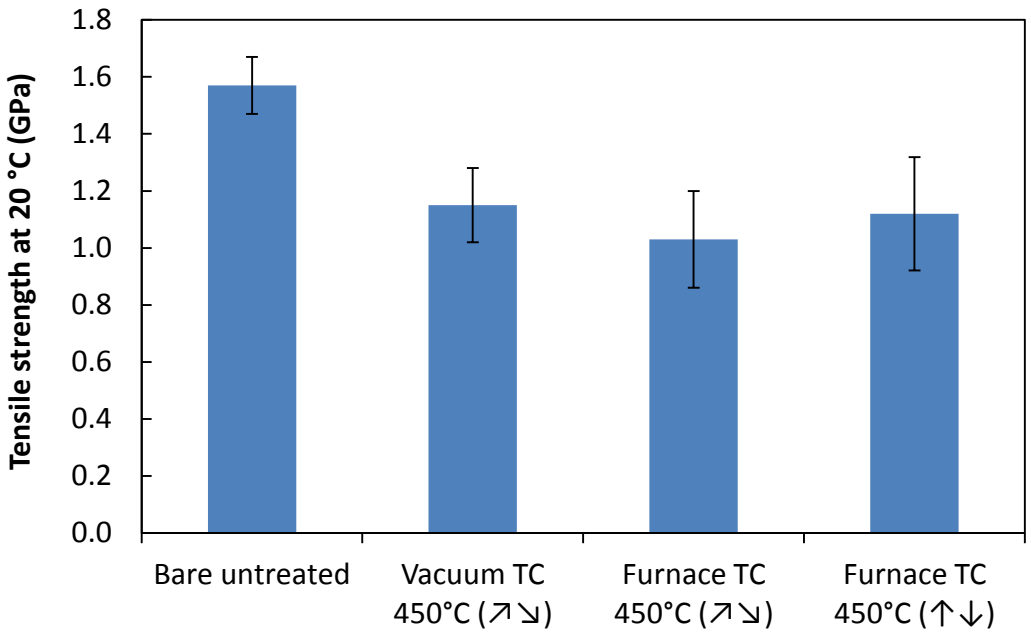

Figure 5-2: average tensile strengths of bare E-glass: (i) untreated, (ii) vacuum treated in TVA at 450 °C, (iii) furnace treated at 450 °C at approximately same heating/cooling rate as TVA, (iv) furnace treated at 450 °C using standard single fibre heat treatment procedure

Alongside the tensile strength of untreated bare fibre, as reported in Chapter 4, the strength data obtained following 3 heat treatment experiments are shown. These were all carried out using a treatment temperature of 450 °C. Excluding the far left column, from left to right in Figure 5-2 the average strengths of fibres after the following treatments are presented:

1. ***Vacuum TC 450 °C (↗↘)***: Vacuum treatment as described in 3.2.3.2 where the fibres were initially pre-dried under vacuum at room temperature for 2 hours

2. ***Furnace TC 450 °C (↗↘)***: A furnace treatment in air which simulated as closely as possible the thermal profile of the vacuum treatment described immediately above, described as gradual heating/cooling
3. ***Furnace TC 450 °C (↑↓)***: A furnace treatment in air following the method outlined in 3.2.1.2 wherein fibres were inserted into a pre-heated furnace and removed immediately to room temperature at the end of the treatment period, described as instantaneous heating/cooling

Thus, the variables between these sets of data included the rate of heating and cooling of the fibres, as well as the presence of water on the surface of fibres, the effect of whose removal was under investigation.

5.3.1 Effects of variables in heat treatment process on retained fibre strength

5.3.1.1 Effect of heating/cooling rate

A change in the heating and cooling rates used during heat treatment did not produce a significant change in the retained fibre strength, however this result was expected. During instantaneous heat treatment fibres spent a total time of 25 minutes in the furnace, approximately 15 minutes of which was at the target temperature. Conversely, the gradual heat treatment process required that fibres were inside the furnace for longer; approximately 15 minutes to reach 450 °C, a 15 minute isothermal period immediately thereafter and a cooling period of the order of 1 hour to cool fully back to room temperature. Following the established understanding of the effect of temperature on fibre strength (outlined in 2.3.1) the portion of this treatment spent at the highest temperature has the most significant effect on reducing strength. The initial phase of gradual cooling in the furnace saw the most rapid rate of temperature decrease; as a consequence the time spent at 450 °C was roughly equivalent for both furnace heat treatments. It therefore follows that the strengths of fibre after these two treatments should also be the same, which was statistically shown to be the case.

5.3.1.2 Effect of heat treatment under vacuum

No significant effect, dependent on whether heat treatment was performed in air or under vacuum, was found on the retained strength of fibre. This agrees with previous studies (summarised in Section 5.1) that showed no change in fibre strength when heat treatment was carried out using air or an inert gas. Although a

vacuum is not the same as an inert gas atmosphere, both will prevent (or at least significantly retard) the progress of oxidative reactions. In addition to the vacuum treatment preventing oxidative reactions, it was also shown that the application of a suitably high vacuum could remove water adsorbed on the surface of fibres by allowing a suitably long period of pre-drying at room temperature. The subsequent heat treatment was therefore performed in the absence of surface water normally found on glass fibres.

Numerous explanations for the strength loss of heat treated glass fibres have been proposed in the literature; however the possibility of an interaction between glass fibre and water at its surface has not been investigated. There is reason to suppose that such an interaction could cause a strength decrease. As discussed in 2.1.4.1, atmospheric moisture is known to weaken glass fibres from the moment at which they are pulled from the bushing. In this way, the intrinsic strength of the glass is irreversibly lost, and a lower level of extrinsic strength is reached. It is known that a stress corrosion reaction causes the decrease in strength; while the precise nature of this reaction is not fully understood all suggested mechanisms are based on processes facilitated by water. Considering the heat treatment of glass fibres, in addition to water present on the fibre surface, energy in the form of heat is available to the system. Despite the presence of surface water, the strength at room temperature of the unsized fibres studied is generally stable; suggesting that the stress corrosion reaction is not active. Given, however, the addition of heat energy during heat treatment it is not unreasonable to suppose that a similar corrosion reaction could take place, reducing the strength of the fibre. This possible mechanism was investigated by using a relatively high vacuum to dry the fibres before performing the in situ heat treatment immediately thereafter.

The results presented in Figure 5-2 show that no difference in strength was found between fibres pre-dried and treated under vacuum and those treated in an air furnace using the same thermal profile during heat treatment. This suggests that removal of the physically adsorbed water present on the surface of E-glass fibres does not have an effect on the strength loss behaviour due to heat treatment. This result would appear to rule out the possibility of a reaction similar to the stress corrosion reaction that causes a decline in strength of pristine glasses. Furthermore, the mechanism that is in fact responsible for the observed strength loss must occur irrespective of the presence of water at the fibre surface.

Chapter 6. Analysis of the surface of heat treated glass fibres

As part of the investigation into the strength loss of heat treated glass fibre, a study of changes to the fibre surface was undertaken. The direct analysis of the surface of glass fibres can be challenging as they are not flat and their dimensions are relatively small; the reinforcement fibres studied in this work had a nominal diameter of 17 µm. Nonetheless, it is of particular importance to investigate the surface of a brittle material such as glass, as the state of the surface is understood to directly influence the strength of the material. When considering a glass fibre placed under increasing tension, it is assumed that failure will initiate at the most severe Griffith crack; it is also possible, however, for surface features other than cracks to act as stress concentrators and as such imaging of the surface at the nano-scale can provide useful information when attempting to explain the strength behaviour of the fibre. An imaging method with very high resolution is necessary as, due to the relatively high strength of glass fibre, the theoretical critical crack length to initiate failure tends to be of the nano-scale. Techniques were employed to study possible changes in the chemistry, topography and crystallinity of heat treated glass fibres.

6.1 Surface chemical changes

6.1.1 Introduction

Previous investigations into the chemical nature of the surface of E-glass were reviewed extensively in 2.1.3.2. Studies using X-ray Photoelectron Spectroscopy (XPS) and Auger Electron Spectroscopy (AES) have shown that the surface of E-glass fibres tends to be rich in Si. It may also be considered likely that they are depleted in Ca and Mg at the surface in comparison with the fibre bulk. Little in the way of examination of the surface of heat treated E-glass has been previously reported, but some tentative evidence suggested that the concentration of Ca, initially depleted before treatment, increased following heat treatment, suggesting that some migration process took place. The investigation undertaken utilising XPS added further data to this field and attempted to replicate findings in the literature.

Due to the nature of the analysis performed and instrument settings selected (as described in 3.5) a maximum of the outermost 10 nm of the material was probed

using XPS. The atomic percentages of elements that are presented were calculated from survey scans of the spectrum of each sample; improved smoothness of the baseline was achieved by performing several passes in each scan.

6.1.2 Results

An investigation into possible changes in the surface chemical composition of glass fibres before and after heat treatment was carried out using XPS. The fibres used in the study were thermally treated as bundles following the method outlined in 3.2.1.1.

Table 6-1: Results of surface and bulk analyses of boron-free E-glass fibre from Chapter 6, presented alongside comparable compositional data taken from the literature. No heat treatments (HT) applied unless explicitly stated. All values given in atomic percentage (At%)

		O	Si	Ca	Al	Mg	Na	Ti	Fe	K
Surface	*XPS results (Chapter 6)*	70.3	19.0	5.4	3.9	1.1	0.31	x	x	x
	XPS results (taken from [105]*)*	65.8	22.1	6.5	4.3	0.65	0.54	x	x	x
Bulk	*XRF results (taken from* [105]*)*	62.2	21.8	8.4	5.5	1.7	0.4	x	x	x
	From glass melt formulation [106]	62.1	21.6	8.5	5.5	1.6	0.42	0.14	0.05	0.09
	SEM-EDX results_no HT (Chapter 6)	53.6	27.1	10.1	6.5	1.8	0.47	0.31	x	0.13
	SEM-EDX results_700°C HT (Chapter 6)	54.4	26.6	9.8	6.4	1.8	0.47	0.30	x	0.25

XPS is a highly surface sensitive technique therefore many of the glass constituent elements were detected; in addition to carbon from surface contamination, oxygen, silicon, calcium, aluminium, magnesium and sodium were identified. The results obtained, calculated as the average values of the two series shown in Figure 6-1 to Figure 6-3, are presented in their entirety in Table 6-1. The data for non-heat treated fibre were found to be in generally close agreement with previously published XPS data using similar fibre [105]. Comparison of surface and bulk fibre compositions

shows that these XPS data sets support the existence of a calcium depleted surface region.

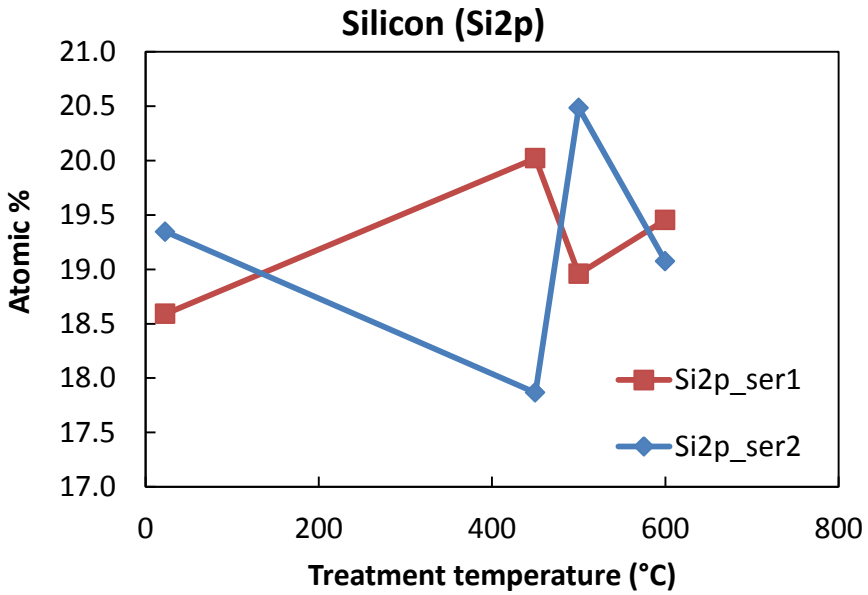

Figure 6-1: Atomic percentages of Si at E-glass fibre surface with respect to heat treatment temperature. Measurements of 2 series of samples were carried out using XPS, at an interval of approximately 1 month

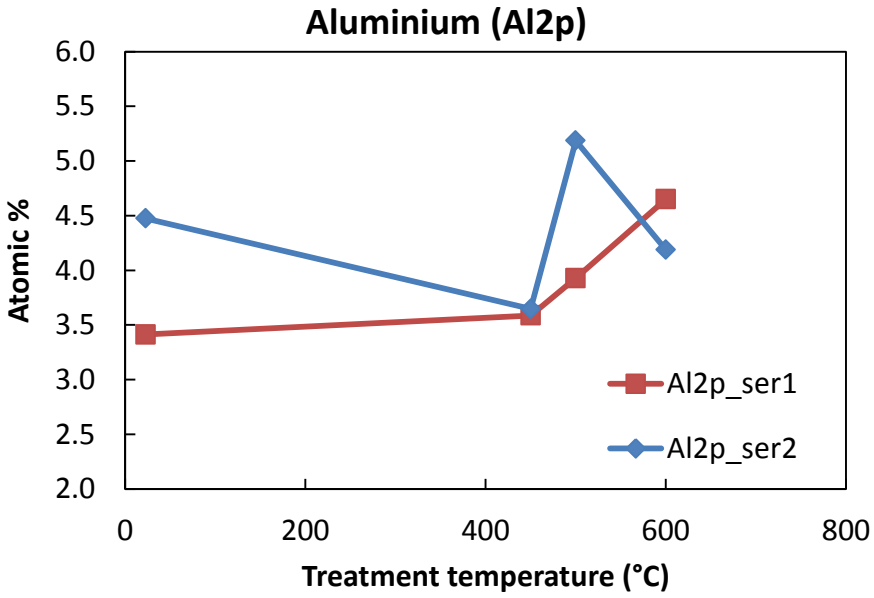

Figure 6-2: Atomic percentages of Al at E-glass fibre surface with respect to heat treatment temperature. Measurements of 2 series of samples were carried out using XPS at an interval of approximately 1 month

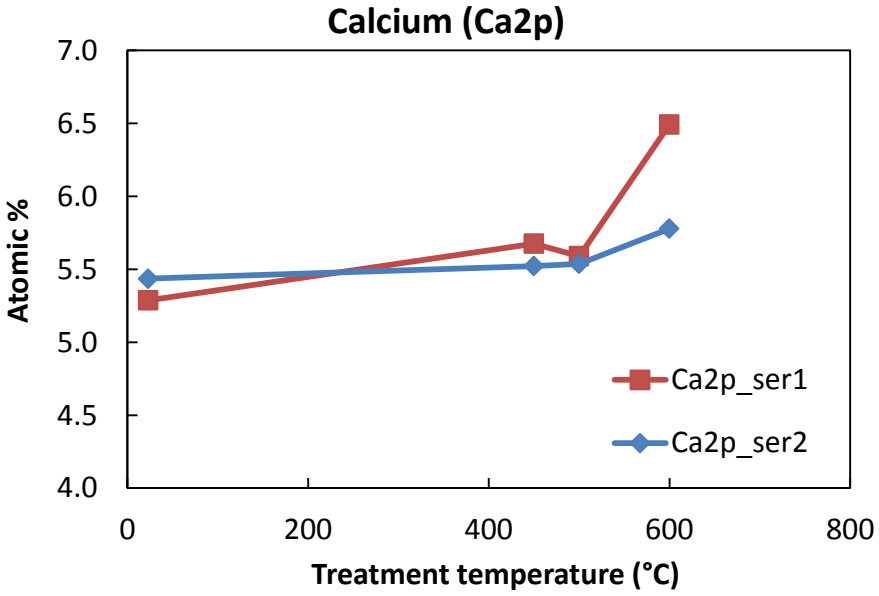

Figure 6-3: Atomic percentages of Ca at E-glass fibre surface with respect to heat treatment temperature. Measurements of 2 series of samples were carried out using XPS at an interval of approximately 1 month

In Figure 6-1 to Figure 6-3 data are presented from 2 series of XPS data gathered at a 1 month interval. Values were obtained from quantification of individual survey scans. Samples were not progressively heat treated and analysed; as such the data represent the results of measurements made using 8 different samples. Data are shown for the 3 most common glass constituent elements (other than oxygen). Figure 6-1 shows that no consistent trend was found in the atomic percentage content of silicon. Inconsistent results regarding the atomic content of aluminium were also found, as shown in Figure 6-2: suggestions of a progressive increase in atomic % of aluminium with heat treatment temperature observed in series 1 were not reproduced in the second set of results collected.

The atomic % of calcium at the surface showed an increase with heat treatment temperature in both series. Only one data point contradicted this trend, in series Ca2p_ser1 at 500 °C. Taking an average value (calculated from the 2 values for atomic % of untreated fibre shown in Figure 6-3) for the atomic % of Ca on the surface of untreated glass as 5.4 %, the maximum increases in calcium concentration for the series 1 and 2 were approximately 21 % and 8 % respectively.

6.1.3 Discussion

For the majority of the glass constituent elements detected by XPS no consistent change in their surface atomic concentrations with respect to heat treatment temperature was found. This was the case for silicon and aluminium as shown in Figure 6-1 and Figure 6-2 respectively, but similar results were also found for minor glass constituents such as sodium and magnesium.

An increase in the surface atomic percentage of calcium was observed; this finding is consistent with those of Nichols et al. [26] who suggested that a diffusion of calcium to the surface of E-glass fibres occurred during heat treatment, which they performed for a period of 3 hours at temperatures of between 150 to 720 °C. Their discussion, however, did not include any reference to strength loss of the glass.

There exists little evidence in the literature to suggest what effect a change in the surface concentration of calcium might have on the strength of glass. Calcium acts as a network modifier in E-glass, balancing the charge associated with oxygen ions which is caused by non-silicon species being incorporated into the network while itself being present in the interstices. Another interstitial network modifier is sodium; the effect of its addition to silica was investigated by Kennedy et al. [107] and summarised by Freiman [108]. Upon increasing the concentration of sodium Kennedy et al. tested the strength of specimen rods using 4 point bending and found that the fracture toughness, and therefore also strength, increased with increasing sodium content. They postulated that the explanation of the effect may be related to changes in straining or bending of the Si-O bonds; the bonding will be affected by changes in composition which has a knock-on effect on the size of a so-called “process zone” near the crack tip in which linear elastic fracture mechanics may no longer apply.

Similarly, there is evidence to suggest that an increase in calcium content in silica glasses effects an increase in fracture toughness [109] although in this case it was not a simple binary system that was investigated. It appears that, if it has any effect, an increase in calcium at the glass fibre surface would lead to an increase in fracture toughness or strength. Based on this it is unlikely to be the source of an explanation of the strength loss of heat treated glass fibre, as observed at the same treatment temperatures for which the surface calcium enrichment was demonstrated.

6.2 Surface physical changes

Changes in the physical surface of glass fibres, as well as other types of glasses, can be directly observed using the correct type of microscopy at sufficient resolution. When working with glass fibres of microscopic dimensions, such as reinforcement E-glass fibres, techniques providing a high resolution are required. Atomic Force Microscopy (AFM) and Scanning Electron Microscopy (SEM) are two possible choices. Of these, AFM is capable of producing a greater variety of useful data; unambiguous topographical data of a surface can be produced, as opposed to SEM images in which convex and concave structures can often be confused. One of the most commonly reported parameters is the surface roughness, which can be calculated from the topographical data of an area produced by AFM.

The study of glass fibre by AFM has been previously reported in the literature. Rondinella et al. [110] reported a Root Mean Square (RMS) roughness R_q, as calculated using Equation (3.5), for silica optical fibre of 0.3 nm. These fibres were freshly drawn before analysis and as such did not have time in which to age under atmosphere. Roughness analysis of a boron-containing E-glass formulation was reported by Gupta et al. [111]. Similarly low RMS roughness of between 0.15 – 0.19 nm was obtained for freshly drawn fibres, produced by melting and hand-drawing E-glass beads. Analysis using a calcium aluminosilicate fibre, similar to E-glass, was reported by Mellott and Pantano [112]. The surface roughness of untreated fibre was 0.26 nm; once again these were laboratory produced fibres which experienced only relatively short periods of exposure to atmosphere during which aging could occur, prior to surface analysis by AFM.

No rigorous studies of change in surface roughness following annealing or heat treatment have been presented in the literature and neither has there been any investigation of any possible link between nano-level surface state and fibre strength, despite the accepted model that failure initiates at the surface unless a significant internal pore has been introduced as a manufacturing flaw. An investigation of possible nano-scale changes at the heat treated fibre surface was examined using AFM in a systematic manner.

6.2.1 Surface roughness

6.2.1.1 Surface of non-heat treated E-glass

A large number of AFM analyses of fibre surfaces were carried out, following the procedure discussed in 3.6. The numbers of individual areas analysed for each heat treatment condition are given in Table 6-2.

Table 6-2: number of areas analysed by AFM at each temperature condition

Heat treatment temperature (°C)	20	200	300	400	500	600	700
No. of areas analysed, n	24	4	4	4	5	4	3

A significantly larger sample size was generated for untreated, room temperature fibres (“heat treatment” = 20 °C) due to an earlier set of experiments in which it was attempted to compare the surfaces of the same fibres both before and after a heat treatment was applied. This comparison was ultimately unsuccessful but did generate a sufficiently large dataset for the roughness of untreated fibre to calculate a representative average value with relatively small confidence limits. The average roughness R_{q_20} = 0.58 nm with 95 % confidence limits of 0.14 nm. This is approximately double some of the values referenced for ‘pristine’ or ‘melt-surface’ glass or silica fibres [110–112]. This might be explained in part because the E-glass fibres used in this work were not pristine; they had been exposed to water spraying during manufacture followed by moist atmospheric conditions which has been shown to have a roughening effect on the surface over time [113]. Furthermore, the effect of surface contaminant particles present on the surface of fibres could not be removed from the analysis of roughness, producing an artificially higher value.

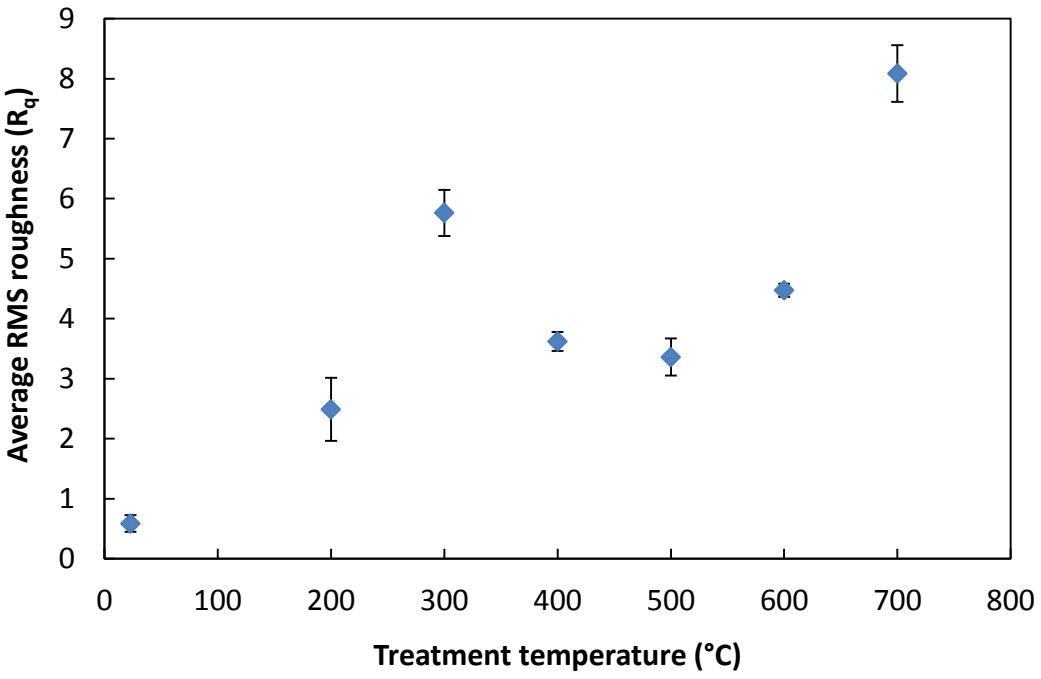

Figure 6-4: average RMS roughness of E-glass fibre with respect to heat treatment temperature

A typical topography plot of an untreated unsized glass fibre is shown in Figure 6-5, as both a 3D and 2D image. The scale of the 3D image is fixed so as to be identical to those of all other 3D topography plots presented in 6.2.1; this allows easier comparison of the development of surface features with increasing heat treatment temperature. The scale on the 2D image is automatically generated such that the maximum and minimum z-values obtained correspond with the limits of the z-scale; thus an improved contrast of the image is achieved making features more easily visible.

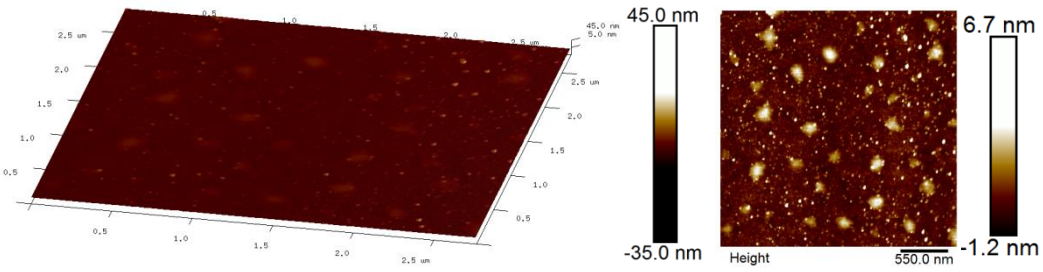

Figure 6-5: 3D and 2D topography plots of a typical untreated unsized E-glass fibre

Two types of surface feature were visible; numerous mounds with x-y dimensions of between 100 – 200 nm and smaller spikes of an average 20 nm across. Both of these types of surface features had a maximum height of approximately 5 to 6 nm.

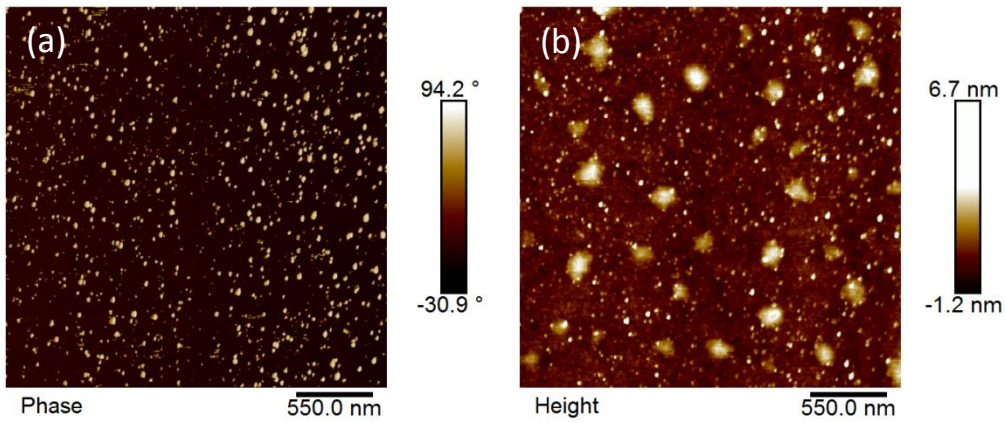

Figure 6-6: (a) phase contrast and (b) 2D topography plot of a typical untreated unsized E-glass fibre

These features could be further distinguished using phase imaging data, as shown in Figure 6-6 (a). In intermittent contact AFM, phase is essentially a measurement of the amount of energy dissipated by the tip as it makes contact with the sample surface. The topography of the sample has some effect on phase, but it is more dependent on adhesion and the viscoelastic properties of the material surface. A very clear phase contrast was visible in Figure 6-6 (a), between the bright white particles and the dark colour of the remaining area of glass fibre surface. This observation confirmed that the small spike-like features were due to contamination of the surface and were not related to the topography of the glass itself. These particles also appeared sensitive to temperature as they were not found on the surface of any heat treated fibres between 200 – 700 °C. It was thus concluded that the surface of E-glass fibre was largely flat and featureless apart from some large rounded structures of 100 – 200 nm across and with height of no more than 5 nm. As no phase difference was found between these and the remaining fibre surface area they are assumed to be a part of the glass, given that there is no apparent difference in viscoelastic properties, adhesion or composition.

6.2.1.2 Surface of heat treated E-glass

Following heat treatment, significant changes in the surface topography of E-glass fibres were measured; these changes were reflected in a general trend in increased surface roughness as shown in Figure 6-4. The typical topography of a fibre heat treated at 200 °C is shown in Figure 6-7. The surface appearance was notably different compared to the non-heat treated fibre. The total z-range more than doubled to approximately 19 nm. Furthermore, the general appearance changed significantly; rather than the mostly flat surface with randomly dispersed mounds

observed for non-heat treated fibres the surface was almost uniform with a textured appearance. The development of this roughness, although relatively minor with maximum height of 12 nm, explained the observed increase in RMS roughness from R_{q_20} = 0.58 to R_{q_200} = 2.49 nm.

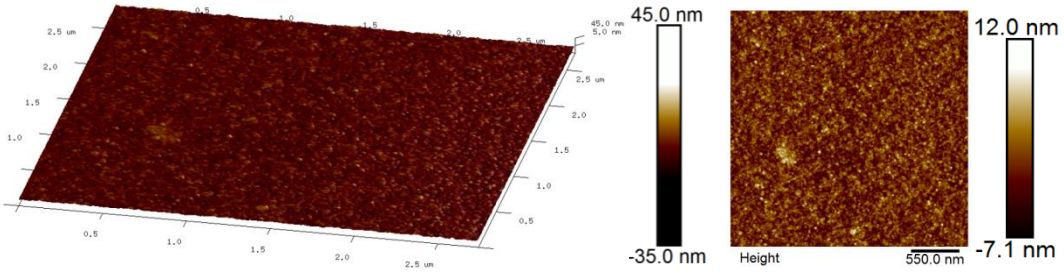

Figure 6-7: 3D and 2D topography plots of a typical 200 °C treated unsized E-glass fibre

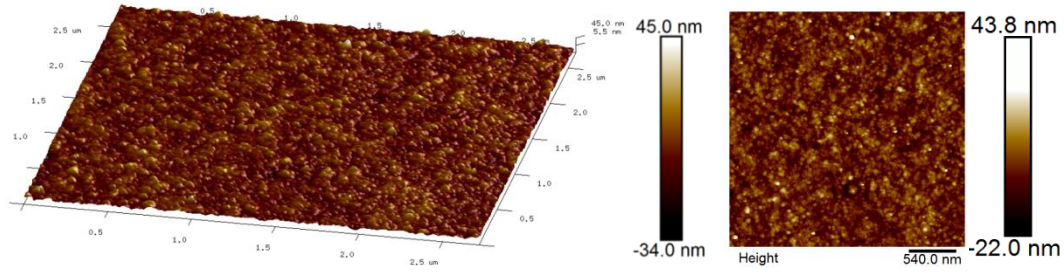

Figure 6-8: 3D and 2D topography plots of a typical 300 °C treated unsized E-glass fibre

As shown in Figure 6-4, following heat treatment of unsized fibre at 300 °C a large increase in the surface roughness was measured with R_{q_300} = 5.76 nm. In the plots of topography, Figure 6-8, it is clear that the surface is indeed rougher; the 3D plots with fixed z-scale elucidate clearly that the z-dimensions of the surface features increased significantly. A maximum height of almost 45 nm was measured, although this was limited to two small peaks of 50 – 60 nm in diameter in the x-y plane; the maximum height of the remainder of the surface was in the range 20 – 30 nm, while the minimum trough depth also increased in magnitude to approximately –20 nm. Similar to fibres heat treated at 200 °C, the distribution of the surface roughness was quite uniform, with little evidence of defined peaks. In terms of surface roughness, this result at 300 °C was the only one which does not fit with a trend of continuously increasing roughness with increasing fibre treatment temperature.

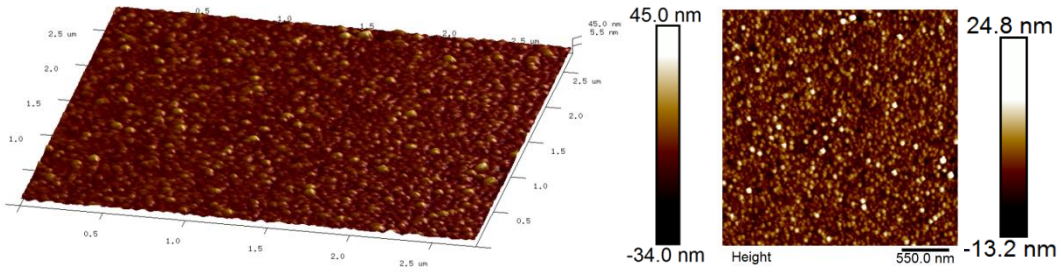

Figure 6-9: 3D and 2D topography plots of a typical 400 °C treated unsized E-glass fibre

In contrast, the surface of fibre treated at 400 °C was generally different in appearance. Development of many more defined peaks was observed; these were round in shape and measured between about 50 – 70 nm in the x-y plane. The RMS roughness R_{q_400} = 3.62 nm was lower than following heat treatment at 300 °C, which was against the expected trend of continuously increasing roughness with increase in heat treatment temperature. However, R_{q_400} was significantly greater than R_{q_200}.

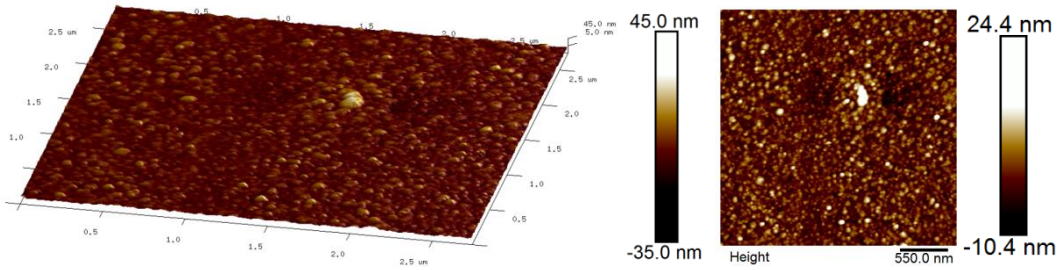

Figure 6-10: 3D and 2D topography plots of a 500 °C treated unsized E-glass fibre (1 of 2)

The average roughness of fibres treated to 500 ° was not statistically different to those heat treated at 400 °C; as shown in Figure 6-4, R_{q_500} = 3.36 nm.

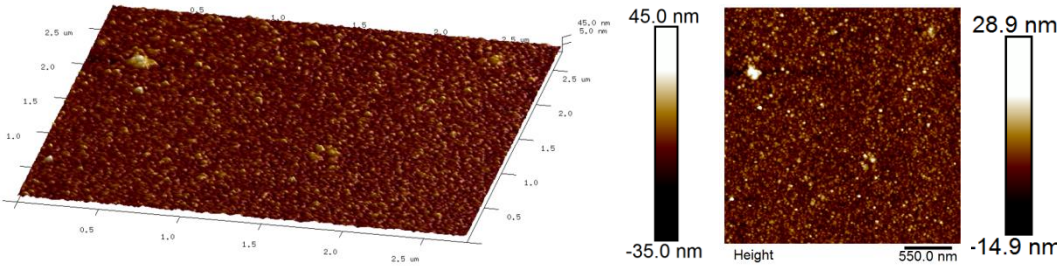

Figure 6-11: 3D and 2D topography plots of a 500 °C treated unsized E-glass fibre (2 of 2)

The magnitudes of peak height and trough depth were very similar for fibres treated at both 400 and 500 °C. The surface appearances were also largely similar; the

topography plots in Figure 6-9 and Figure 6-10, for example, both show evidence of similar surface features, although there was less prevalence of defined peaks with rounded profile on the 500 °C treated sample. The topography of a second fibre treated at 500 °C is also presented in Figure 6-11; the surface of this fibre showed evidence of almost no defined peaks however the roughness was unchanged. This inconsistency between individual fibres was unusual and only occurred with samples treated at 500 °C. It was not clear whether this effect was random and due to the generally arbitrary selection of fibres for surface imaging by AFM.

Typical surface topography images obtained when analysing fibres heat treated to 600 and 700 °C are presented in Figure 6-12 and Figure 6-13 respectively.

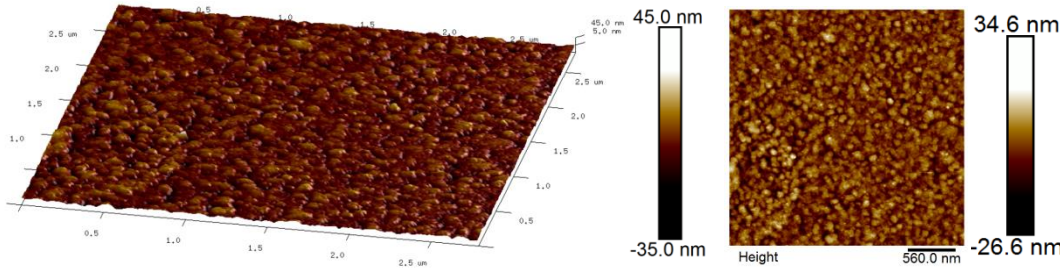

Figure 6-12: 3D and 2D topography plots of a typical 600 °C treated unsized E-glass fibre

Upon performing heat treatment at these temperatures, another visible change in the general topography was observed. At lower temperature, particularly after treatment at 400 °C, defined rounded ‘spikes’ were visible across the surfaces of fibres. This type of feature is particularly clear in the 2D topography plot in Figure 6-9. The topography of fibres treated at ≥ 600 °C no longer exhibited these spikes of relatively small x-y dimensions; instead surfaces appeared more mottled.

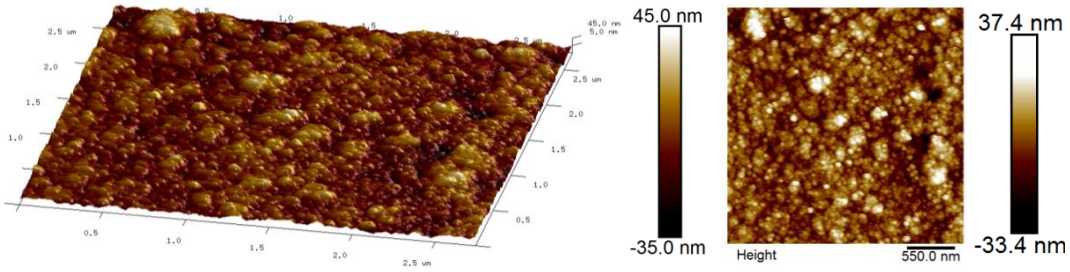

Figure 6-13: 3D and 2D topography plots of a typical 700 °C treated unsized E-glass fibre

It was not possible to ascertain from the images whether the increase in roughness represents the development of some process that progresses with increasing temperature. There appeared to be step changes in the general topography

between certain temperatures; namely 300 – 400 °C and 500 – 600 °C. Similarly, it was observed that general topography was comparable at both 200 and 300 °C, equally so at 400 and 500 °C. The topography of fibres treated at 600 and 700 °C may appear significantly different; however evidence presented in 6.2.2.2 suggests that, over this temperature range, the development of a distinct surface structure took place.

6.2.2 SEM observations

6.2.2.1 Comparability of AFM and SEM images

In addition to surface imaging by AFM, high resolution Scanning Electron Microscopy was employed in the examination of fibres heat treated at temperatures up to and including the maximum investigated of 700 °C. From the topography plots of fibres heat treated at this temperature, and to a lesser extent at 600 °C, it was noted that features were of a sufficient size that they should be observable by SEM. Initially, fibres heat treated at 700 °C were imaged and compared with a typical AFM topography plot of a similarly treated fibre as shown in Figure 6-14.

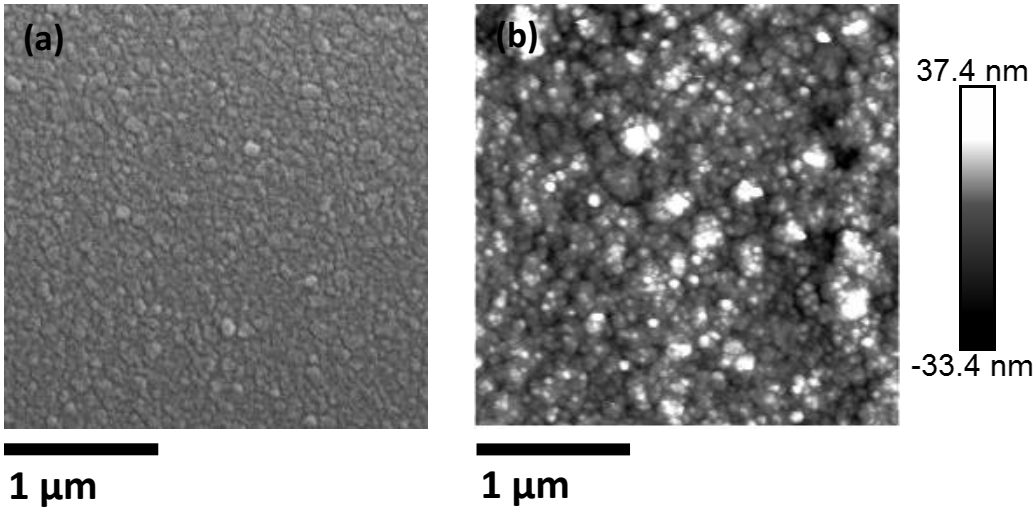

Figure 6-14: Images of 700 °C heat treated glass fibre obtained using (a) SEM [8000x magnification] and (b) AFM

By visual inspection of the two images presented in Figure 6-14 it appeared quite clear that the surface structures were demonstrably the same; although the AFM image (b) showed significantly greater contrast in the z-axis as expected. While this was a clear advantage of AFM as a surface imaging method, considerable

disadvantages compared with SEM imaging included the significantly greater time required to obtain images and the difficulties in following the fibre curvature, making imaging of only small areas with dimensions of a few micrometres possible. Having demonstrated that both methods were capable of successfully imaging the studied surface phenomenon, further SEM images were captured to complement the AFM data shown in 6.2.1.

6.2.2.2 SEM of fibres treated ≥ 600 °C

It is shown by the topography plots in Figure 6-7 to Figure 6-13 that there was a general increase in fibre roughness with increasing heat treatment. The maximum height of features upon the surface increased from a few nanometres on untreated fibre, to the order of several tens of nanometres after treatment at 700 °C. Until the roughness, and corresponding approximate height, of these surface features increased above a certain threshold it was not possible to visualise, with sufficient resolution using SEM, the effect that was evident by AFM. Therefore, SEM images are shown only for fibres heat treated at, or in excess of, 600 °C. With reference to Figure 6-4 it is observed that a significant increase in roughness occurred over this 100 °C interval.

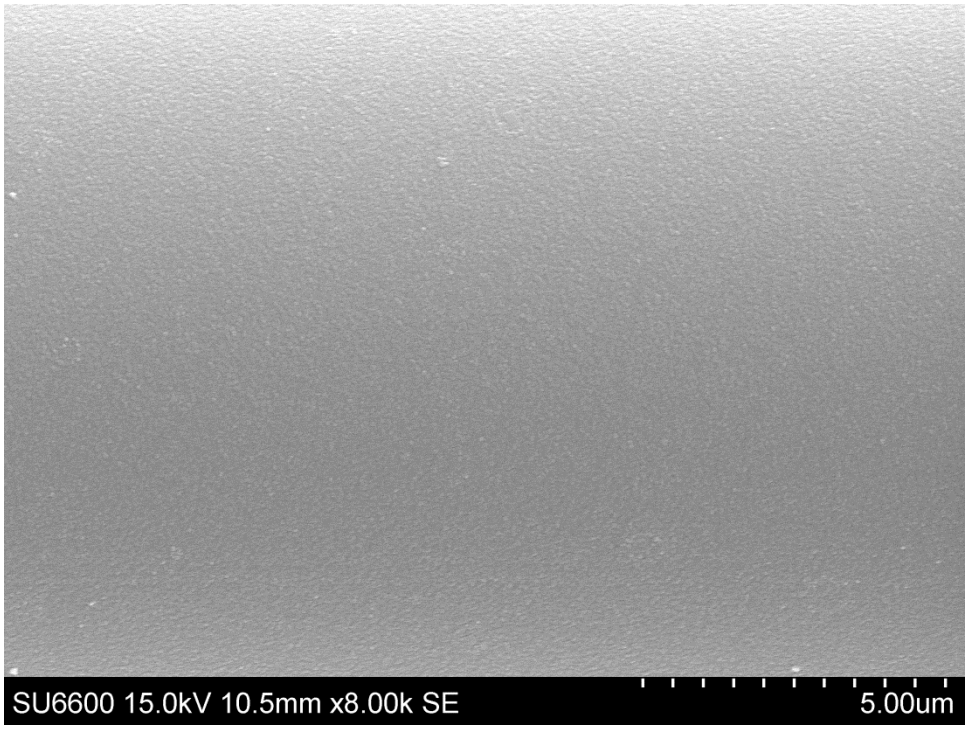

Figure 6-15: SEM image of fibre surface following heat treatment at 600 °C (scale marker subdivisions represent 500 nm)

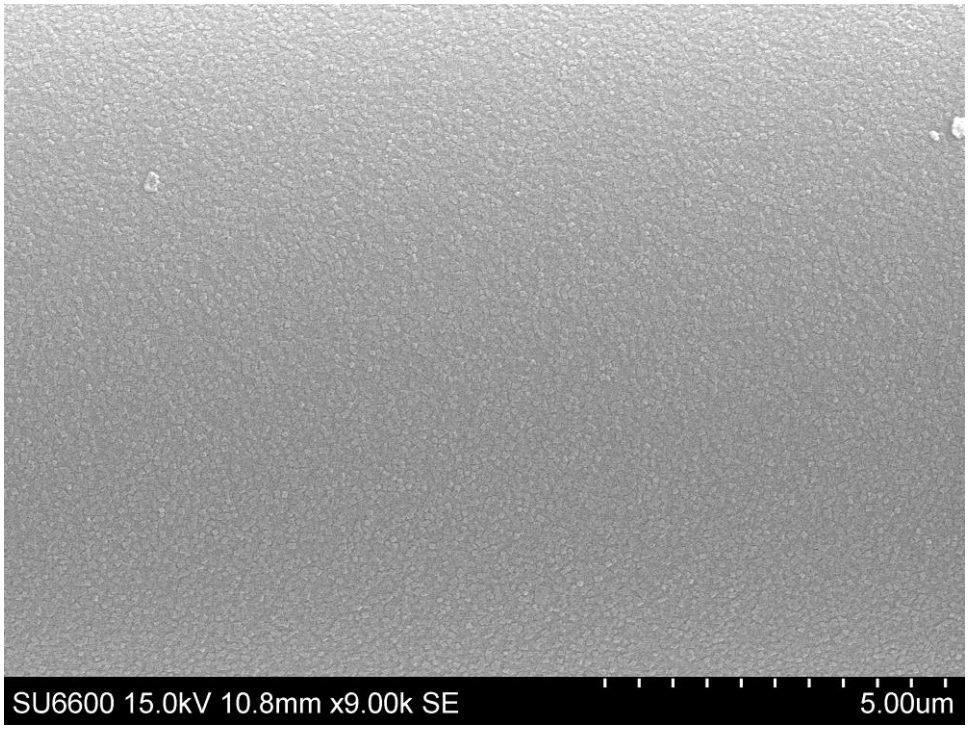

Figure 6-16: SEM image of fibre surface following heat treatment at 625 °C (scale marker subdivisions represent 500 nm)

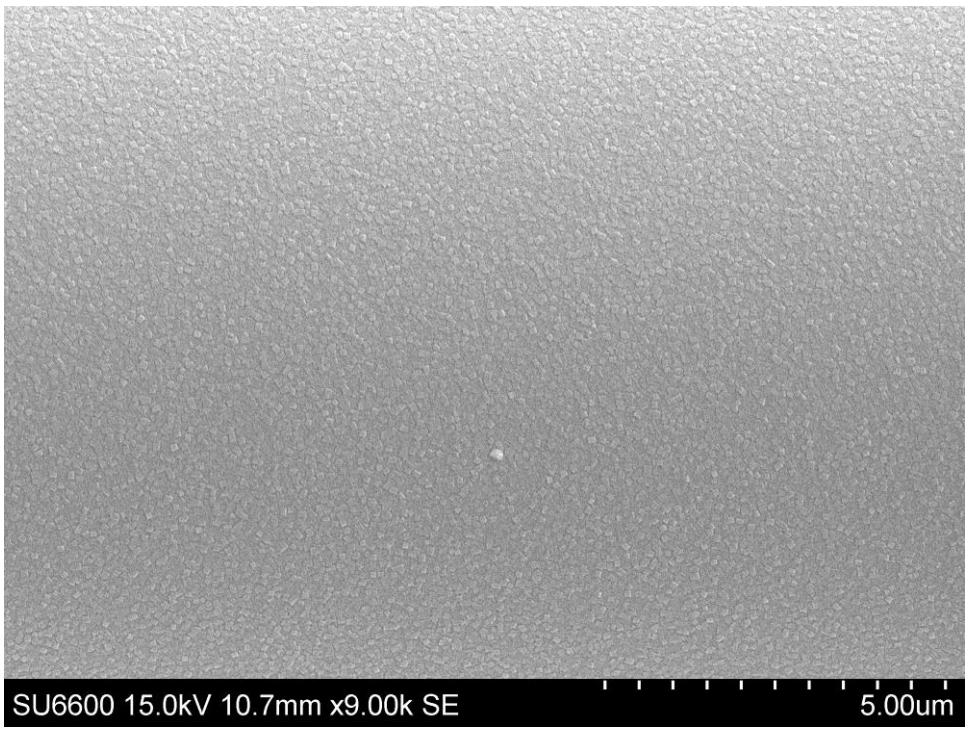

Figure 6-17: SEM image of fibre surface following heat treatment at 650 °C (scale marker subdivisions represent 500 nm)

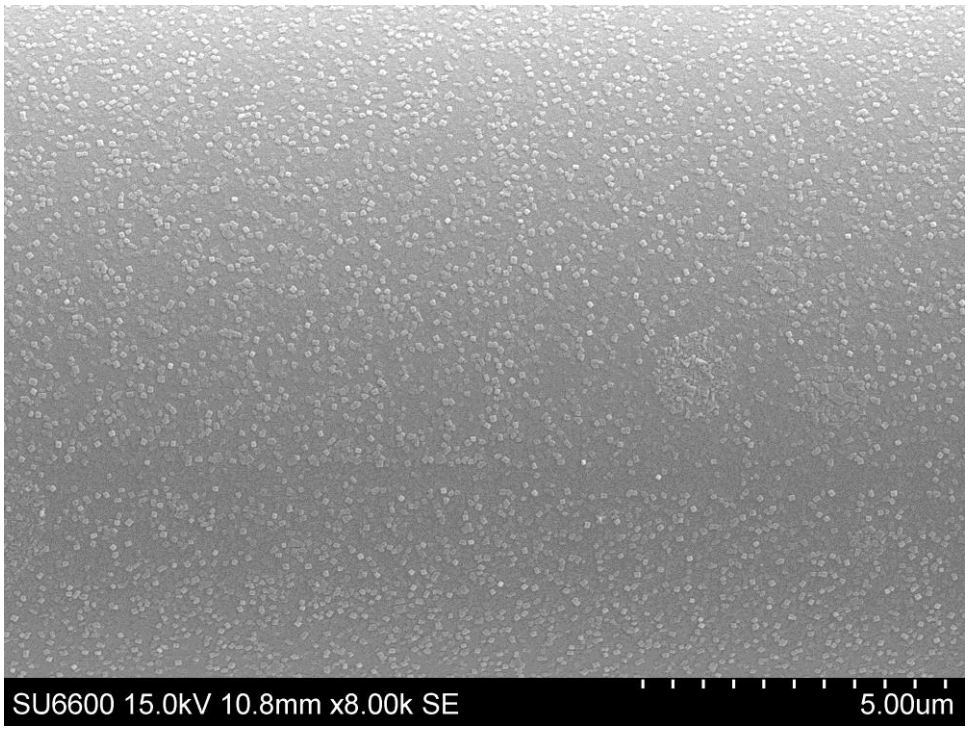

Figure 6-18: SEM image of fibre surface following heat treatment at 675 °C (scale marker subdivisions represent 500 nm)

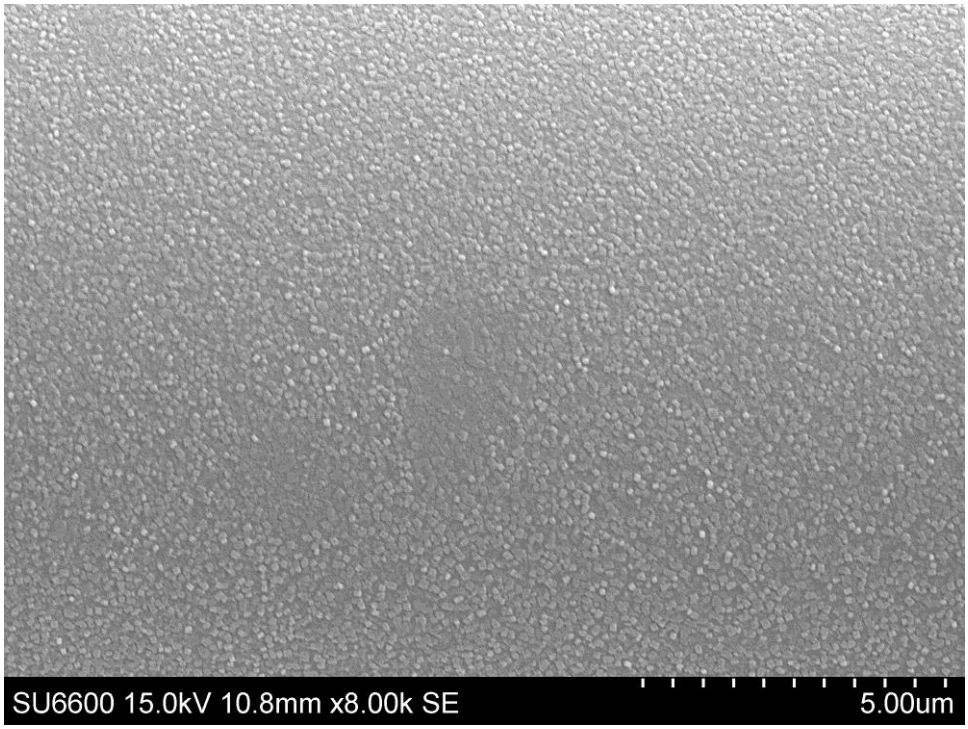

Figure 6-19: SEM image of fibre surface following heat treatment at 700 °C (scale marker subdivisions represent 500 nm)

In Figure 6-15 to Figure 6-19 it is possible to observe a progressive development of features on the surface of glass fibres. Significantly, the images provide strong evidence that the process which produced these features took place across the whole surface. In addition, visualisation of the surface at the whole-fibre scale indicated that the surface structure was not entirely consistent: for example, in Figure 6-20 several rounded regions may be observed, in which the observed features appear different to the rest of the surface. This may explain some of the variations in roughness found between individual AFM images, as these roughness values are calculated from what are essentially randomly selected 3x3 µm squares.

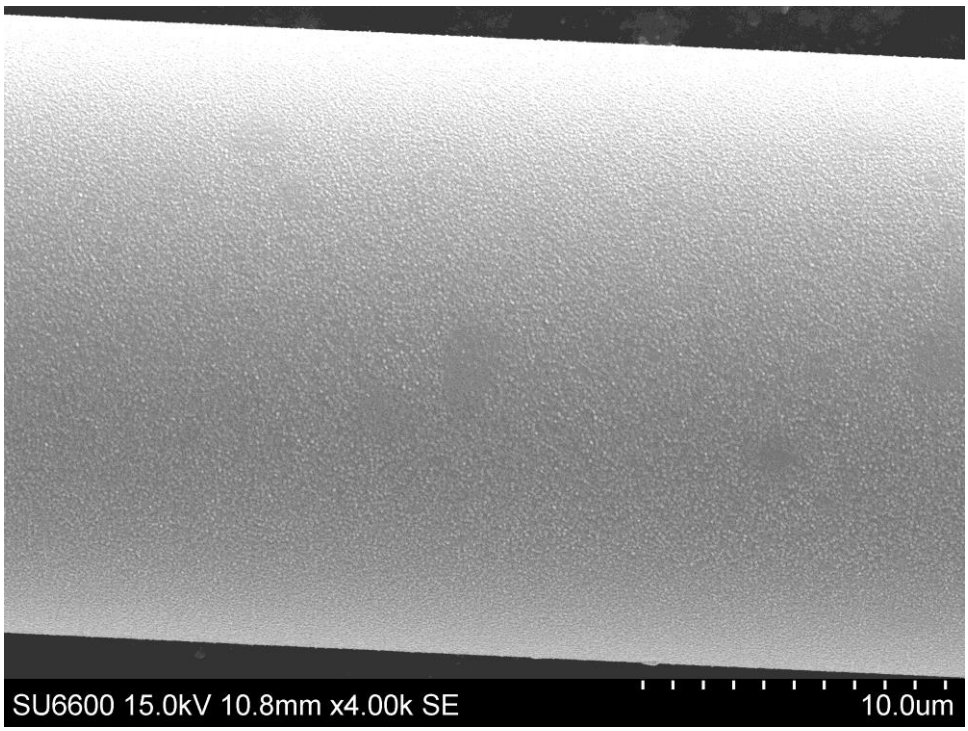

Figure 6-20: larger scale SEM image of fibre shown in Figure 6-19; heat treated at 700 °C (scale marker subdivisions represent 1 µm)

6.2.2.3 Image analysis of surface features on fibres treated ≥ 600 °C

Image analysis was performed using the procedure outlined in 3.10. Typical binary black and white images produced from areas of the original SEM pictures are shown for the 4 heat treatment temperatures investigated in Figure 6-21.

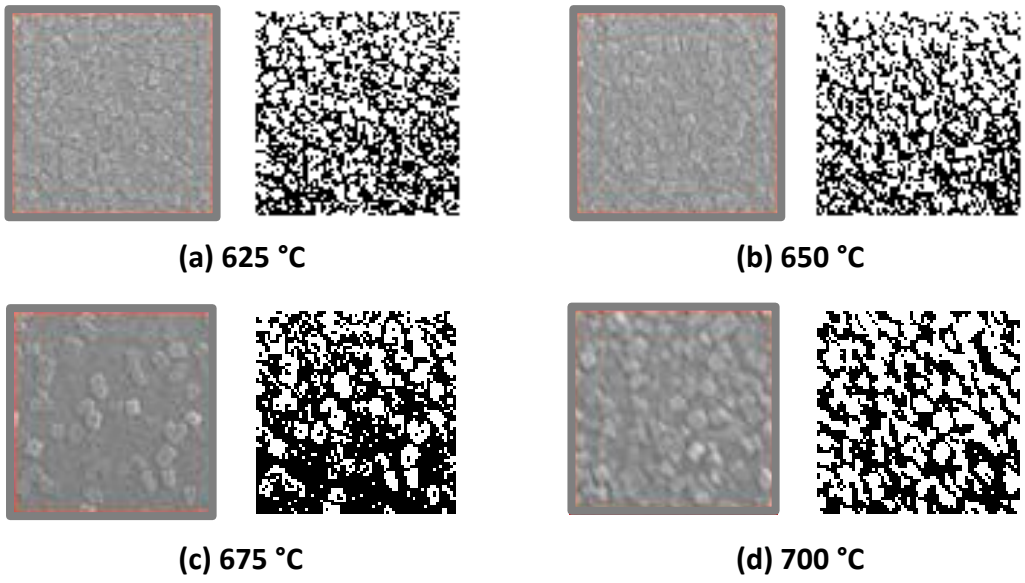

Figure 6-21: Examples of segments (2 x 2 µm) of SEM images of bare glass fibre heat treated between 625 – 700 °C and their counterparts following image conversion to black and white. Images captured at 8000 – 9000 times magnification

As noted in 3.10 some issues were encountered when attempting to produce binary images due to the lack of contrast, particularly those of fibres treated at lower temperatures of 625 and 650 °C. The associated increased difficulty in identifying edges affected the conversion to binary images. This effect is most evident in Figure 6-21 (a); the edges of the surface particles formed during heat treatment are visible in the left hand image but these edges were not captured perfectly in the binary image. Some joined together to form larger shapes and very often there were black speckles within the white particle areas. In contrast, in Figure 6-21 (d), for example, there was far less black speckling although the joining of neighbouring particle areas occurred once again. The production of representative binary images was of great importance as discussed in 3.10.2; despite the issues mentioned this was achieved to an acceptable degree.

The ratio of white to black pixels was calculated for several areas at each heat treatment temperature and an average calculated; these results are shown in Figure 6-22.

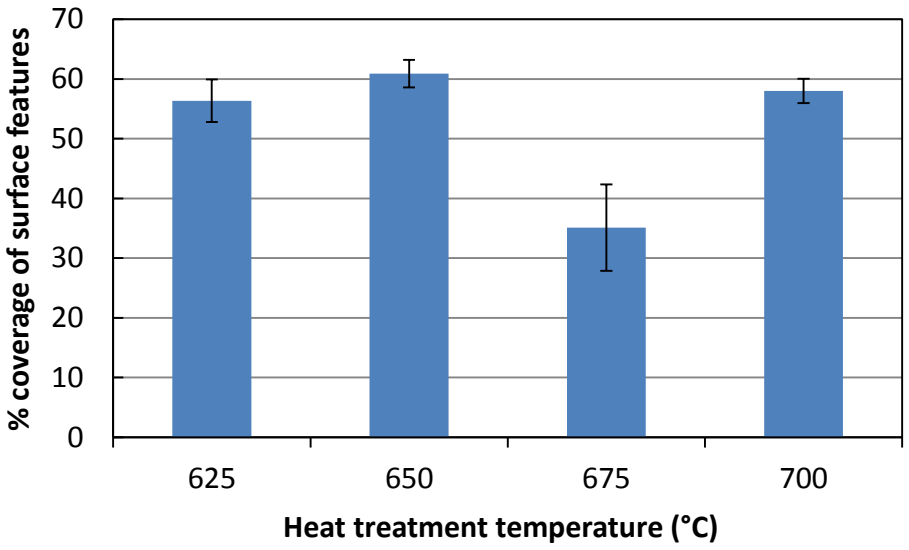

Figure 6-22: Average percentage coverage of surface features formed due to high temperature heat treatment, calculated from analysis of binary images

The results shown agree with what can be noted from visual inspection of the binary images in Figure 6-21, wherein image (c) comprises a greater proportion of black while the other three appear approximately similar to one another. The distribution of surface features was least uniform on fibres that were treated at 675 °C, as shown by the images in Figure 6-16 to Figure 6-19. This finding was reproduced for several

different heat treated fibres but an explanation within the framework of the development of the surface structures observed is not possible based on the data collected. It may be that the spaces between the features formed become 'filled in' themselves as treatment temperature is further increased to 700 °C but this is not clear.

It can, however, be stated from the image analysis that, based on the results following heat treatment at 625, 650 and 700 °C, the percentage of surface area occupied by the surface structure formed is almost unchanged. In addition the distribution of sizes of the individual particles did not seem to change significantly with increasing temperature; there was only an increase in the z-direction as elucidated from both the AFM results at 600 compared with 700 °C and the continuous increase in contrast of SEM imaging between the same temperatures. Although these data are only preliminary, the findings regarding development of the surface features may be informative. The apparent appearance across the entire fibre surface at similar temperature and time, and the lack of growth in the x-y plane suggests that it is unlikely to be related to a nucleation and growth phenomenon, while some spinodal decomposition process remains as a possible explanation.

6.2.2.4 Rinsing of fibres treated ≥ 600 °C

The surface features found on high temperature treated single fibres were further investigated by attempting to remove them. An initial attempt to rinse the fibres in what were deemed to be relatively non-aggressive conditions was made using room temperature deionised water. Several short lengths of 700 °C treated fibre, of around 30 mm, were suspended in a beaker containing approximately 200 ml of still water. After an hour the fibres were removed and viewed using SEM.

A comparison of SEM images is presented in Figure 6-23. Image (a) depicts the surface of a typical clean, bare fibre while image (b) shows a fibre which was rinsed in still deionised water as described following heat treatment at 700 °C. Image (c) shows an unrinsed fibre that was treated at 700 °C. Examination of the images shown in Figure 6-23 strongly suggested that there was no difference in the appearance of the surface of the untreated bare fibre and the heat treated then rinsed fibre.

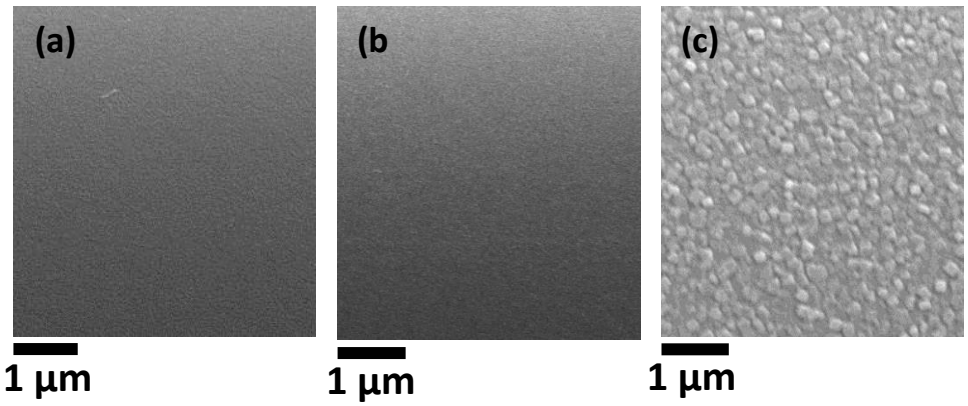

Figure 6-23: SEM images of bare E-glass fibres; (a) untreated (b) TMA heat treated to 700 °C and rinsed in still deionised water for 1h (c) TMA heat treated to 700 °C unrinsed

It was found that the relatively gentle fibre rinsing process employed was sufficient to remove the features that were produced during heat treatment at 700 °C. This suggested that the observed features either dissolved in water or, alternatively, that they did not adhere to the surface of the heat treated glass fibre particularly strongly. Nonetheless observation of the AFM phase plots of fibres heat treated at 600 or 700 °C but not rinsed (examples of which are shown in Figure 6-24 and Figure 6-25) suggested that the surface structure which developed belonged to the same phase as the glass surface. Unlike the example shown in Figure 6-6 of a contaminated fibre surface, the whole surface region analysed by AFM displayed little phase contrast for these heat treated fibres.

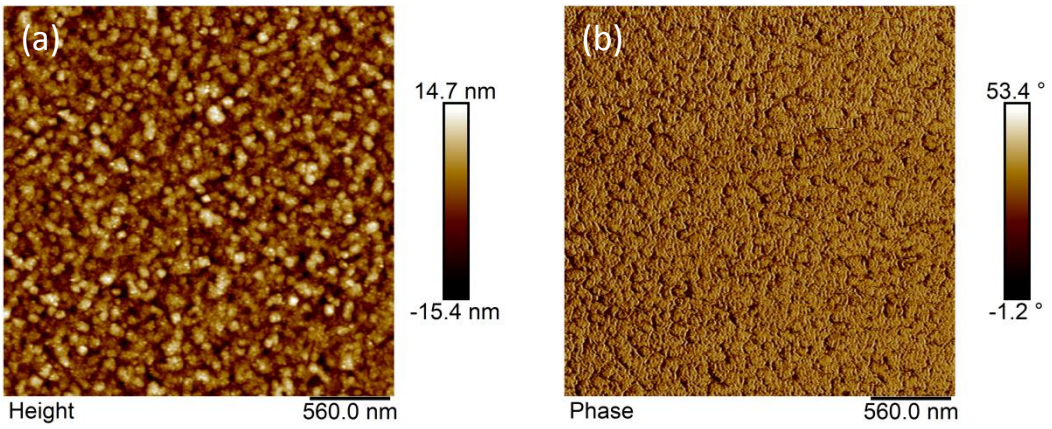

Figure 6-24: (a) 2D topography and (b) phase contrast plot of a typical 600 °C heat treated unsized E-glass fibre

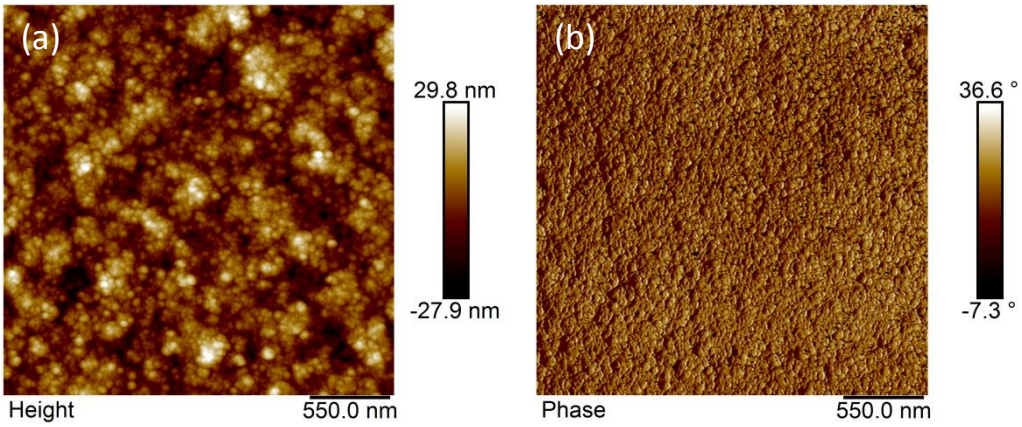

Figure 6-25: (a) 2D topography and (b) phase contrast plot of a typical 700 °C heat treated unsized E-glass fibre

6.2.3 Chemical analysis of features by SEM-EDX

Initial chemical analysis of high temperature (≥ 600 °C) conditioned fibres, treated as described in 3.2.3.2, was carried out using the Energy Dispersive X-ray spectroscopy function of the SEM as outlined in 3.9. The results of these analyses are presented in Figure 6-26: data shown in black are for major glass constituents (with normalised weight percentage in excess of 1) and those in red are minor components. The analysis depth of this technique is in the range 1 – 3 µm [114] therefore it is not particularly surface sensitive, in contrast to XPS. It was of interest to compare the results obtained by SEM-EDX with those from other techniques which are optimised to measure either surface or bulk chemical composition. This comparison is presented in Table 6-1; with respect to SEM-EDX data only those obtained for non- and 700 °C heat treated fibres are included. It can be seen that the results neither agree with those from surface analysis nor those from bulk analysis, whether by XRF or calculation based on glass formulation. The oxygen content was approximately 8 At% lower with respect to bulk glass values which it was expected to most closely replicate, balanced by higher atomic percentages of major glass elements Si, Ca and Al. With respect to potassium content, for which the only consistent trend was found (Figure 6-26) only tentative agreement with bulk results was found: a value of 0.13 At% was measured by EDX for untreated E-glass. This is of approximately similar magnitude as the value from a typical E-glass composition of 0.09 At%, although represents an increase of around 40 %. XPS data with a measured K component have not been reported, and similarly one was not found during the XPS conducted as part of this work.

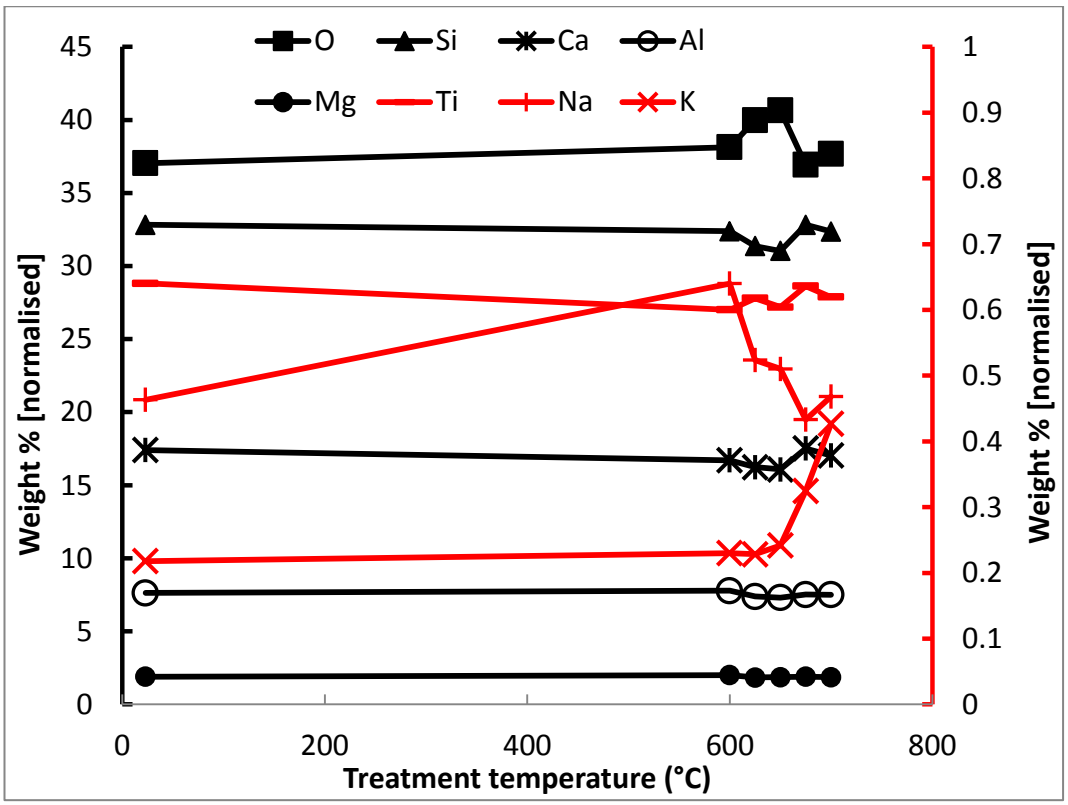

Figure 6-26: weight percentages (normalised) obtained by SEM-EDX of bare glass fibre following various heat treatments

Considering the results obtained directly from EDX, expressed in normalised weight percentage, the majority of glass constituents – major and minor – demonstrated little to no change in weight percentage and where small changes were found there was no consistent trend. The Si and O contents scaled inversely with each other, a finding in agreement with observations also made during XPS measurements. Changes in weight % of Na were found but they were inconsistent: between 600 – 700 °C values were measured that were less than, equal to and greater than the initial room temperature value for an untreated fibre.

In contrast, the weight percentage of potassium, K, experienced a consistent increase with heat treatment temperature once a temperature of 625 °C was exceeded. Although the magnitudes of normalised weight percent were relatively small, less than 0.5 %, they doubled following treatment at the maximum 700 °C compared with the initial value for untreated fibre.

Similar SEM-EDX analysis was also carried out on fibres rinsed as described in 6.2.2.4, at the same time as they were imaged. No significant differences were found in the normalised weight percentages of any glass constituents. Regarding

potassium specifically an average value of 0.44 % was obtained. These findings suggest that the surface structure which formed progressively between 600 – 700 °C was not itself rich in potassium.

6.2.4 Discussion of physical surface changes

Various changes to the physical surface of heat treated glass fibres have been presented in 6.2, these findings obtained by AFM and SEM observation. The AFM results showed that surface roughness increased significantly following any heating, in comparison to an untreated fibre. It was also found that the region in which a particularly significant increase in roughness occurred was 600 – 700 °C. From SEM imaging it was proven that changes at the fibre surface over this temperature range were part of a phenomenon affecting the entire fibre surface. This whole fibre SEM investigation was not possible after heat treatment at lower temperatures where the increases in fibre roughness did not produce features that were sufficiently large to be resolved. In tandem with SEM imaging of fibre heated treated at 25 °C intervals between 600 – 700 °C, chemical analysis was performed using SEM-EDX. No changes with reliable trends were found in the normalised weight percentages of major glass constituents such as silicon, calcium, aluminium or magnesium. There was, however, an increase in the normalised wt% of potassium which doubled from 600 to 700 °C. In summary, significant changes in physical appearance, and potentially also chemical composition, of the near surface region occurred following heat treatment in the range 600 – 700 °C. At lower temperature no chemical changes were detected by EDX, but physical surface changes occurred nonetheless following heat treatment in the range 200 – 500 °C. XPS results presented in 6.1.2 suggested that a slight increase in the concentration of calcium at the surface occurred following heat treatment at 450, 500 and 600 °C.

6.2.4.1 Links with strength loss

With respect to the strength loss of heat treated E-glass fibres, conclusions were drawn based on the work presented in Chapter 4. By developing a single fibre heat treatment and applying it to the treatment of bare fibre, fundamental thermal strength loss of the material was measured. The most critical strength loss appeared to take place after heat treatment in excess of approximately 450 °C. A maximum treatment temperature of 600 °C was used for the bulk of the work carried out,

however an attempt to investigate retained strength following heating to 700 °C was presented and discussed in 4.5.2.3. These data are shown here in Figure 6-27, in which the treatment temperature range has been divided into two distinct regions termed ‘low temp’ and ‘high temp’ which intersect at 450 °C.

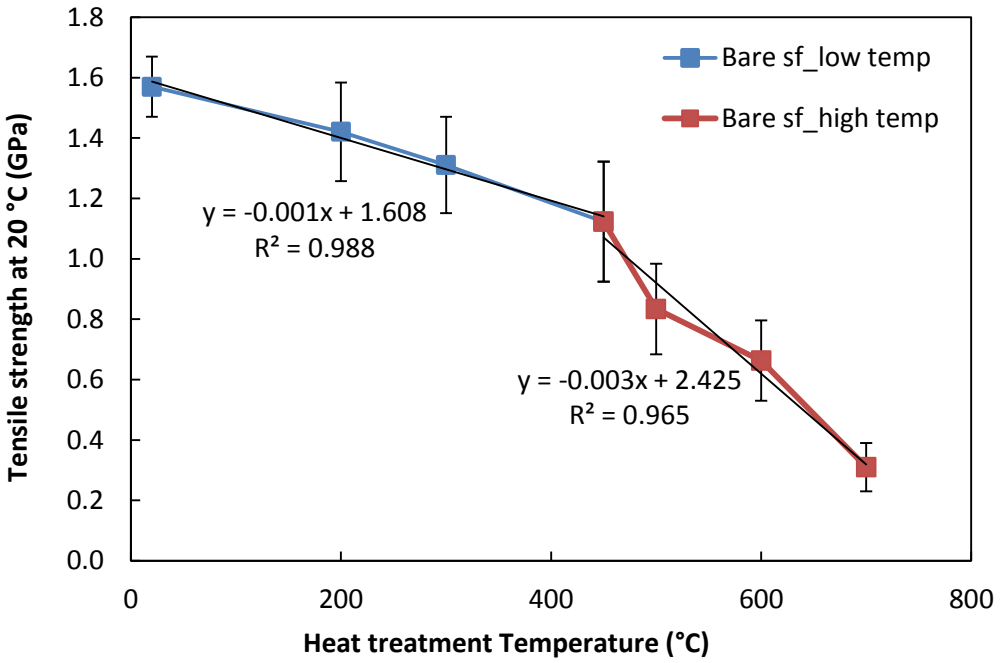

Figure 6-27: Tensile strengths of bare fibres after single fibre heat treatment for 25 minutes. Data are divided into a low temp and high temp zone either side of 450 °C and linear best fits for each of these zones are shown

In each of the two zones a relatively good linear fit was achieved. The gradient of the best fit line in the high temp region was triple that of the low temp region, reflecting that the most significant thermally induced strength loss took place at temperatures of 450 °C and above. Therefore, between 600 – 700 °C a strength loss was observed that was consistent with the thermally induced strength loss found for fibre treated at lower temperatures in the region 450 – 600 °C. In this same temperature range (600 – 700 °C) there occurred the progressive development of a surface structure and an apparent increase of potassium in the region of the first few microns at the surface. The precise mechanism responsible for the formation of this surface structure has not been identified at this time and is a topic for further research.

It is not known whether or not there is any relationship between observed surface roughness and the fibre strength loss. On the one hand, it is known that nano- or micro- scale roughness has the potential to negatively affect the strength of glass

[112]. In this case, however, such an effect appears unlikely due to the relatively small increases in the nano-scale roughness. This is discussed in greater detail in 6.3.3. Furthermore, as heat treatment temperature increases there is no apparent correlation between decreasing fibre strength and increasing RMS roughness of fibres.

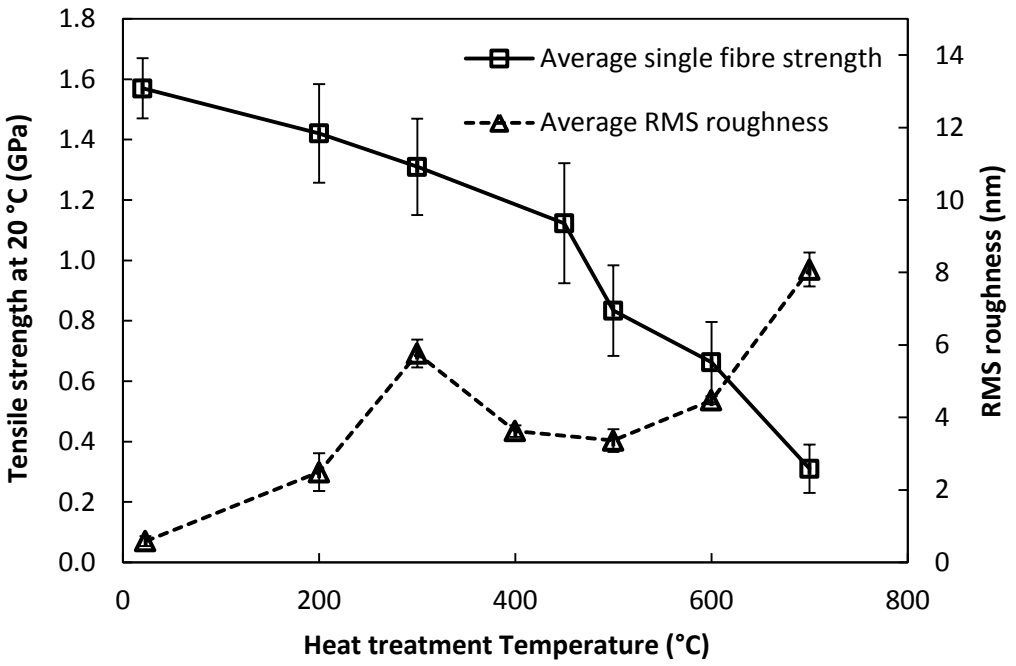

Figure 6-28: O-C unsized E-glass fibre; average fibre tensile strength and fibre surface RMS roughness against 25 minute heat treatment temperature

As shown in Figure 6-28, in the region where a significant decrease in fibre strength was found, from approximately 450 – 600 °C, there was in fact only a relatively modest increase in RMS roughness.

6.2.4.2 Known surface roughening effects

Changes in the surface roughness of glass fibre following heat treatment have not been reported and are not well understood: on the other hand, there is work in the literature of studies of surface roughness following exposure to various aqueous media which can be delineated as acid, base or neutral. Exposure of freshly produced glass surfaces to atmospheric moisture has a roughening effect, and further exposure to liquid water can promote this effect further [29, 113]. The effect of treating fibres in acidic or alkaline conditions has also been studied [112, 115]. Acidic conditions are understood to cause preferential leaching of glass ions leaving a silica rich surface; under alkaline conditions non-preferential network dissolution

occurs. Of the two processes network dissolution has a more significant surface roughening effect. Some evidence also suggests that leaching leads to an increase in specific surface due to pore formation, but that this is not evident when network dissolution under alkaline conditions takes place [115].

The continuing development of nano-scale roughness following heat treatment at progressively increasing temperatures was found, as indicated by increase in RMS roughness shown in Figure 6-4 and the series of images of heat treated fibre in 6.2.1.2. However, these images were taken at 100 °C intervals. Although the increases in roughness (with exception of R_{q_300}) were in agreement with increasing treatment temperature, as stated in 6.2.1.2, there were apparent step changes in general surface appearance. It was therefore not possible to say that surface roughening was due to a single effect which progressed with heat treatment temperature.

6.2.4.3 Potential sources of surface structure/roughness

The nano level roughness which formed on the surface of heat treated fibres was demonstrated by AFM measurements and, at sufficiently high treatment temperatures, was also shown in SEM images of fibre surfaces. An explanation for the observed surface changes, however, is missing and constitutes an area where further study may be required.

Based on AFM phase images such as those presented in Figure 6-24 and Figure 6-25 it was concluded that the surface structure formed had a similar composition to the rest of the surrounding glass surface. Some evidence of changes in surface chemistry was found by XPS and SEM-EDX, namely increases in the relative concentrations of Ca and K respectively. These results suggest the possibility that diffusion of these E-glass constituents through the glass during heat treatment may have occurred. Evidence of diffusion of Ca towards the surface of E-glass fibres has been reported before [26] and was summarised in 2.1.3.2. It is also established that diffusion of ions of alkali metals through silica is possible given sufficient heat input [116] and ions with smaller ionic radius will diffuse more readily. Further, monovalent alkali metal ions such as Na and K have a significantly greater mobility through silica networks than alkali earth metals, for example Ca [117].

An alternative effect that has been studied for silicate glass systems, although not for E-glass specifically, is phase separation. Typical examples of systems studied,

however, include SiO_2 – Na_2O [118] and SiO_2 – B_2O_3 – Na_2O – K_2O [119]; all of which are typically found in E-glass, with the exception of B_2O_3 which is now generally eliminated due to environmental concerns. Study of phase separation of these systems was carried out at temperatures in the range of 600 – 800 °C primarily utilising AFM. Before imaging, however, samples were subjected to an acid etching process to enhance the clarity of imaging; this works successfully if phase separation has occurred as the concentrated phases rich in silica resist etching more effectively. In the topography images presented in these works [118, 119] phase separation is clearly observed with respect to its progression with both increasing temperature and elapsed heat treatment time.

From observation of both AFM images of the SiO_2 – Na_2O system in [118] and topographic plots from this thesis of heat treated E-glass at 600 or 700 °C (Figure 6-12 and Figure 6-13), some potentially interesting comparisons may be drawn. Although the known content of Na_2O in [118] is around an order of magnitude greater than that estimated for the E-glass studied, in addition to being a far simpler binary system, some general similarities could be interpreted.

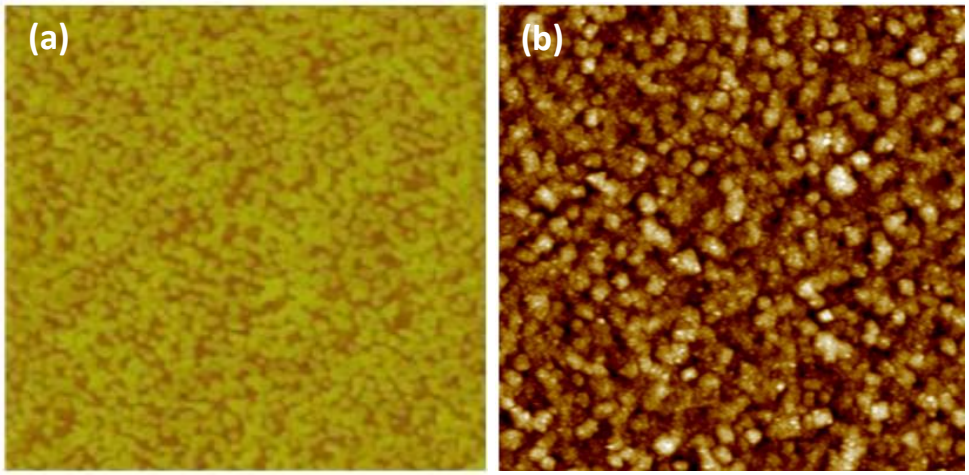

Figure 6-29: AFM topography, 2x2 µm images of: (a) 12.5Na_2O . 87.5SiO_2 heat treated at 650 °C for 160 minutes, taken from reference [118]; (b) bare E-glass fibre heat treated at 600 °C for 25 minutes

Two topography images produced using AFM are shown in Figure 6-29: (a) is taken from [118] and represents a molar composition 12.5Na_2O . 87.5SiO_2 sample heat treated at 650 °C for 160 minutes, while (b) is typical of images obtained in this work for bare E-glass fibre heat treated at 600 °C for approximately 25 minutes. It is not possible to comment on the relative z-scales as none are given with the images from [118]; in any case these would not be directly comparable as the sodium

silicate samples were lightly acid etched where E-glass fibres were imaged as produced following heat treatment. In Figure 6-29 (a) silica rich areas are also artificially high in comparison to phase separated regions rich in sodium which were etched, whereas in Figure 6-29 (b) there appears to be a steadier gradient between peak and trough regions. Despite these differences in sample preparation, there are similarities in the general surface appearance between (a) which demonstrates spinodal decomposition of the two phases, and the E-glass surface in (b). It would be of significant interest if some kind of phase separation of E-glass during heat treatment was found to occur, which contributes to changes in surface topography and roughness.

6.3 Fracture and flaws in glass fibres

6.3.1 Introduction

As discussed in 2.2.2 the strength of glass fibres is understood to be governed by the distribution of flaws as first described by Griffith [11]. This theory adequately explains why a correlation between increasing gauge length and decreasing fibre strength is found [95]. Despite the accepted framework of flaws and strength, the visualisation of these flaws has proved consistently challenging for fibres. Images of in-situ flaws have been reported [120] but the production of these requires specially designed equipment and, generally, the use of pure silica.

When working with glass fibre the visualisation of flaws has been demonstrated, at times, to be possible after fracture of tensile specimens has occurred, using Scanning Electron Microscopy of carefully prepared samples [59, 95, 100, 121, 122]. Even when fracture surfaces are successfully imaged at high resolution, in many cases it nonetheless remains impossible to observe the flaw from which fracture initiated [59]. The dimension of the critical flaw at which fracture occurs, a, is related to the fracture toughness, K_{Ic}, of a material through (6.1).

$$K_{Ic} = \frac{\sigma_f Y}{(\pi a_c)^{-1/2}} \tag{6.1}$$

In equation (6.1) σ_f is the fibre fracture stress and Y is a geometric factor dependent on the position, shape and dimensions of the critical flaw. The equation may be re-arranged in terms of flaw dimension, a_c.

$$a_c = \frac{1}{\pi}\left(\frac{K_{Ic}}{\sigma_f Y}\right)^2 \quad (6.2)$$

From equation (6.2) the theoretical critical flaw dimension can be calculated for an E-glass fibre if the failure stress, fracture toughness and geometric factor are known. Failure stress is relatively straightforward to measure by single fibre tensile test; if fractographic examination of the tensile sample is possible thereafter, an acceptable estimate of factor Y may be made. In most cases, however, there will be no clearly visible flaw at the fracture origin and assumptions about the geometry of this flaw must be made. The fracture toughness of E-glass can be obtained from the literature. A value of K_{Ic} = 0.93 MN $m^{3/2}$ was reported by Ghosh et al. for bulk E-glass [123] and a similar value K_{Ic} = 0.91 MN $m^{3/2}$ was found by Feih et al. using E-glass fibre [122]. Additionally, they reported that the fracture toughness was not altered by heat treatment of the fibres; this observation was based on heat treatments carried out at 450 °C.

6.3.2 Fractography of heat treated E-glass fibre

In agreement with the general findings of Lund and Yue [59], in many of the fibre fracture surfaces investigated in the work undertaken it was not possible to observe any flaw at the point of fracture origin. An example of this is given in Figure 6-30.

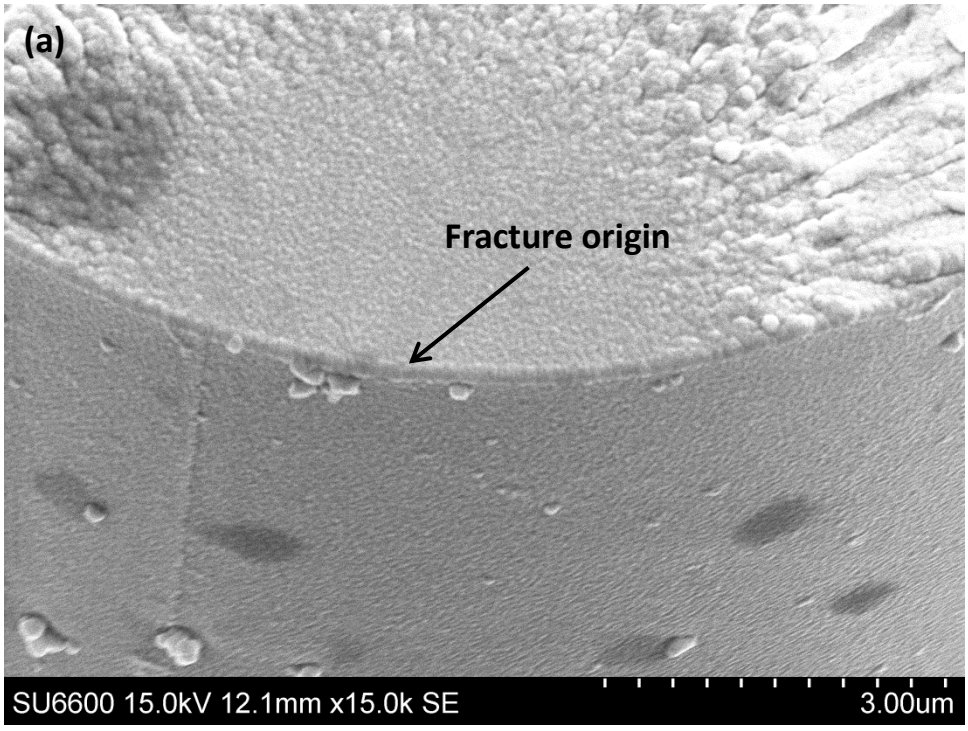

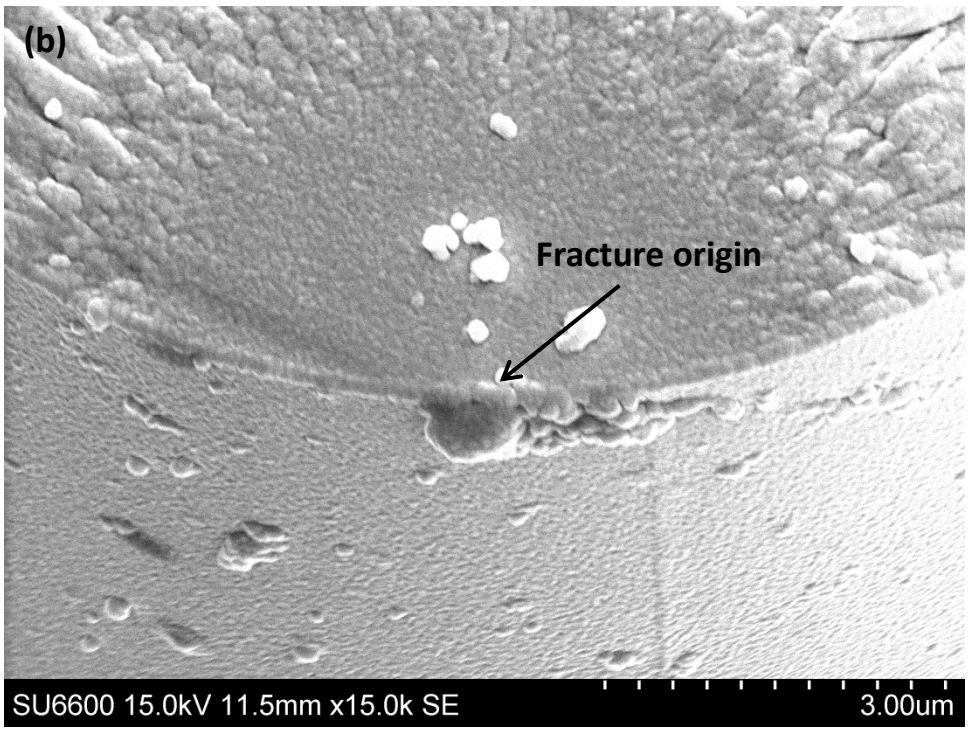

Figure 6-30: fracture mirror and mist regions (a) and (b) of the same 450 °C vacuum heat treated fibre with strength 1.23 GPa, with approximate fracture origin indicated

On fracture surface (a) no indication of a flaw to initiate fracture was found; at the expected fracture origin of surface (b) some surface structure was observed. The general appearance of this structure suggested some form of contamination which may have obscured a flaw beneath.

Conversely, the fracture surface of another fibre with similar strength is presented in Figure 6-31 upon which an obvious source of fracture could be observed. The mating fracture surface is not shown, deviating from the method outlined in standard ASTM C1322-05b, as it was not possible to achieve a suitable image due to localised contamination and charging issues.

The apparent critical surface flaw on this fibre is clearly visible; the shape is estimated as approximately circular, meaning the geometric factor Y = 1.29. Fracture stress was measured as 1.2 GPa and fracture toughness taken from the literature as 0.91 MN $m^{3/2}$. Using equation (6.2) the critical flaw dimension was calculated to be a_c = 0.11 µm, in very close agreement with the measured dimension as shown in Figure 6-31.

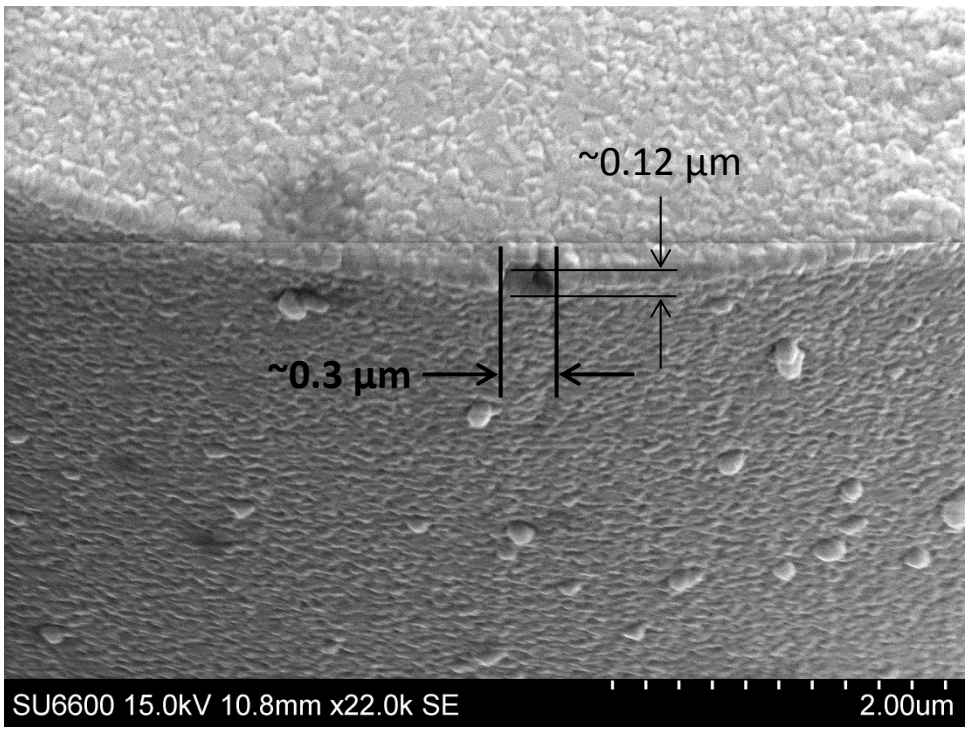

Figure 6-31: fracture origin of a 450 °C vacuum heat treated fibre with strength 1.2 GPa

Nonetheless, the inconsistencies reported by other researchers regarding availability of observable flaws on fibre fracture surfaces were confirmed in this work. In addition, in some cases where an apparent critical surface flaw was found at the origin of the mirror region the apparent measured dimension of this flaw did not agree with the calculated value based on the known single fibre strength, fracture toughness and geometric factor.

6.3.3 Comparison of flaw theory with observed AFM data

6.3.3.1 Topography data for non-heat treated bare fibre

There has yet to be reported in the literature clear and unambiguous evidence of a critical surface flaw on the surface of a glass fibre found before fracture of the fibre has been achieved. From the fractography conducted, examples of which are presented in 6.3.2, and from other work [59, 122] it has been shown post-fracture that often no visible flaw is found at the origin of fracture. In other cases a straight or circular edge flaw may be present.

Based on knowledge of Equation (6.2) it is possible to calculate the fibre strengths associated with a range of values of a_c. Presented in Table 6-3 are calculated failure stresses, $\sigma_{f\text{-}c}$, based on either the straight or circular edge flaw.

Table 6-3: Calculated E-glass fibre failure stresses with change in flaw depth according to (2.1), for straight (Y=1.12) and circular (Y=1.29) edge crack

Flaw depth, a_c (nm)	Calculated fibre strength, $\sigma_{f\text{-}c}$ (GPa)	
	[Y=1.12]	*[Y=1.29]*
1	14.50	12.59
2	10.25	8.90
3	8.37	7.27
4	7.25	6.29
5	6.48	5.63
10	4.58	3.98
15	3.74	3.25
20	3.24	2.81
30	2.65	2.30
40	2.29	1.99
50	2.05	1.78
75	1.67	1.45
100	1.45	1.26
150	1.18	1.03
200	1.03	0.89
300	0.84	0.73
400	0.72	0.63
500	0.65	0.56
600	0.59	0.51
700	0.55	0.48
800	0.51	0.44
900	0.48	0.42
1000	0.46	0.40
1250	0.41	0.36
1500	0.37	0.32

The z-height parameters obtained by AFM of untreated bare fibre samples are also presented in Table 6-4. Taken from each individual image analysed, these include the maximum and minimum z-values and their difference , the total z-range.

Table 6-4: measurements (all in nm) in z-direction for individual bare E-glass fibres analysed by AFM. Approximately 3 µm squares were analysed for each sample

Sample name	z_{max}	z_{min}	z-range
gf_4a_cs020	3.9	-1.3	5.2
gf_4a_cs021	4.4	-1.4	5.8
gf_5a_cs025	2.9	-1.5	4.4
gf_5a_cs026	6.4	-1.9	8.3
gf_5b_cs027	1	-0.9	1.9
gf_5b_cs028	1.4	-0.7	2.1
gf_7a_cs012	1.2	-0.8	2
gf_7a_cs013	1.6	-0.9	2.5
gf_7a_cs015	3.5	-1.6	5.1
gf_9a_cs018	1.5	-1	2.5
gf_9a_cs019	2.1	-1.2	3.3
gf_10a_cs000	2.4	-1.2	3.6
gf_10a_cs001	3	-1.3	4.3
gf_11a_cs004	3.8	-1.3	5.1
gf_11a_cs005	4.1	-2.6	6.7
gf_11b_cs006	3.1	-1.8	4.9
gf_11b_cs007	3.6	-1.4	5
gf_12a_cs008	3.4	-1.4	4.8
gf_12a_cs009	4.1	-1.3	5.4
gf_12b_cs010	5.4	-1.7	7.1
gf_12b_cs011	4.5	-2	6.5

From examination of Table 6-4 it is found that the average image z-range was 4.6 with a maximum of about 8 nm; the average z_{min} was -1.4 with a minimum of -2.6 nm.

6.3.3.2 Implications of AFM topography and fibre strengths

The subject of glass fibre strength was covered extensively in 2.2, including the difference between intrinsic and extrinsic strength. The strength data presented in this work are all extrinsic: the intrinsic strength of E-glass has, however, been reported and is of the order of 6 GPa [56]. Considering the upper limit of intrinsic strength and with reference to Table 6-3, if failure of an E-glass fibre were to occur at the surface then this would suggest the presence of a flaw with critical dimension of between approximately 4 – 5 nm, or potentially slightly less depending on the geometric factor.

Through measurement of extrinsic strength it has been shown that there is a correlation between gauge length of tensile specimens and the average strength

found; shorter gauge lengths leading to higher measured strengths [95, 124]. When investigating fibre topography by AFM in effect only a relatively small area of surface can be analysed; in this work squares of sides approximately 3 µm. If we consider the potential strength of the fibre based on such a small effective gauge length it must be considerably greater than the 1.5 GPa measured using a 20 mm gauge length. Nonetheless an absolute upper limit remains, that is the intrinsic strength of the material. Examining the data in Table 6-4 it was found that the topographic features imaged by AFM were small: total z-ranges were all well below 10 nm and so called 'troughs' below the z=0 plane measured no more than (minus) 2 nm. According to Table 6-3 if a surface flaw was represented by such a trough depth it would correspond to a failure stress close to the theoretical strength of glass [54]; therefore the troughs observed can probably be discarded as a features related to fibre fracture. Considering full z-range values, the strengths that are computed are just below the intrinsic material strength but greater than many reported strengths obtained for freshly drawn fibres tested immediately after manufacture, which approach 4 GPa [5, 55]. In any case, full z-range is not a reasonable choice of dimension in the z axis on which to base estimations of strength as maxima and minima do not tend to occur adjacent to each other on the fibre surface. This may be interpreted to suggest that the AFM measurements performed as described may not be capable of visualising a surface flaw, critical or otherwise. The surface features and roughness measured may be indicative of other processes causing surface roughening but do not directly relate to strength of untreated fibres. This would appear to be the case for heat treated fibres also: as shown in Table 6-5 and Table 6-6 the average z-range or z_{min} found at each heat treatment temperature correspond to a fibre strength far greater than the measured value.

Table 6-5: comparison of measured average strengths of heat treated fibres, with calculated strengths based on z-ranges taken from AFM topography of heat treated fibres

Treatment temp. (°C)	Measured avg. strength (GPa)	Avg. z-range (nm)	Calculated strength (GPa)	Calculated strength (GPa)
			Y = 1.12	Y = 1.29
200	1.42	35	2.4	2.2
300	1.31	67.2	1.8	1.6
400/450	1.12	38.7	2.3	2.0
500	0.83	39	2.3	2.0
600	0.66	43.3	2.2	1.9
700	0.31	80.6	1.6	1.4

Table 6-6: comparison of measured average strengths of heat treated fibres, with calculated strengths based on z_{min} values taken from AFM topography of heat treated fibres

Treatment temp. (°C)	Measured avg. strength (GPa)	Avg. z_{min} (nm)	Calculated strength (GPa)	Calculated strength (GPa)
			Y = 1.12	Y = 1.29
200	1.42	-8.1	5.1	4.4
300	1.31	-19.3	3.3	2.9
400/450	1.12	-11.1	4.4	3.8
500	0.83	-10.3	4.5	3.9
600	0.66	-14.8	3.7	3.2
700	0.31	-27.9	2.7	2.4

6.4 Crystallisation behaviour

6.4.1 Introduction

As discussed in 2.4.3 crystallisation of glass fibre has been reported for some formulations [63, 77], but not previously in relation to E-glass. Basaltic fibres, with some compositional similarity to E-glass, have been shown to exhibit both surface crystallisation and loss of tensile strength following heat treatment [77] therefore an investigation of E-glass was carried out following the method described in 3.4.

6.4.2 Results

The results of X-Ray Diffraction measurements on unsized fibre, before and after heat treatment, are presented in Figure 6-32. Details of the heat treatment applied are outlined in 3.2.1.3.

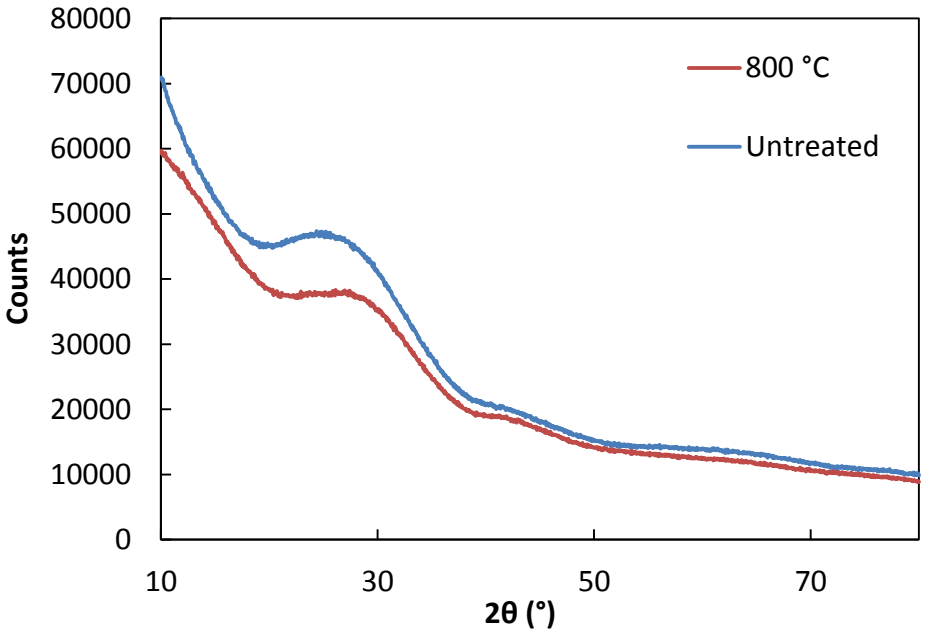

Figure 6-32: X-ray diffraction patterns for unsized E-glass fibre: untreated (blue) and heat treated to 800 °C and furnace cooled (red)

A difference in total counts during the analysis at 2θ < 40° was found, however this can be attributed to slight differences in the preparation of the samples. The diffraction patterns obtained were largely featureless; in both a broad band between approximately 20° < 2θ < 40° was found. This band is a typical feature of the diffraction patterns of amorphous glasses containing a majority of silica, regardless of whether or not some form of heat treatment or annealing has been applied [77–79, 125].

6.4.3 Discussion

A similar broad band (sometimes referred to as halo) but no diffraction spikes were found in the diffraction spectra for untreated and heat treated E-glass. This strongly suggests that no crystallisation occurred as a result of the heat treatment and the structure of the E-glass remained amorphous.

It was noted by Yue et al. [77] that the crystallisation of stone wool fibre (SWF) occurred only at the fibre surface, with the formation of a layer up to approximately 100 nm in thickness. In their case the effect on the X-ray diffraction spectrum was quite subtle, but a distinct change in the surface topography was measured by AFM; namely there was a significant increase in maximum z-dimension. In general terms

this surface change was similar to the development of surface features observed in the AFM imaging of heat treated E-glass fibre surfaces as presented in 6.2. Although similar in character, there are reasons to conclude that the development of surface roughness observed in E-glass fibre is not related to a crystallisation phenomenon as it is in SWF. The mechanism by which magnesium (as well as calcium and iron) ions migrated to the surface of SWF and formed a crystalline layer was explained as a consequence of the oxidation of the ferrous component of these relatively iron-rich fibres. The content of both magnesium and iron oxides in E-glass is considerably lower than that of SWF: respectively, in E-glass versus SWF there is 3 – 4 % compared with approximately 11 % MgO and no FeO where in SWF there may be a content of 7 %. These chemical compositions are sufficiently different that it would be unlikely that a similar mechanism of surface crystallisation could occur during the heat treatment of E-glass fibres, in agreement with the negative finding of the XRD analysis in this work.

Chapter 7. Conclusions

7.1 Statement on the novelty of the work presented

A statement regarding the novelty of the work presented in this thesis is included here ahead of the more detailed conclusions of the work that was presented in each of the three results chapters 4 – 6.

1. The development and utilisation of a single fibre approach to heat treatment of glass fibres allowed the minimisation of strength loss due to mechanical damage, making it possible to study strength loss due to fundamental thermal effects.
2. Use of a system in which it was possible to simultaneously heat teat single fibres while holding them under vacuum allowed the effect of removal of physical water from the treatment atmosphere and fibre surface to be studied for the first time.
3. A systematic study of physical and chemical changes to glass fibres following heat treatment was carried out using a large variety of techniques such as AFM, XPS, SEM-EDX and XRD. These changes were alongside data on fundamental strength loss to assess any possible relationships.

7.2 Strength loss of heat treated fibres (chapter 4)

7.2.1 Degradation of surface coating

The sized E-glass fibre (as opposed to the unsized or bare fibre) used in the work presented was coated with AminoPropyltriethoxySilane (APS). The degradation of this aminosilane, in both oxidative and non-oxidative atmospheres was explored using the thermal analysis techniques TGA, DSC and CATLAB.

Mass loss at relatively low temperature, below 200 °C, was attributed to volatilisation of both water and carbon dioxide. The onset of degradation of the organic fraction of APS was found to begin between approximately 300 – 350 °C depending on the nature of treatment atmosphere, onset occurring at higher temperatures in a non-oxidative atmosphere. The maximum rate of mass loss, and peak in the exothermic degradation reaction, occurred at approximately 450 °C.

XPS surface analysis of APS coated fibres suggested that a heat treatment of 450 °C for 25 minutes was sufficient to remove the organic fraction of the silane, as no nitrogen N1s signal was detected. Removal of the nitrogen-containing amine group occurs by scission of a C-N bond; scission of this bond requires energy of 305 kJ/mole. The energies of other bonds within the organic primary amine terminated group are slightly greater: C-C 347 kJ/mole and Si-C 360 kJ/mole. It is possible that a percentage of the coating is retained after this heat treatment, but as discussed in 4.4.1 it was not possible to distinguish the carbon of the APS from that associated with surface contamination.

SEM observation of the surfaces of APS fibres treated at 300 °C showed some evidence of the degradation of the silane coating at this temperature, in support of findings from TGA and DSC that this marks the initiation temperature of degradation in air.

In general, an understanding of the degradation of the APS fibre coating was developed in order to aid in the interpretation of fibre strength retention results following heat treatment with respect to possible fibre surface damage.

7.2.2 Mechanical handling damage

The retained strength of heat treated E-glass fibre was previously known to be an effect of both temperature and time of treatment. The work presented in Chapter 4 additionally showed that it can be highly dependent on the nature of the heat treatment method used. This was achieved by the use of two distinct heat treatment processes, bundle and single fibre, in which fibres for tensile testing were separated respectively after or before heat treatment was performed. In cases where the fibre surface was not suitably protected by a silane based sizing – either because it was not applied to the fibre during manufacture, or because it had degraded at high temperature – a significant difference in retained fibre strength was measured between the two methods.

When surface protection was not afforded by the silane, significantly greater strength was measured by using single fibre heat treatment rather than bundle. Such results were found using APS coated fibres heat treated at greater than 300 °C up to 500 °C; and for bare fibres treated between 200 – 600 °C. Supported by

the results of thermal analysis of APS degradation (7.2.1), insufficient surface protection due to silane degradation was identified to explain the significant difference in strengths depending on the heat treatment procedure applied. In such cases, where there was a difference in retained fibre strength, the strength loss measured using bundle heat treatment consisted of two components: a fundamental heat treatment component and additional mechanical handling damage.

7.2.3 Thermal strength loss

Application of the novel single fibre heat treatment procedure allowed separation of the mechanical handling damage and thermal damage effects to be achieved, as handling damage was minimised to the smallest possible value. The procedure was applied to bare E-glass fibres whose strength after heat treatment, unlike APS sized fibres, is not a function of degradation of the surface coating. The strength loss measured after heat treatment therefore represented that which occurred due only to thermal effects. By application of this process the critical strength loss zone associated with the thermal effect was identified as between approximately 450 – 600 °C. It was then possible to conduct further analyses within this temperature zone to attempt to identify the phenomena responsible. Following application of single fibre heat treatment to APS sized fibre it was found that, similar to bare fibre, the critical temperature range with respect to strength loss occurred between 450 – 600 °C. This could be interpreted to suggest that surface coating degradation was not important when mechanical handling damage was minimised and the same thermal strength loss phenomenon affecting the bare fibre was dominant; this is somewhat in contrast with the possible ‘flaw healing’ mechanism that has been proposed previously [94].

7.3 Effect of the presence of water during heat treatment (chapter 5)

The effect of atmospheric water to weaken glass has previously been reported in the literature and was summarised in 2.1.4.1. This effect, which is most probably caused by a diffusion process, is significant when considering freshly drawn fibres [29].

Following production the glass fibre strength steadily approaches a constant value, far less than the value immediately after drawing. It is known, however, that adsorbed water exists on the surface of glass fibres; it was the possible effect of this, in addition to atmospheric, water during heat treatment of glass fibres that was investigated as it has never previously been studied. Despite the paucity of systematic investigations of the contribution of water to strength loss of heat treated fibre, it has at times been invoked as a possible explanation for at least part of the well-established decrease in strength.

In contrast to some previous investigations instead of an extremely dry inert gas in the heat treatment chamber, a vacuum heat treatment using a Thermal Volatilisation Analyser (TVA) was developed, allowing the application of relatively high vacuum and temperature simultaneously. Application of a sufficiently strong vacuum facilitates the removal, in addition to atmospheric moisture, of surface adsorbed water from amorphous glasses [19]. Using the TVA the efficacy of a 2 hour vacuum drying procedure at room temperature to remove surface water from glass fibre samples was demonstrated.

Single fibre heat treatment of bare E-glass was performed under vacuum at 450 °C. It was found that there was no significant difference in retained fibre strength when comparing the vacuum heat treatment including room temperature pre-drying of the fibre, and a standard treatment in an air furnace. From the experimental work conducted it was concluded that:

1. As reported in the literature using dry inert gas as the furnace atmosphere, the presence of water in the treatment atmosphere does not have an effect on strength loss.
2. The surface adsorbed water on glass fibres does not take part in a reaction which contributes to the fibre strength loss; although further study of this effect would be of great benefit as only one heat treatment temperature was studied in this work.

7.4 Glass fibre surface changes due to heat treatment (chapter 6)

7.4.1 Chemical

7.4.1.1 Surface calcium content (XPS)

XPS analysis of the surface of heat treated bare E-glass fibres suggested an increase in the concentration of calcium in approximately the outermost 10 nm following heat treatment at 600 °C, consistent with the findings of Nichols et al. [26]. Changes in the atomic percentages (At%) of other glass constituent elements were measured but no consistent trends were observed. The data produced did not exhibit any correlation between fibre strength loss and atomic percentage of calcium at the surface: little change in At% occurred between room temperature (non-heat treated) and 500 °C, whilst a significant decrease in fibre strength was measured. It should therefore be considered unlikely that change in surface calcium concentration provides a direct explanation for the strength loss phenomenon.

7.4.1.2 Physio-chemical: K content increase with development of surface structure

The progressive development of a surface structure following heat treatment at temperatures of ≥ 600 °C was observed by both AFM and SEM. Chemical analysis of individual fibres during SEM imaging was carried out using EDX; an increase in normalised weight percentage (wt%) of potassium was found with a maximum at 700 °C. As potassium is only a very minor glass constituent in E-glass it is suggested that further confirmation of this behaviour after relatively high temperature heat treatment should be carried out using a more sensitive surface analysis technique, as outlined in Chapter 8.

7.4.2 Physical

Changes in the surface roughness of bare fibres following heat treatment in the range 200 – 700 °C were studied in detail by AFM. A precise correlation was not found between the average RMS roughness of fibres and their average single fibre tensile strengths after heat treatment over the temperature range investigated.

However, a general trend of decreasing fibre strength and increasing surface roughness was found (Figure 6-28).

Considering individual topography plots, the trough depths were not of sufficient dimensions in the z-direction that they were likely to represent a critical flaw at which failure could initiate. Examination of total z-ranges yielded a similar conclusion; in this case the values obtained could translate by calculation to possible, although very high, strengths below the intrinsic strength of E-glass, but significantly higher than commonly reported values. These high strengths might be considered plausible given the framing effect produced by analysis of areas of the order of only a few microns squared, similar to the well-established gauge length dependence of measured fibre strength. However, the minima and maxima of z-height did not tend to occur adjacent to one another on the analysed fibre surface areas; this suggests that they were also unlikely candidates for a critical flaw for the initiation of failure. Theoretical calculations of fibre strength were made based on fracture toughness, flaw dimension and a range of reasonable geometric factors of a surface flaw; the total z-range or z_{min} from AFM images was used in place of flaw dimension. In the case of untreated fibres, the calculated strengths were greater than the intrinsic strength of E-glass using z_{min}; the average value of z-range equated to a strength of approximately the intrinsic value, or just below for the highest z-ranges. The calculated strength values for heat treated fibres were between 1.5 to 5 times (z-range) or 2 to 9 times (z_{min}) greater than the experimentally measured strengths; the disparity increased with increasing conditioning temperature. These results suggest that the AFM observed surface roughness does not appear to relate directly to tensile strength of bare fibre, and that observation of a feature that could reasonably be interpreted as a critical surface flaw was not achieved. Changes in surface roughness with heat treatment may be indicative of other processes causing surface roughening; a close correlation with strength was not evidenced although a general trend between increasing roughness and decreasing fibre strength does exist.

Between 600 – 700 °C the development of a distinctive surface structure was observed by AFM and SEM. Concurrently, an increase in K content was measured using EDX as outlined in 7.3.1.2. The physical appearance of this structure bears resemblance to some high temperature phase separated glasses of Si-Na systems. Further work is required to investigate the phenomenon. E-glass phase separation has not been previously reported and substantial further data would be required to

either prove or disprove it as a mechanism affecting heat treated E-glass fibre at temperatures exceeding 600 °C.

7.4.3 Crystallisation

Data were gathered by XRD using ground samples of both untreated E-glass fibre and fibres heat treated to 800 °C and allowed to cool slowly back to room temperature. Similar ‘halo’ diffraction patterns were produced for both the treated and untreated fibres. This evidence suggests that crystallisation does not occur during heat treatment of E-glass fibre, and as such does not play a role in the strength decrease observed.

Chapter 8. Future work

8.1 Surface analysis

8.1.1 Further study of surface roughening due to heat treatment

8.1.1.1 Continuing AFM study

If single fibre heat treatment is carried out using a relatively low temperature, in the range 200 – 300 °C, then a steady state minimum strength will be reached after a sufficiently long conditioning time. The conclusion based on the data presented in Chapter 4 is that, by heat treating individual fibres, the strength loss observed is attributable to thermal effects on the fibre rather than physical damage to the fibre surface. This should hold regardless of the length of heat treatment, although in Chapter 4 the treatment time was constant for all experiments. Whether fibre surface damage is minimised by careful single fibre heat treatment or not, a decrease in fibre strength necessitates that there was an enhancement of critical surface flaws in line with Griffith's theory [11].There is evidence to suggest that the fracture toughness of E-glass fibres is unchanged following heat treatment [122]; this suggests that to satisfy the decrease in fracture strength there must occur either; (a) an increase in critical flaw dimension or (b) a change in surface flaw such that the geometric factor Y increases.

It was shown in Chapter 6 that – in addition to significant fundamental thermal based strength loss – heat treatment for approximately 30 minutes at relatively low temperatures such as 200 or 300 °C also caused a significant change to the surface of fibres in terms of their topography and an associated increase in RMS roughness was found by analysis of AFM images obtained. These images constituted snapshots taken after heating and cooling had been completed. Some progression of the surface roughening effect was visible in images taken at progressively increasing temperature but the effect was not clear and unambiguous. For this reason it is proposed that further study of fibre surface changes by AFM should be carried out. One approach that would aid in assessing the progression of the surface changes is to capture topographic images at smaller HT temperature intervals, for example every 50 °C. This would be particularly interesting over the range 400 – 600 °C: in this range of temperatures significant changes in surface occurred but there was no clear development of surface structure. Rather, as described in

Chapter 6, there appeared to be a step change between 500 and 600 °C. As the most significant strength loss was found to take place in this temperature range it is of particular interest to study and understand the surface changes that take place.

8.1.1.2 AFM analysis of vacuum heat treated fibres

The AFM analysis conducted used only fibres that were heat treated in an air furnace. It would be of interest to observe the topography of fibres treated at similar temperatures under vacuum, to investigate whether the presence of surface water has any effect on the development of surface roughness of bare fibres. Similar investigation could be carried out using the environmental AFM described in 8.1.1.3 however the maximum operating temperature available would be restricted.

8.1.1.3 Environmental AFM study

An alternative option that is only available for the further study of changes at lower temperature is the use of an environmental AFM in whose analysis chamber it is possible to control both temperature and humidity. Using equipment within the Laboratory of Biophysics and Surface Analysis at University of Nottingham (as utilised in previous work) it is possible to perform environmental AFM with humidity between approximately 10 – 80 % and temperature up to 200 °C. Although this is a lower temperature limit than ultimately desired, a roughening effect was nonetheless found following heat treatment at 200 °C so it would therefore be possible to investigate the development of this over time with this AFM setup. Proper execution of this experiment would require an investigation of the strength of bare E-glass fibres, using the single fibre heat treatment method, following conditioning at 200 °C for various lengths of time. As discussed in 6.2.4.1 no relationship between fibre strength and average RMS surface roughness was found through the range of treatment temperatures investigated. However, in this case it is not yet understood if the surface roughening observed is the product of different processes that occur and potentially overlap at different temperatures. In the case of a time dependent study at constant temperature of 200 °C it is more reasonable to assume that the potential issue of multiple competing processes will be removed. It would then be of interest to compare the time dependent strength loss with RMS roughness over the same time scale.

8.1.1.4 Investigation of potential phase separation at high temperature

The topic of phase separation in silicate glasses was discussed in 6.2.4.3 in relation to E-glass. It was noted that topographic features on the surface of E-glass heat

treated to 600 °C or higher were similar in appearance to those observed during the phase separation of $12.5Na_2O$. $87.5SiO_2$ conditioned at similar temperatures [118]. It would be of interest to expand the investigation of E-glass by applying some of the methodology from this work. This would entail obtaining multiple AFM images after various lengths of heat treatment time to assess whether there is a development of the surface structure with time. Additionally, before analysis the fibres might be acid etched with a solution similar to the 0.5 % HF solution suggested in [118]. If some phase separation had occurred during heat treatment it is expected that topography images would have a similar appearance whether or not an acid etch were applied: in the case that an acid etch was used the trough depth of regions with lower silica content would increase giving an increased z-range in all images.

8.1.2 Further chemical analysis by SEM-EDX

The analysis using SEM-EDX that was presented in 6.3.2 was focused on samples that were heat treated between 600 – 700 °C and compared against a baseline where no treatment was applied. The majority of glass constituent elements exhibited minimal variation in their relative normalised weight percentages (wt%): the largest variations were observed for minor constituents, monovalent alkali metals Na and K. The wt% of K increased consistently between 625 – 700 °C whereas the wt% of Na fluctuated with no apparent trend. This approach to the investigation of chemical changes could be extended.

8.1.2.1 Extension of temperature range investigated

It may be of interest to perform chemical analyses using fibres treated at temperatures between room temperature and 600 °C. It is not expected that any significant changes would be found for the majority of E-glass constituents; however it is of interest to investigate whether there are any trends in the wt% of Na. If diffusion of these monovalent ions takes place during heat treatment of E-glass fibre it is expected that Na would diffuse more easily than K because of its smaller ionic radius [116] so possible changes in its concentration may occur at lower temperature.

8.1.2.2 Wavelength Detection X-ray spectroscopy

As described in Chapter 3, chemical analyses were conducted using the Energy Dispersive X-ray spectroscope which is part of the SEM instrumentation suite. An

alternative method to SEM-EDX is WDX – Wavelength Dispersive X-ray spectroscopy. EDX measures the energies of photons from a sample surface which are emitted when an outer shell electron moves to a space created in a lower energy shell due to impingement from an X-ray source. WDX differs in that it measures the wavelengths rather than energies of X-rays from the analysed surface; counting at a single wavelength at a time. This technique is more labour intensive as it requires careful calibration for each element that is desired to be analysed using a standard, prior to any measurements being taken. However, the results obtained may be considered superior compared to EDX; primarily they are more accurate because it is simpler to distinguish between the emitted wavelengths from the sample surface than it is the emitted energies of photons that are used for EDX analysis. Repetition of the measurements reported in this thesis, and extension of the investigation (for example over a greater temperature range), using WDX is likely to yield useful further results.

8.2 Further heat treatment & strength loss experiments

8.2.1 Investigation of the influence of production parameters (axial drawing stress) on strength retention following heat treatment

As summarised in the literature review (2.3.1), from some of the work of Lund & Yue, tentative evidence was presented that there may be an influence from either enthalpy or birefringence relaxation on retained strength of continuous E-glass fibre after heat treatment. This, however, was not clear as it was not the goal of their investigations but rather came out from analysis of the data they presented in the paper. The possibility of either of these phenomena relating to fibre strength loss is intriguing.

It is proposed that a series of experiments could be carried out using bare/unsized E-glass fibre produced under certain conditions, in a similar way to the investigation carried out by Stockhorst and Brückner [47]. The data presented by Lund and Yue [51] could be interpreted to suggest that either enthalpy relaxation, or birefringence relaxation, was related to strength decrease following heat treatment/annealing of continuous E-glass. Enthalpy and birefringence are production related properties so it would be necessary to manufacture fibres of identical E-glass composition, without

any surface sizing, in which these parameters were varied. A possible approach would be to maintain constant nozzle pressure and temperature; this would ensure a constant mass flow of glass through the nozzle and therefore a constant drawing force [126]. Birefringence is linked to drawing stress and this stress can be influenced by changes in fibre radius which is itself a function of drawing speed. This approach was used by Lund and Yue [51] to produce continuous E-glass fibres with a range of diameters and therefore drawing stresses between approximately 10 and 70 MPa. In their work they showed that changes in drawing stress do not affect fibre strength at room temperature.

Using at least two different fibres/fibre rovings with significantly different axial drawing stresses, the strength retention following heat treatment at a range of temperatures could be investigated, initially using a fixed treatment time. It would be necessary to use single fibre heat treatment in all cases, such that the strength loss observed was comprised of only a thermal component, rather than including mechanical handling damage. In addition to a study of fibre strength retention with both heat treatment temperature and time it would be necessary to study the relaxation over time of both enthalpy and birefringence of the same fibres. It would then be possible to identify critical zones in terms of the loss of fibre strength, and the relaxation of enthalpy and birefringence. If the temperature and time associated with significant strength loss correlated with either of these relaxations it would suggest that they may in fact be linked.

An additional factor that would be important to keep in consideration is the effect of changing diameter on the quenching of the fibre during manufacture: a reduction in fibre diameter with increase in axial drawing stress must take place. As discussed by Bateson [127] different modes of flaw formation, which would have an effect on fibre strength, might be possible during quenching if there was a sufficient radial thermal gradient. In order to minimise any such effect it would be advisable to limit the fibre diameters investigated to a relatively small range.

8.2.2 Further investigation of the effect of water on the fibre surface during heat treatment

The work presented in Chapter 5 on the effect of the presence of water during heat treatment of single glass fibres represented an initial investigation of this variable, using a novel testing setup devised to work in the vacuum chamber of a Thermal Volatilisation Analyser (TVA). It is accepted that the investigation presented is, in many senses, still only preliminary. A more detailed analysis of the volatilisation of water with vacuum pressure, time and temperature could yet be completed. Furthermore, only one heat treatment temperature of 450 °C was investigated. It would be significantly more informative to expand the range of heat treatment temperatures studied, particularly into the range 500 – 600 °C as this zone has been demonstrated to be particularly critical in terms of strength loss of the E-glass fibre studied.

8.2.3 The effect of water on flaws in glasses

It was shown in work by Feih et al. [122] that it is possible to create flaws of a desired depth in the surface of glass fibres by the process of Focused Ion Beam (FIB) milling. They demonstrated through fractographic analysis that fibre will fail at these engineered notches of nanometre dimensions. The SEM images of these milled notches represent the only images in the literature of a flaw at which a fibre will then fail during tensile testing, but taken before fracture has occurred. These engineered flaws, although causing initiation of failure, could however be considered as not representative of an ordinary surface flaw that would otherwise cause fibre failure. What a normally present flaw does look like remains unknown.

Although there is uncertainty about the representativeness of the FIB milled flaw, the technique developed could provide an interesting avenue of investigation, into the effects of high temperature water based treatments and their ability to increase the strength of glasses. Li and Tomozawa and Hirao and Tomozawa [128–130] have presented evidence of this strengthening effect on silica, and proposed a mechanism by which it may progress. Further, results produced by the Advanced Composites Group at University of Strathclyde have shown similar improvements in the strength of E-glass using water-based treatments at greater than room

temperature [131, 132]. The results of these treatments strongly suggest that they are altering the existing surface flaws in some fundamental way. It would be of interest to investigate the efficacy of the same water-based treatments on the strength of fibres in which an artificial flaw has been produced using FIB milling. If the treatment were to be unsuccessful it would imply that there is a significant fundamental difference between the milled flaw and that which would otherwise cause fibre failure.

References

1. Thomason JL, Yang L, Meier R (2014) The properties of glass fibres after conditioning at composite recycling temperatures. Compos Part A Appl Sci Manuf 61:201–208. doi: 10.1016/j.compositesa.2014.03.001

2. Job S (2013) Recycling glass fibre reinforced composites – history and progress. Reinf Plast 57:19–23. doi: 10.1016/S0034-3617(13)70151-6

3. Pickering SJ (2006) Recycling technologies for thermoset composite materials—current status. Compos Part A Appl Sci Manuf 37:1206–1215. doi: 10.1016/j.compositesa.2005.05.030

4. Sakka S (1957) Effect of Reheating on Strength of Glass Fibers. Bull Inst Chem Res 34:316–320.

5. Thomas WF (1960) An investigation of the factors likely to affect the strength and properties of glass fibres. Phys Chem Glas 1:4–18.

6. Cameron NM (1962) The Effect of Annealing on the Room Temperature Strength of Glass Fibres. Illinois

7. Jenkins PG, Yang L, Liggat JJ, Thomason JL (2015) Investigation of the strength loss of glass fibre after thermal conditioning. J Mater Sci 50:1050–1057. doi: 10.1007/s10853-014-8661-x

8. Emsley J (1983) Glass: past elegant, future thin. New Sci 728–732.

9. Wallenberger FT (2000) Structural Silicate and Silica Glass Fibers. In: Wallenberger FT (ed) Adv. Inorg. Fibers Process. Struct. Prop. Appl. Kluwer Academic Publishers, pp 129–168

10. (2011) Global glass-fibre production: changes across the board. In: JEC Compos. http://www.jeccomposites.com/news/composites-news/global-glass-fibre-production-changes-across-board. Accessed 16 Nov 2012

11. Griffith AA (1921) The Phenomena of Rupture and Flow in Solids. Philos Trans R Soc A Math Phys Eng Sci 221:163–198. doi: 10.1098/rsta.1921.0006

12. Wallenberger FT, Watson JC, Hong L (2001) Glass Fibers. In: Miracle DB,

Donaldson SL (eds) ASM Handbook, Vol. 21 Compos. ASM International, Ohio, pp 1–8

13. Wallenberger FT (2010) Commercial and Experimental Glass Fibers. In: Wallenberger FT, Bingham PA (eds) Fiberglass Glas. Technol. Springer US, Boston, MA, pp 3–91

14. Hair ML (1975) Hydroxyl groups on silica surface. J Non Cryst Solids 19:299–309.

15. Fry R a, Tsomaia N, Pantano CG, Mueller KT (2003) 19F MAS NMR quantification of accessible hydroxyl sites on fiberglass surfaces. J Am Chem Soc 125:2378–2379. doi: 10.1021/ja0275717

16. McDonald RS (1958) Surface Functionality of Amorphous Silica by Infrared Spectroscopy. J Phys Chem 62:1168–1178.

17. Peng L, Qisui W, Xi L, Chaocan Z (2009) Investigation of the states of water and OH groups on the surface of silica. Colloids Surfaces A Physicochem Eng Asp 334:112–115. doi: 10.1016/j.colsurfa.2008.10.028

18. Bakaev VA, Pantano CG (2009) Inverse Reaction Chromatography. 2. Hydrogen/Deuterium Exchange with Silanol Groups on the Surface of Fumed Silica. J Phys Chem C 113:13894–13898.

19. Zhuravlev LT (1993) Surface characterization of amorphous silica - a review of work from the former USSR. Colloids Surfaces A Physicochem Eng Asp 74:71–90.

20. Wesson SP, Jen JS, Nishioka GM (1992) Acid-base characteristics of silane-treated E glass fiber surfaces. J Adhes Sci Technol 6:151–169.

21. Carré A, Lacarrière V, Birch W (2003) Molecular interactions between DNA and an aminated glass substrate. J Colloid Interface Sci 260:49–55. doi: 10.1016/S0021-9797(02)00147-9

22. Liu XM, Thomason JL, Jones FR (2009) The Concentration of Hydroxyl Groups on Glass Surfaces and their Effect on the Structure of Silane Deposits. In: Mittal KL (ed) Proc. Sixth Int. Symp. Silanes Other Coupling Agents. Brill Academic Publishers, Cincinatti, pp 25–38

23. Pantano CG (2003) Effect of boron oxide on surface hydroxyl coverage of aluminoborosilicate glass fibres: a (19)F solid state NMR study. Phys Chem Glas 44:64–68.

24. Wong R (1972) Recent aspects of Glass Fiber-Resin Interfaces. J Adhes 4:171–179.

25. Thomason JL, Dwight DW (1999) The use of XPS for characterisation of glass fibre coatings. Compos Part A Appl Sci Manuf 30:1401–1413.

26. Nichols D, Hercules DM, Peek RC, Vaughan DJ (1974) Application of X-ray Photoelectron Spectroscopy to the Study of Fiberglass Surfaces. Appl Spectrosc 28:219–222.

27. Wang D, Jones FR, Denison P (1992) TOF SIMS and XPS study of the interaction of hydrolysed γ-aminopropyltriethoxysilane with E-glass surfaces. J Adhes Sci Technol 6:79–98. doi: 10.1163/156856192X00070

28. Fowkes FM, Dwight DW, Cole DA, Huang TC (1990) Acid-Base Properties of Glass Surfaces. J Non Cryst Solids 120:47–60.

29. Martin DM, Akinc M, Oh SM (1978) Effect of Forming and Aging Atmospheres on E-Glass Strength. J Am Ceram Soc 61:308–311.

30. Proctor BA, Whitney I, Johnson JW (1967) The Strength of Fused Silica. Proc R Soc A Math Phys Eng Sci 297:534–557. doi: 10.1098/rspa.1967.0085

31. Orowan E (1948) Fracture and strength of solids. Reports Prog Phys 12:185–232. doi: 10.1088/0034-4885/12/1/309

32. Ito S, Tomozawa M (1982) Crack Blunting of High-Silica Glass. J Am Ceram Soc 65:368–371. doi: 10.1111/j.1151-2916.1982.tb10486.x

33. Tomozawa M (1998) Stress corrosion reaction of silica glass and water. Phys Chem Glas 39:65–69.

34. Agarwal A, Tomozawa M (1997) Correlation of silica glass properties with the infrared spectra. J Non Cryst Solids 209:166–174. doi: 10.1016/S0022-3093(96)00542-X

35. Michalske TA, Freiman SW (1982) A molecular interpretation of stress corrosion

in silica. Nature 295:511–512.

36. Michalske TA, Freiman SW (1983) A Molecular Mechanism for Stress Corrosion in Vitreous Silica. J Am Ceram Soc 66:284–288.

37. Michalske TA, Bunker BC (1993) A chemical kinetics model for glass fracture. J Am Ceram Soc 76:2613–2618. doi: 10.1111/j.1151-2916.1993.tb03989.x

38. Nogami M, Tomozawa M (1984) Effect of Stress on Water Diffusion in Silica Glass. J Am Ceram Soc 67:151–154. doi: 10.1111/j.1151-2916.1984.tb09634.x

39. Tomozawa M, Kim D-L, Agarwal A, Davis KM (2001) Water diffusion and surface structural relaxation of silica glasses. J Non Cryst Solids 288:73–80. doi: 10.1016/S0022-3093(01)00648-2

40. Akinc M, Martin DM (1983) Heat of adsorption of water on E glass fibre surfaces. Phys Chem Glas 24:117–121.

41. Carman LA, Pantano CG (1990) Water-Vapor Adsorption on Calcium-Boroaluminosilicate Glass Fibers. J Non Cryst Solids 120:40–46.

42. Nishioka GM, Schramke JA (1983) Desorption of water from glass fibers. In: Ishida H, Kumar G (eds) Mol. Charact. Compos. Interfaces. Plenum Press, New York, pp 387–400

43. Brannan RT (1953) Further Evidence Against the Orientation of Structure in Glass Fibers. J Am Ceram Soc 36:230–231.

44. Goldstein M, Davies TH (1955) Glass Fibers with Oriented Chain Molecules. J Am Ceram Soc 38:1953–1956.

45. Miller PJ, Exarhos GJ, Risen WMJ (1973) Vibrational spectral study of molecular orientation in vitreous fibers. J Chem Phys 59:2796. doi: 10.1063/1.1680411

46. Bartenev GM (1969) The Structure and Strength of Glass Fibers of Different Chemical Composition. Mater Sci Eng 4:22–28.

47. Stockhorst H, Brückner R (1982) Structure sensitive measurements on E-glass fibers. J Non Cryst Solids 49:471–484.

48. Otto WH, Preston FW (1950) Evidence Against Oriented Structure in Glass

Fibres. J Soc Glas Technol 34:63–68.

49. Kroenke WJ (1966) Mechanical Test for Anisotropy; Failure of Aluminoborosilicate Glass Fibers Under Combined Loadings of Tension and Torsion. J Am Ceram Soc 49:508–513.

50. Mueller H (1938) Theory of photoelasticity in amorphous solids. J Am Ceram Soc 21:27–33. doi: 10.1111/j.1151-2916.1938.tb15726.x

51. Lund MD, Yue Y (2010) Impact of Drawing Stress on the Tensile Strength of Oxide Glass Fibers. J Am Ceram Soc 93:3236–3243. doi: 10.1111/j.1551-2916.2010.03879.x

52. Ya M, Deubener J, Yue Y (2008) Enthalpy and Anisotropy Relaxation of Glass Fibers. J Am Ceram Soc 91:745–752. doi: 10.1111/j.1551-2916.2007.02100.x

53. Lu X, Arruda E., Schultz W. (1999) The effect of processing parameters on glass fiber birefringence development and relaxation. J Nonnewton Fluid Mech 86:89–104. doi: 10.1016/S0377-0257(98)00203-1

54. Sugarman B (1967) Strength of Glass (A Review). J Mater Sci 2:275–283.

55. Cameron NM (1968) The effect of environment and temperature on the strength of E-glass fibres. Part 2. Heating and ageing. Glas Technol 9:121–130.

56. Gupta PK (2002) Strength of Glass Fibers. In: Elices M, Llorca J (eds) Fiber Fract. Elsevier Ltd, Oxford, United Kingdom, pp 125–153

57. Roylance D (2001) Introduction to Fracture Mechanics. 1–17.

58. ASTM C1322-05b (2010) Standard Practice for Fractography and Characterization of Fracture Origins in Advanced Ceramics. doi: 10.1520/C1322-05BR10.2

59. Lund MD, Yue Y (2008) Fractography and tensile strength of glass wool fibres. J Ceram Soc Japan 116:841–845. doi: 10.2109/jcersj2.116.841

60. Cameron NM (1965) Effect of Prior Heat Treatment on the Strength of Glass Fibers Measured at Room Temperature. J Am Ceram Soc 48:385.

61. Brearley W, Holloway DG (1963) The effect of heat-treatment on the breaking

strength of glass. Phys Chem Glas 4:69–75.

62. Piggott MR, Yokom JC (1968) The weakening of silica fibres by heat treatment. Glas Technol 9:172–175.

63. Aslanova MS (1960) The Effect of Different Factors on the Mechanical Properties of Glass Fibers. Steklo i Keramika 17:10–15.

64. Dorzhiev DB, Khazanov VE, Gorbachev V V (1990) Some features of the structure and strength of a magnesium aluminosilicate fiber. Sov J Glas Phys Chem 15:99–102.

65. Feih S, Boiocchi E, Mathys Z, et al. (2011) Mechanical properties of thermally-treated and recycled glass fibres. Compos Part B Eng 42:350–358. doi: 10.1016/j.compositesb.2010.12.020

66. Lund MD (2010) Tensile Strength of Glass Fibres. Aalborg University

67. Kennerley JR, Fenwick NJ, Pickering SJ, Rudd CD (1997) The properties of glass fibers recycled from the thermal processing of scrap thermoset composites. J Vinyl Addit Technol 3:58–63. doi: 10.1002/vnl.10166

68. Bartenev GM, Motorina LI (1965) Effect of Tensile Stresses on the Strength of Heat-Treated Glass Fibers. Mekhanika Polim [Translated] 1:89–92.

69. Lezzi PJ, Xiao QR, Tomozawa M, et al. (2013) Strength increase of silica glass fibers by surface stress relaxation: A new mechanical strengthening method. J Non Cryst Solids 379:95–106. doi: 10.1016/j.jnoncrysol.2013.07.033

70. Lezzi PJ, Seaman JH, Tomozawa M (2014) Strengthening of E-glass fibers by surface stress relaxation. J Non Cryst Solids 402:116–127. doi: 10.1016/j.jnoncrysol.2014.05.029

71. Otto WH (1961) Compaction Effects in Glass Fibers. J Am Ceram Soc 44:68–72.

72. Aslanova MS, Ivanov N V, Balashov YS (1970) Effect of chemical composition on the relaxation properties of thin glass fibers. Steklo i Keramika 8:21–24.

73. Yue Y, Jensen SL, Christiansen J de C (2002) Physical aging in a hyperquenched glass. Appl Phys Lett 81:2983–2985. doi: 10.1063/1.1514386

74. Yue Y (2005) Features of the relaxation in hyperquenched inorganic glasses during annealing. Phys Chem Glas 46:354–358.

75. Deubener J, Yue Y, Bornhöft H, Ya M (2008) Decoupling between birefringence decay, enthalpy relaxation and viscous flow in calcium boroalumosilicate glasses. Chem Geol 256:299–305. doi: 10.1016/j.chemgeo.2008.06.052

76. Yang L, Thomason JL (2013) The thermal behaviour of glass fibre investigated by thermomechanical analysis. J Mater Sci 48:5768–5775. doi: 10.1007/s10853-013-7369-7

77. Yue Y, Korsgaard M, Kirkegaard LF, Heide G (2009) Formation of a Nanocrystalline Layer on the Surface of Stone Wool Fibers. J Am Ceram Soc 92:62–67. doi: 10.1111/j.1551-2916.2008.02801.x

78. Wakasugi T, Burgner LL, Weinberg MC (1999) A DTA study of crystal nucleation in Na2O-SiO2 glasses. J Non Cryst Solids 244:63–73.

79. Hasanuzzaman M, Olabi AG (2012) Effect of Nucleation Temperature and Time on Crystallization Behaviour of Zirconia/Zircon Added Borosilicate Glass. ECCM15 - 15th Eur. Conf. Compos. Mater.

80. Gy R (2008) Ion exchange for glass strengthening. Mater Sci Eng B 149:159–165. doi: 10.1016/j.mseb.2007.11.029

81. Varshneya AK (2010) Chemical Strengthening of Glass: Lessons Learned and Yet To Be Learned. Int J Appl Glas Sci 1:131–142. doi: 10.1111/j.2041-1294.2010.00010.x

82. Kistler SS (1962) Stresses in Glass Produced by Nonuniform Exchange of Monovalent Ions. J Am Ceram Soc 45:59–68.

83. Pugh AC, Stratton RP, Lewis DB (1994) Investigation of elemental diffusion during the drawing and heat treatment of glass optical fibres. J Mater Sci 29:1036–1040.

84. Mäder E, Jacobasch H-J, Grundke K, Gietzelt T (1996) Influence of an optimized interphase on the properties of polypropylene/glass fibre composites. Compos Part A Appl Sci Manuf 27:907–912. doi: 10.1016/1359-835X(96)00044-9

85. Thomason JL (2012) Glass Fibre Sizings, 1st ed.

86. Thomason JL, Adzima LJ (2001) Sizing up the interphase : an insider's guide to the science of sizing. Compos Part A Appl Sci Manuf 32:313–321.

87. Plueddemann EP (1991) Silane coupling agents, 2nd ed. New York: Plenum Press

88. Thomason JL (2007) Interfaces and interfacial effects in glass reinforced thermoplastics. Proc. 28th Risø Int. Conf. Mater. Sci. pp 75–92

89. Sáez Rodríguez E, Yang L, Thomason JL (2013) Investigation of Strength Recovery of Recycled Heat Treated Glass Fibres through Chemical Treatments. 19th Int. Conf. Compos. Mater.

90. Child MJ, Heywood MJ, Pulton SK, et al. (1982) Infrared Studies of the Adsorption of Triethylamine on Silica at the Solid/Vapor and Solid/Liquid Interfaces. J Colloid Interface Sci 89:202–208.

91. Bellmann C, Plonka R, Caspari A, Luxbacher T (2007) Characterization of the interaction between silanes and solid surfaces by the streaming potential method. Silanes and other Coupling Agents 4:1–9.

92. Liu XM, Thomason JL, Jones FR (2008) XPS and AFM Study of Interaction of Organosilane and Sizing with E-glass Fibre Surface. J Adhes 84:322–338.

93. Zinck P, Mader E, Gerard JF (2001) Role of silane coupling agent and polymeric film former for tailoring glass fiber sizings from tensile strength measurements. J Mater Sci 36:5245–5252.

94. Zinck P, Pays MF, Rezakhanlou R, Gerard JF (1999) Mechanical characterisation of glass fibres as an indirect analysis of the effect of surface treatment. J Mater Sci 34:2121–2133.

95. Yang L, Thomason JL (2012) Effect of silane coupling agent on mechanical performance of glass fibre. J Mater Sci 48:1947–1954. doi: 10.1007/s10853-012-6960-7

96. Tiefenthaler A, Urban MW (1989) Thermal stability of silane coupling agents on Nextel fibres. Composites 20:145–150. doi: 10.1016/0010-4361(89)90642-3

97. Mizuguchi J, Tsukada Y, Takahashi H (2013) Recovery and Characterization of Reinforcing Fibers from Fiber Reinforced Plastics by Thermal Activation of Oxide Semiconductors. Mater Trans 54:384–391.

98. Lewicki JP, Liggat JJ, Patel M (2009) The thermal degradation behaviour of polydimethylsiloxane/montmorillonite nanocomposites. Polym Degrad Stab 94:1548–1557. doi: 10.1016/j.polymdegradstab.2009.04.030

99. Lewicki JP, Pielichowski K, De La Croix PT, et al. (2010) Thermal degradation studies of polyurethane/POSS nanohybrid elastomers. Polym Degrad Stab 95:1099–1105. doi: 10.1016/j.polymdegradstab.2010.02.021

100. Feih S, Manatpon K, Mathys Z, et al. (2008) Strength degradation of glass fibers at high temperatures. J Mater Sci 44:392–400. doi: 10.1007/s10853-008-3140-x

101. Masmoudi M, Rahal C, Abdelmouleh M, Abdelhedi R (2013) Hydrolysis process of γ-APS and characterization of silane film formed on copper in different conditions. Appl Surf Sci 286:71–77. doi: 10.1016/j.apsusc.2013.09.018

102. Culler SR, Naviroj S, Ishida H, Koenig JL (1983) Analytical and Spectroscopic Investigation of the Interaction of CO2 with Amine Functional Silane Coupling Agents on Glass Fibers. J Colloid Interface Sci 96:69–79.

103. Thomason JL, Kao CC, Nagel U, Yang L (2015) Recover: Regenerating the Strength of Glass Fibres Thermally Recycled From End-of-Life. 20th Int. Conf. Compos. Mater. pp 19–24

104. (2011) Water. In: NIST (National Inst. Stand. Technol. http://webbook.nist.gov/cgi/cbook.cgi?ID=C7732185&Type=IR-SPEC&Index=1#IR-SPEC. Accessed 13 Apr 2015

105. Liu XM (2006) Interaction of organosilane with glass surfaces. University of Sheffield

106. Eastes WL, Hofmann DA, Wingert JW (1998) Boron-free glass fibers.

107. Kennedy CR, Bradt RC, Rindone GE (1973) Fracture Mechanics of Binary Sodium Silicate Glasses. In: Bradt RC, Evans AG, Hasselman DPH, Lange FF

(eds) Fract. Mech. Ceram. Vol. 2. Plenum Press, New York, pp 883–893

108. Freiman SW (2012) The Fracture of Glass: Past, Present, and Future. Int J Appl Glas Sci 3:89–106. doi: 10.1111/j.2041-1294.2012.00091.x

109. Dériano S, Jarry A, Rouxel T, et al. (2004) The indentation fracture toughness (Kc) and its parameters: The case of silica-rich glasses. J Non Cryst Solids 344:44–50. doi: 10.1016/j.jnonerysol.2004.07.021

110. Rondinella V V., Matthewson MJ, Kurkjian CR (1994) Coating Additives for Improved Mechanical Reliability of Optical Fiber. J Am Ceram Soc 77:73–80. doi: 10.1111/j.1151-2916.1994.tb06959.x

111. Gupta PK, Inniss D, Kurkjian CR, Zhong Q (2000) Nanoscale roughness of oxide glass surfaces. J Non Cryst Solids 262:200–206. doi: 10.1016/S0022-3093(99)00662-6

112. Mellott NP, Pantano CG (2013) A Mechanism of Corrosion-Induced Roughening of Glass Surfaces. Int J Appl Glas Sci 4:274–279. doi: 10.1111/ijag.12035

113. Radlein E, Frischat GH (1997) Atomic force microscopy as a tool to correlate nanostructure to properties of glasses. J Non Cryst Solids 222:69–82.

114. Brussel VU Scanning Electron Microscopy & Energy Dispersive X-Ray Spectroscopy. http://www.surfgroup.be/semedx. Accessed 17 Aug 2015

115. Fernández A, Nieto MI, Oteo JL (1988) Characterization and surface modification on silicoaluminate glass fibre. J Mater Sci Lett 7:7–8. doi: 10.1007/BF01729897

116. Rothman SJ, Marcuso TLM, Nowicki LJ, et al. (1982) Diffusion of Alkali Ions in Vitreous Silica. J Am Ceram Soc 65:578–582. doi: 10.1111/j.1151-2916.1982.tb10786.x

117. Mehrer H, Imre AW, Tanguep-Nijokep E (2008) Diffusion and ionic conduction in oxide glasses. J Phys Conf Ser 106:1–9. doi: 10.1088/1742-6596/106/1/012001

118. Wheaton BR, Clare AG (2007) Evaluation of phase separation in glasses with

the use of atomic force microscopy. J Non Cryst Solids 353:4767–4778. doi: 10.1016/j.jnoncrysol.2007.06.073

119. Dalmas D, Lelarge a., Vandembroucq D (2007) Quantitative AFM analysis of phase separated borosilicate glass surfaces. J Non Cryst Solids 353:4672–4680. doi: 10.1016/j.jnoncrysol.2007.07.005

120. Pallares G, Grimaldi A, George M, et al. (2011) Quantitative analysis of crack closure driven by laplace pressure in silica glass. J Am Ceram Soc 94:2613–2618. doi: 10.1111/j.1551-2916.2011.04471.x

121. Jaras AC, Norman BJ (1983) The measurement of glass fibre strength in composites from studies of their fracture surfaces. J Mater Sci 18:2459–2465.

122. Feih S, Mouritz AP, Case SW (2015) Determining the mechanism controlling glass fibre strength loss during thermal recycling of waste composites. Compos Part A Appl Sci Manuf 76:255–261. doi: 10.1016/j.compositesa.2015.06.006

123. Ghosh SB, Jones FR, Hand RJ (2010) A novel indentation based method to determine the threshold stress intensity factor for sub-critical crack growth in glass. Glas Technol Eur J Glas Sci Technol Part A 51:156–160.

124. Thomason JL, Kalinka G (2001) A technique for the measurement of reinforcement fibre tensile strength at sub-millimetre gauge lengths. Compos Part A Appl Sci Manuf 32:85–90. doi: 10.1016/S1359-835X(00)00122-6

125. Liu H, Wang X, Zhang B, et al. (2012) Structure and properties of CaO-MgO-SiO2 inorganic glass fiber with additives (Al2O3, Y2O3). J Wuhan Univ Technol Sci Ed 27:58–62. doi: 10.1007/s11595-012-0407-5

126. Stockhorst H, Brückner R (1986) Structure sensitive measurements on phosphate glass fibers. J Non Cryst Solids 85:105–126.

127. Bateson S (1958) Critical Study of the Optical and Mechanical Properties of Glass Fibers. J Appl Phys 29:13. doi: 10.1063/1.1722934

128. Li H, Tomozawa M (1994) Mechanical strength increase of abraded silica glass by high pressure water vapor treatment. J Non Cryst Solids 168:287–292. doi: 10.1016/0022-3093(94)90341-7

129. Hirao K, Tomozawa M (1987) Dynamic Fatigue of Treated High-Silica Glass: Explanation by Crack Tip Blunting. J Am Ceram Soc 70:377–382. doi: 10.1111/j.1151-2916.1987.tb05654.x

130. Hirao K, Tomozawa M (1987) Kinetics of Crack Tip Blunting of Glasses. J Am Ceram Soc 70:43–48. doi: 10.1111/j.1151-2916.1987.tb04851.x

131. Yang L, Sáez E, Nagel U, Thomason JL (2015) Can thermally degraded glass fibre be regenerated for closed-loop recycling of thermosetting composites? Compos Part A Appl Sci Manuf 72:167–174. doi: 10.1016/j.compositesa.2015.01.030

132. Thomason JL, Nagel U, Yang L, Sáez ER (2015) Regenerating the strength of thermally recycled glass fibres using hot sodium hydroxide (submitted). Compos Part A Appl Sci Manuf. doi: 10.1017/CBO9781107415324.004

Appendix A : Principles of XPS

Introduction

The X-ray Photoelectron Spectroscopy technique is based on the photoelectron effect, which was first described by Einstein. The technique can provide information about the elemental composition and chemical binding characteristics of samples within approximately the first 1 – 10 nm of the surface by analysing the core electrons that are expelled by an incident X-ray beam. It is usual for the X-ray source to produce photons of a single energy; common choices include Mg Kα (1253.6 eV) and Al Kα (1486.6 eV).

Photoelectron effect

In general, electrons are bound to the positive nucleus of an atom. This can be expressed in terms of a binding energy: this increases as you move through the electron shells closer to the nucleus. In XPS it is the innermost core electrons that are of interest because their binding energies are characteristic of the particular element to which they belong therefore can be used to qualify and quantify the atomic composition of a material surface.

A representation of the photoelectron emission effect that occurs during XPS analysis is shown in Figure A-1.

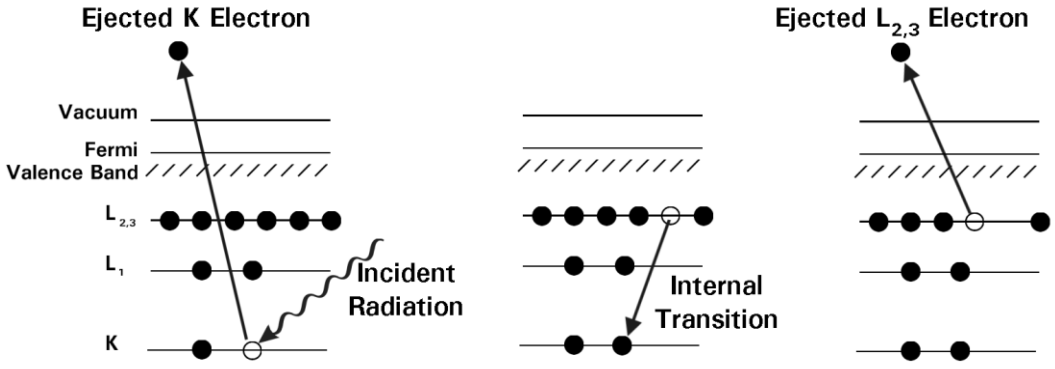

Figure A-1: From left to right; emission of kinetic electron due to incident photoelectron, internal transition to fill core hole, ejection of Auger electron due to transition energy

The incident (X-ray) radiation causes the expulsion of a core electron which is necessary for material identification in the analysis stage. Figure A-1 also shows the ejection of an Auger electron. This is produced as a result of the hole created in the

core electron shell. An electron from a higher shell moves in to fill this hole; the transition energy involved in this movement is imparted to another outer shell electron which is then expelled.

XPS instrumentation and analysis

The procedure described here is representative of the instrument settings used in the experiments described in this thesis; in reality numerous subtle differences in operation may persist based on the instrumentation available or the information desired from the experiments.

Electrons that are emitted from the sample surface pass through several stages in the XPS instrument before analysis. Initially, they are collected and transferred by an electrostatic lens system. The lens system also either accelerates or retards the electrons such that they all possess the same kinetic energy as they enter the next stage, the Concentric Hemispherical Analyser (CHA). Using this mode, the lens is scanned for a range of energies such that a spectrum can be constructed.

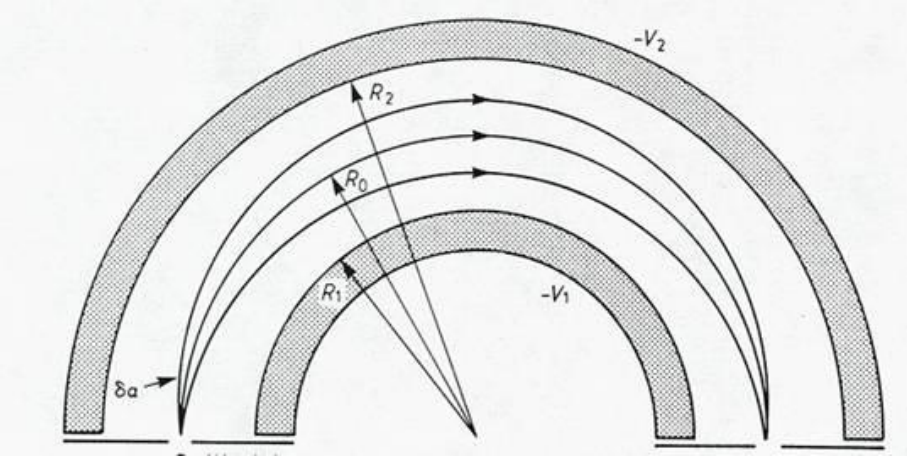

Figure A-2: Concentric Hemispherical Analyser (CHA) present in many XPS instruments

In the CHA a potential difference is created by applying voltage to the inner and outer plates as indicated in Figure A-2. Therefore, only photoelectrons with a particular kinetic energy will be able to pass through the analyser to reach the detector. The immediate output of this analysis process is a spectrum of relative intensities of photoelectrons with various kinetic energies. The following step involves conversion of this data into the characteristic binding energies that can then be used to perform identification of the surface chemistry.

$$KE = hv - BE - \varphi \quad \text{A1.1}$$

Binding energies are found through use of Equation A1.1. In the equation KE is the kinetic energy of photoelectrons that is measured by the instrument. The term hv is the energy of photons from the selected X-ray source which is fixed; the term φ is a work function specific to the XPS instrument which is found through proper calibration. In Equation A1.1 there is, therefore, only a single unknown BE the binding energy; solving for this allows production of spectra in which elements can be qualified and quantified by this characteristic.

Appendix B : Principles of AFM

Introduction

Atomic Force Microscopy (AFM) is a technique commonly used in the analysis of surfaces. At its most simple it can facilitate high resolution images of surfaces in the x, y and z directions: limits of the dimensions of images produced are of the order of tens to hundreds of micrometres in the x-y plane and a few micrometres in the z direction although these values are dependent on the instrument used. In general the strength of AFM is the ability to measure surface features with an accuracy of fractions of a nanometre in all directions, allowing production topography images. Analysis of these images often yields further useful information such as surface roughness, identification of structures with repeating phases or identification of the presence of contamination. Numerous more advanced techniques, based around the basic AFM, have been developed but are not considered here.

General principles of AFM

AFM images are produced by the interaction between a studied surface and a probe used to analyse it. Probes are commonly manufactured from silicon or silicon nitride; they consist of cantilever beam with a tip at or near the free end as shown schematically in Figure B-1.

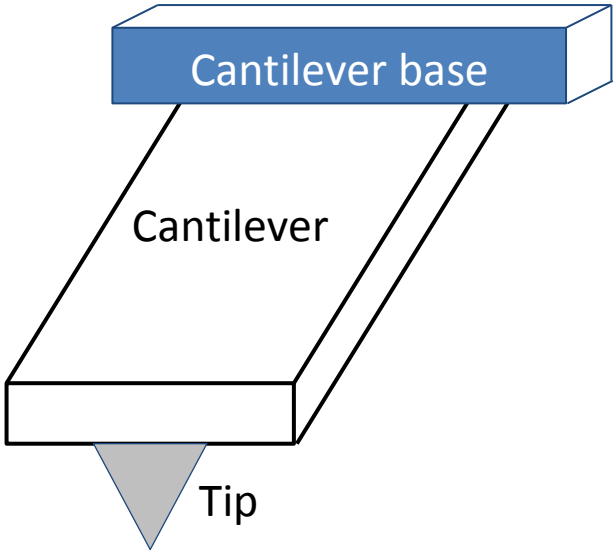

Figure B-1: Schematic of AFM probe showing cantilever and tip

The movement of the probe is controlled by a scanner which usually takes the form of a piezoelectric tube. By altering the applied voltage the position of the probe can be accurately controlled in the x, y and z directions. During analysis the probe is positioned extremely close to the surface of interest using stepper motors and the piezo based controller. Once engaged with the surface it scans in the x-y plane and follows the topography. Local increases in height cause the tip to move up, bending the cantilever upwards; similarly troughs or decreases in height cause a downward bend in the cantilever. These tiny movements of the cantilever are measured using a laser: the laser shines onto the rear face of the cantilever and is reflected on to a photodiode based detector as indicated in Figure B-2.

Intermittent contact AFM

Intermittent contact, or tapping mode, AFM is a variation of the more simple contact AFM and is used in many applications. It is advantageous primarily because it minimises damage to both samples and tips.

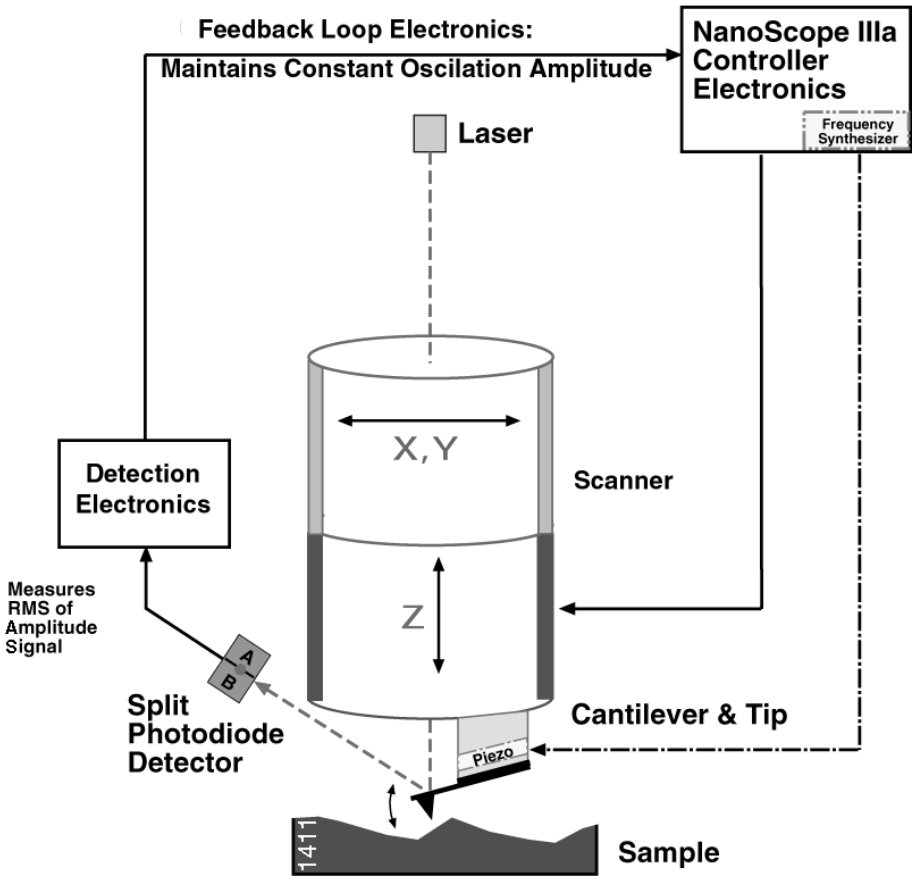

Figure B-2: Feedback loop electronics for AFM working in intermittent contact mode

A diagram of an AFM in tapping mode is shown in Figure B-2, including the feedback control system used. In tapping mode, the tip does not touch the sample surface as described for contact mode operation. Instead the piezoelectric controller oscillates the cantilever at or just above its resonant frequency which corresponds to an amplitude of no more than a few nanometres. As with contact AFM, the probe is moved relative to the sample in the x-y plane in a raster to measure the topography. In tapping mode, however, the function of the control system is to maintain a constant oscillation amplitude of the cantilever as indicated in Figure B-2. The tip does not make contact with the sample surface but as it approaches it is subjected to atomic forces which apply a corresponding force on the cantilever decreasing the amplitude of oscillation. The closer the tip is to the surface the greater this amplitude decrease would be. To maintain constant amplitude the piezoelectric tube therefore adjusts the position of the cantilever in the z direction as it scans back and forth. These adjustments in height constitute the data from which a plot of the sample topography will then be constructed.